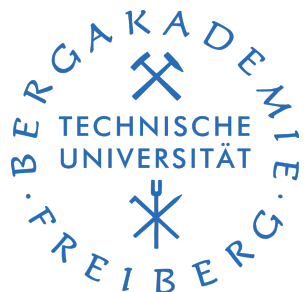


Development and implementation of user material subroutines for fibre reinforced plastics in a commercial FEM software

Master thesis



Presented by: Arun Prakash Ganapathy

Matriculation number: 63876

Course: Computational Materials Science
Institute of Mechanics and Fluid Dynamics

First Examiner: Prof. Dipl.-Ing. Björn Kiefer, Ph.D.

Second Examiner: Dr.-Ing. Stephan Roth

Supervisor: Dr.-Ing. Andreas Seupel

External supervisor: Dr.-Ing. Dominik Laveuve
Fraunhofer-Institut für Betriebsfestigkeit
und Systemzuverlässigkeit (LBF)

TU Bergakademie Freiberg

August 2021

Abstract

Composite materials, especially fibre-reinforced plastics, are replacing conventional materials like metals because of their superior strength and lightweight properties not only in advanced structural components but also in everyday applications. Fraunhofer LBF specializes in the safety and reliability of sustainable, lightweight structures. So numerical and experimental analysis and efficient manufacturing of fibre-reinforced plastics are essential in designing and developing lightweight, sustainable, and reliable components. An ongoing project at Fraunhofer LBF investigates the fatigue and creep behaviour of short fibre-reinforced thermoplastics. The damage behaviour in composite materials must be understood first in order to analyze complex phenomena such as fatigue, creep, etc. The main aim of this master thesis is to develop progressive damage models that can predict the initiation and propagation of damage when the composite material exceeds its failure strength. The constitutive equations necessary for simulating the behaviour of damaged materials are established in the framework of continuum damage mechanics (CDM). Because of the complex material behaviour, an anisotropic damage mechanism is employed to represent the damage distribution. A non-linear damage evolution law utilizing fracture energy regularization technique is employed to calculate the damage evolution. First, the damage models are implemented and tested at integration point levels. After that, representative structural examples are used to analyze how the damage models behave under various loading conditions. The global force-displacement response is examined to address the issue related to numerical implementation such as convergence and mesh sensitivity during strain-softening.

Acknowledgement

I would like to express my sincere thanks to Dr.-Ing. Dominik Laveuve for his guidance, support and valuable insights throughout this master thesis work. I would like to extend my gratitude to Prof.Dr.-Ing.Björn Kiefer for providing me the chance to pursue this thesis work under his supervision and Dr.-Ing. Andreas Seupel for his valuable feedback during the thesis work. I would like to thank Fraunhofer LBF for this opportunity and providing me with the required resources for completion of this thesis work. Last but not least, I am thankful to my friends and family for their constant moral support.

Declaration

Hereby, I formally declare that I have developed and written the enclosed thesis without illegitimate help of a third party and that no other than the indicated aids have been used for its completion; all thoughts from other sources that have been used literally or indirectly are marked as such. The thesis has not been submitted to any other examination committee in this or a similar form.

Arun Prakash Ganapathy

.....
Freiberg, 30.08.2021

Contents

Contents	VII
List of Figures	XI
List of Tables	XV
List of symbols	XVII
List of abbreviations	XIX
1 Introduction	1
1.1 Background and Motivation	1
1.2 Scope and Outline	3
2 Continuum Damage Mechanics	5
2.1 Damage	5
2.2 Representative Volume Element(RVE)	6
2.3 Concept of Continuum Damage Mechanics (CDM)	7
2.3.1 Modelling by effective area reduction	7
2.3.2 Modelling by variation of elastic modulus	8
2.4 Mechanical representation of the damage state	9
2.4.1 Scalar damage variable	9
2.4.2 Vector damage variable	9
2.4.3 Damage tensor of second order	10
2.5 Effective Stress Tensors	11
2.5.1 Effective stress tensor for isotropic damage (Lemaitre and Chaboche, 1978)	11
2.5.2 Asymmetric effective stress tensor for anisotropic damage (Murakami, 2012)	11
2.6 Damage effect tensors	11
2.7 Hypothesis of strain equivalence	12
2.8 Hypothesis of strain energy equivalence	14
2.9 Elastic constitutive equation and elastic modulus tensor of orthotropic material	15

3 Working environment	17
3.1 Software tools required	17
3.2 Programming the USERMAT	18
3.3 Compiling the USERMAT	19
3.4 Creating the FE model	20
3.5 Testing the USERMAT	20
3.6 PostProcessing	21
4 Progressive failure analysis of orthotropic composite materials	23
4.1 Fibre-reinforced Composites	23
4.1.1 Longitudinal failure	23
4.1.2 Transverse failure	24
4.2 Failure criteria	24
4.2.1 3D Hashin's quadratic strain criteria	24
4.2.2 Maximum stress criteria	25
4.2.3 Modified Hashin's failure criterion	26
4.3 Types of damage evolution	27
4.3.1 Isotropic damage	27
4.3.2 Anisotropic damage	28
4.4 Localisation and Mesh Regularisation	29
4.5 Numerical implementation of the damage model in ANSYS	30
4.5.1 Strain based damage model	31
4.5.2 Stress based damage model	32
4.6 Schematic of USERMAT implementation	33
5 Results and Discussion	35
5.1 Modelling linear elastic behaviour of orthotropic materials	35
5.2 Damage behaviour at integration point level	38
5.2.1 Uniaxial tension	38
5.2.2 Biaxial tension	43
5.2.3 Triaxial tension	44
5.3 Representative structural examples	45
5.3.1 Notched tensile specimen	46
5.3.2 Compact Tension (CT) Specimen	52
5.3.3 Plate with hole (3D)	59
6 Summary and Conclusion	65
Bibliography	67

Appendix	XX
A Stiffness matrix of the damaged material	XX
B Second term of the tangent stiffness	XXI
C APDL Script	XXII
D Source code for USERMAT	XXIV

List of Figures

1.1	Composite materials used in a Boeing 787 'Dreamliner' (P.Nikethan, 2016)	1
1.2	Strain-softening of composite materials after damage initiation (Rafi et al., 2007)	2
2.1	Scales of damage observation (Murakami, 2012)	6
2.2	Effective area reduction due to microcracks (Murakami, 2012)	7
2.3	Damage of bar under tensile load (Murakami, 2012)	8
2.4	Surface element in RVE of a damaged material (Murakami, 2012) . .	10
2.5	Hypothesis of strain equivalence (Murakami, 2012)	13
2.6	Hypothesis of strain energy equivalence (Murakami, 2012)	15
3.1	Steps involved in developing and testing damage models	18
3.2	USERMAT interface (Lin, 1999)	19
3.3	Table (TB) commands	21
3.4	Time history post processor window	22
4.1	Fracture planes in FRP material (Maimí et al., 2007)	24
4.2	Types of degradation behaviour in damaged composite materials (Wang et al., 2009)	27
4.3	Schematic of USERMAT implementation	33
5.1	Stress-Strain relation (Standard vs user-defined material routine) . .	35
5.2	Bar used for analysis: Mesh and BCs	36
5.3	Contour plots of the stress components σ_{11} , σ_{22} and σ_{33} of the bar obtained using standard material routine (Figures a, c, e on the left) and (Figures b, d, f on the right)	37
5.4	Evolution of stress for uniaxial tension test in 11 direction	38
5.5	Evolution of damage components for uniaxial tension test in 11 direction	39
5.6	Convergence issue: Residual norm of the stress <i>vs</i> no of Newton- raphson iterations	40
5.7	Evolution of stress components (Stress-based damage model)	40
5.7	Evolution of damage components (Stress-based damage model)	41
5.8	Influence of characteristic length L_c on the damage evolution	41

5.9	The strain components ϵ_{22} and ϵ_{33} computed using algorithmic (a) and numerical tangent stiffness (b) under uniaxial tension	42
5.10	Evolution of stress (Figures a, c on the left) and corresponding damage (Figure b, d on the right) components under biaxial tension	43
5.11	Evolution of stress (Figures a, c, e on the left) and corresponding (Figures b, d, f on the right) damage components under triaxial tension	45
5.12	Specimen geometry and boundary conditions. Dimensions are given in mm. Displacement controlled loading U_x is applied.	47
5.13	Considered meshes (h is the length of the element along fracture zone and n the total number of elements)	48
5.14	Convergence study: Global force-displacement response for model with regularization (Figure a on the left) and without regularization (Figure b on the right)	48
5.15	Convergence study for model with (Figures a, c, e) and without (b, d, f) regularization: Damage contour plots d_1 at the end of the loading .	49
5.16	$h = 0.25$ mm	50
5.17	Damage contour plots d_2 at the end of the loading (Loading in transverse direction)	50
5.18	Comparison of force-displacement response in longitudinal and transverse direction for $h = 0.5$ mm discretization	51
5.19	Specimen geometry and boundary conditions. Dimensions are given in mm. Displacement controlled loading U_x is applied	52
5.20	Considered meshes (h is the length of the element along fracture zone and n the total number of elements)	53
5.21	Damage distributions at the end of loading in longitudinal direction: Damage contour plots d_1 and d_2	54
5.22	Damage distributions at the end of loading in transverse direction: Damage contour plots d_1 and d_2 ($h = 1$ mm discretization)	55
5.23	Comparison of force-displacement response in longitudinal and transverse direction for $h = 1$ mm discretization	55
5.24	Comparison of force-displacement response for different shear co-efficient (α) ($h = 1$ mm discretization)	56
5.25	Evolution of stress components during longitudinal tensile loading ($h = 1$ mm discretization)	56
5.26	Damage distributions at the end of longitudinal loading: Damage contour plots d_2 for different shear co-efficients (α)	57
5.27	Evolution of stress components during transverse tensile loading ($h = 1$ mm discretization)	58
5.28	Damage distributions at the end of transverse loading: Damage contour plots d_1 for different shear co-efficient (α)	58

5.29 Specimen geometry and boundary conditions. Dimensions are given in mm. Displacement controlled loading U_x is applied	59
5.30 Finite element discretization used for 3D damage study	60
5.31 Global force-displacement response for the longitudinal tensile load- ing	61
5.32 Contour plots of the damage distribution d_1 , d_2 and d_3 at the end of longitudinal tensile loading	63

List of Tables

4.1	Maximum stress criterion	26
5.1	Material parameters (Integration point studies)	36
5.2	Material parameters (Representative structural examples)	46
5.3	Material parameters (3D Damage model)	60

List of Symbols

Symbols for tensors

Scalar	Light-face letters	a, b, ..., A, B, ..., σ , ϵ , ...,
Vectors	Bold letters	a , b , ..., A , B , ..., Ω , ...,
Second-order tensors	Underlined letters	<u>a</u> , <u>b</u> , ..., <u>A</u> , <u>B</u> , ..., <u>σ</u> , <u>ϵ</u> , ...,
Fourth-order tensors	Uppercase blackboard letters	\mathbb{A} , \mathbb{B} , \mathbb{C} , ...,

Symbols used

D	Damage
σ	Stress
$\tilde{\sigma}$	Effective stress
ϵ	Strain
E	Young's modulus
ν	Poisson's ratio
G	Shear modulus
Ω	Damage (vector)
\underline{D}	Damage tensor
\underline{I}	Identity tensor
$\underline{\sigma}$	Stress tensor
$\tilde{\underline{\sigma}}$	Effective stress tensor
$\underline{\epsilon}$	Strain tensor
\mathbb{M}	Damage effect tensor
α	Internal state variable
\mathbb{S}_0	Compliance tensor of an undamaged material
$\mathbb{S}(D)$	Compliance tensor of a damaged material
\mathbb{C}_0	Elastic stiffness tensor of an undamaged material
$\mathbb{C}(D)$	Elastic stiffness tensor of a damaged material
F_I	Failure indices in each principal material direction ($I = l, t, z$)
X_t, Y_t, Z_t	Tensile strength in each principal material direction
X_c, Y_c, Z_c	Compressive strength in each principal material direction
S	Shear strength

\otimes	Dyadic product
:	Double-contraction
.	Dot product
T	Transpose
L_c	Characteristic element length
$G_{f,i}$	Fracture energy in each principal material direction (i= 1,2,3)
d_i	Damage variable in each principal material direction (i= 1,2,3)
P_i	Softening parameter (i= 1,2,3)

List of Abbreviations

FRPs	Fibre Reinforced Plastics
CDM	Continuum Damage Mechanics
RVE	Representative Volume Element
FEM	Finite Element Methods
FE	Finite Element
IDE	Integrated Development Environment
USERMAT	User Material routine
APDL	ANSYS Parametric Design Language
TB	Table
NTEMPS	Number of Temperature Points
NPTS	Number of material constants at a given temperature
BCs	Boundary Conditions
GUI	Graphical User Interface
ATS	Algorithmic Tangent Stiffness
CT	Compact Tension

Chapter 1

Introduction

1.1 Background and Motivation

Composite materials are made of two or more dissimilar materials of different physical, chemical or mechanical properties, which, when combined, create a material with properties, unlike the individual constituent materials. One of the earliest use of composite materials dates back to 3400 B.C when Mesopotamians glued wood strips at different angles to create plywood (TWI, 2016). Nowadays, advanced composite materials are widely used in structural design in various industries such as aerospace, automobile, marine, petrochemical etc., due to their superior properties over traditional engineering materials.

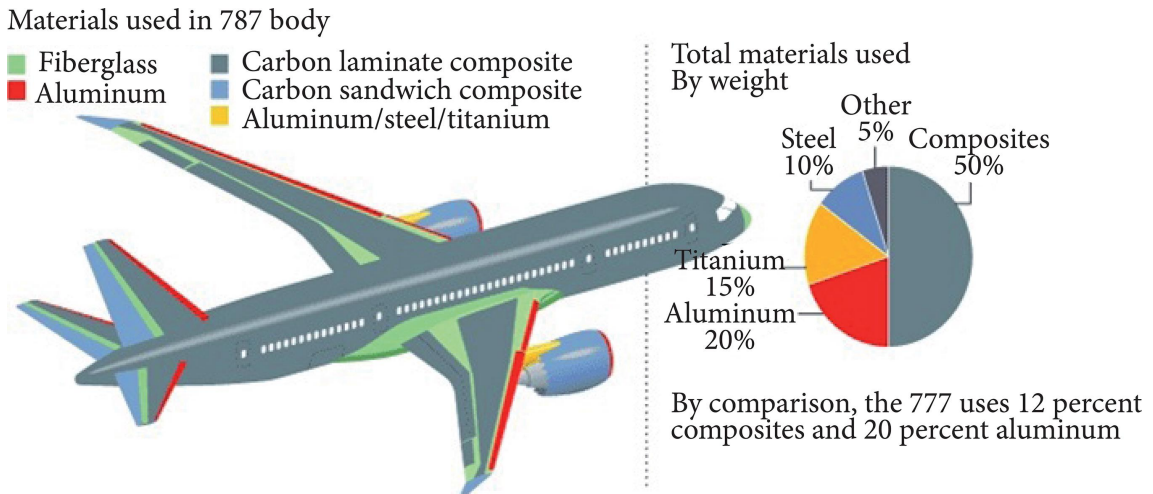


Figure 1.1: Composite materials used in a Boeing 787 'Dreamliner' (P.Nikethan, 2016)

Composite materials are attractive because of their high strength, high stiffness-to-density ratio, lightweight properties etc. (Lapczyk and Hurtado, 2007), Another important reason for using composite materials is the possibility to tailor

the stiffness and strength to specific load applications flexibly (Wang et al., 2009). Despite their superior physical properties, composite materials can be damaged from several sources, both during initial processing and in operation. Since composite materials have a complex material response and a low margin of safety through ductility as offered by metals, the development of damage must be understood for predicting failure of such materials (Lapczyk and Hurtado, 2007). For example, fibre-reinforced plastics exhibit local damage such as fibre breakage, matrix cracking, fibre matrix debonds, under normal operating conditions, which may contribute to the failure (Maimí et al., 2007). Therefore the ability to predict the initiation and growth of damage is important for predicting the performance, safety and reliability of the composite materials for commercial use.

Several methods have been proposed to analyze the failure of composite materials. The simplest of them is to degrade the stiffness of the material instantaneously using a degradation factor once the failure criteria are met (El-Sisi et al., 2015). While easy to implement, the sudden complete failure of the material does not agree well with the real-life behaviour. Progressive failure analysis of composite materials is required to predict the real-life mechanical behaviour under various loading conditions. Over the last few decades, the continuum mechanics approach to the damage model based on the works of (Kachanov, 1958) has been employed to analyze the progressive degradation of the materials. The CDM approach provides a methodology that can determine the full range of material deterioration, starting from no damage to the fully disintegrated material (Falzon and Apruzzese, 2011).

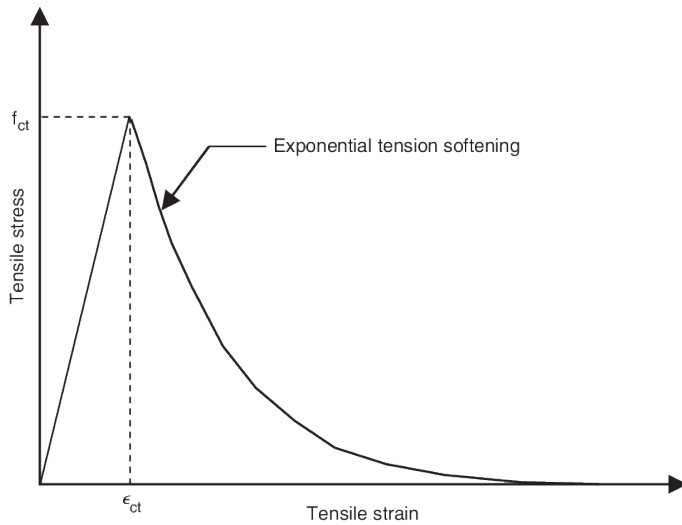


Figure 1.2: Strain-softening of composite materials after damage initiation (Rafi et al., 2007)

In CDM, the damage is represented as a set of damage variables that describe the material's current state and their development using a set of evolution laws.

Once the failure criteria are met, the damage variables are calculated using these evolution laws and the stiffness of the material is degraded with the help of the damage variables (Murakami, 2012) i.e., the material experiences strain-softening as illustrated in the Figure (1.2).

1.2 Scope and Outline

The objective of the thesis is to develop progressive damage models for predicting the initiation and propagation of the damage in fibre-reinforced plastics (FRPs) when subjected to various loading conditions. Continuum damage mechanics (CDM) provides the framework for developing these damage models. A second-order orthotropic damage tensor is employed to show the anisotropic damage development. Therefore one damage variable is assigned to each principal material direction to represent the development of damage, i.e., two damage variables are required when the problem is in 2D/Plane-stress and three variables when the problem is in 3D. The numerical modelling of the strain-softening behaviour results in strong mesh dependency, which results in convergence issues when the mesh is refined (Wang et al., 2009). The fracture energy approach is used to reduce the mesh sensitivity, which includes fracture energy in the damage evolution laws. This reduces the mesh sensitivity of the model by adjusting the energy dissipated by each failure mechanism using a characteristic element length (L_c) (Falzon and Apruzzese, 2011).

The stages of the thesis work are briefly described as follows

Chapter 2 introduces the theoretical framework of continuum damage mechanics (CDM), constitutive relations and constitutive equations necessary for developing the orthotropic material model.

Chapter 3 gives the reader a brief introduction to software used and the instructions to develop, compile and implement a material model.

Chapter 4 gives a brief introduction to the damage mechanisms, different types of failure criteria and evolution equations necessary for developing damage models. Finally, the chapter deals with the regularization technique used to reduce mesh sensitivity and a brief description of how to implement the damage models numerically.

Chapter 5 The results of the finite element simulations are discussed in this chapter. Starting with the implementation of linear elastic behaviour of the orthotropic material, the chapter discusses the behaviour of the damage models at the integration point level and then using representative structural examples. The issues

related to numerical implementation, such as convergence and mesh sensitivity during strain-softening are also discussed in this chapter.

Chapter 2

Continuum Damage Mechanics

Continuum damage mechanics (CDM) is a theory for analyzing failure processes in materials from a continuum mechanics point of view. (CDM) provides a continuum perspective for microcracks initiation, propagation, and their coalescence that results in macroscopic fracture. CDM uses state variables to represent the damaging effect on the stiffness and remaining life of the material that is deteriorating due to load and ageing. A failure criterion is used to predict the initiation of damage, and evolution laws are required to represent the propagation of the damage in a material subjected to load (Murakami, 2012)

2.1 Damage

Consider a body B where a crack of length a has developed when subjected to an external load F , as shown in Figure (2.1). A number of microcracks would be observed around the arbitrary point $P(x)$ near the crack tip. These microcracks develop due to breakage of atomic bonds or defects in the atomic array (Murakami, 2012). From the microscopic point of view, fracture of materials is a process of nucleation of microcracks due to the breakage of atomic bonds. From the macroscopic point of view, it is a process of extension of cracks by the coalescence of these microcracks.

From the mesoscopic point of view, which exists between microscopic and macroscopic scale, it is a process of nucleation, growth and the coalescence of microscopic cavities that leads to the initiation of macroscopic crack. The development of microscopic, mesoscopic and macroscopic fracture processes in materials and the resulting deterioration in their mechanical properties is called damage. Continuum damage mechanics aims to analyse the damage development during mesoscopic and macroscopic fracture processes in the framework of continuum mechanics (Murakami, 2012).

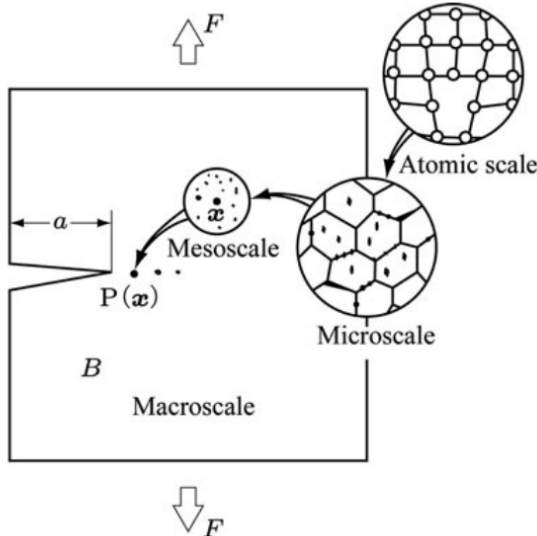


Figure 2.1: Scales of damage observation (Murakami, 2012)

2.2 Representative Volume Element(RVE)

To discuss the effects of microcracks in a material using CDM, one must homogenize the mechanical effects of microstructure and represent them as a continuous macroscopic field. For this purpose, we take a small region of a mesoscale around the material point $P(x)$ in body B , as shown in Figure (2.1). We assume that the material with discontinuities in this region as homogeneous, and the state of the material in this region can be represented by the statistical average of the mechanical variables in that region. This region is said to be the Representative Volume Element (RVE) (Hill, 1963) and (Hashin, 1983). For such RVE, the following two conditions must be satisfied (Murakami, 2012):

- For the material in the RVE to be homogeneous, the RVE should be sufficiently large enough to contain a number of discontinuities
- To represent a non-uniform macroscopic field using a continuum, the size of RVE should be small enough so that the variation of the macroscopic variable in it may be insignificantly small

The size of RVE depends on the microstructure of the relevant material, and their typical sizes are as follows (Lemaitre, 2012)

- Metals and ceramics - 0.1 mm^3
- Polymers and composites - 1 mm^3
- Timber - 10 mm^3
- Concrete - 100 mm^3

2.3 Concept of Continuum Damage Mechanics (CDM)

The basic concept of CDM is that a set of damage variables can represent the microstructural defects in a material. Continuum damage mechanics first represent the state of damage in a material using a set of internal state variables and then describe the mechanical behaviour of the damaged material and the development of damage. The mechanical behaviour of a damaged material can be described using the notion of effective stress, together with the hypothesis of mechanical equivalence between damaged and undamaged material (Murakami, 2012). The concept of effective stress and mechanical equivalence will be discussed in the following sections.

2.3.1 Modelling by effective area reduction

Let us consider body B of Figure (2.2) and take an RVE at a point $P(x)$ in B . If the total void area in dA is dA_D , the mechanical effect of dA will be decreased by dA_D . Then the area,

$$d\tilde{A} = dA - dA_D \quad (2.1)$$

may be interpreted as the area which carries the internal force and is called an *effective area* (Kachanov, 1986). Thus, the damage variable D can be specified as

$$D = \frac{dA - d\tilde{A}}{dA} = \frac{dA_D}{dA} \quad (2.2)$$

where the damage variable D takes a value between 0 and 1 ($0 \leq D \leq 1$). $D = 0$ represents initial undamaged state and $D = 1$ represents fully damaged state.

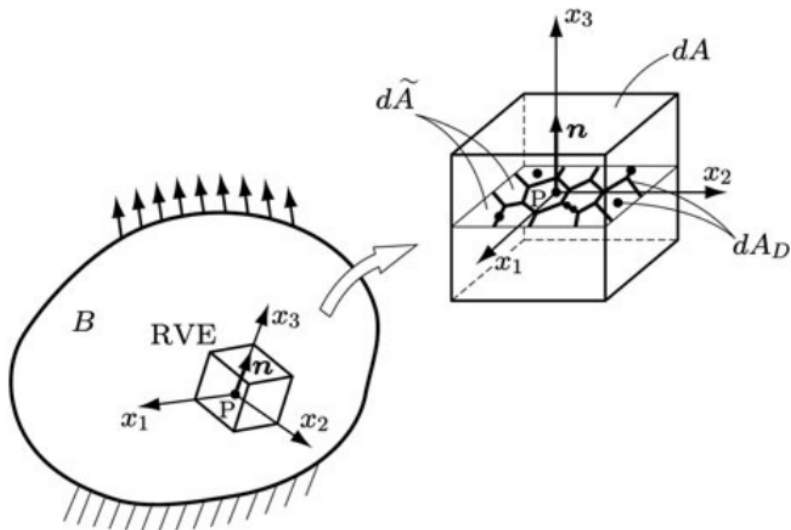


Figure 2.2: Effective area reduction due to microcracks (Murakami, 2012)

Suppose a cylindrical bar of cross-sectional area dA is subject to a tensile load dF as shown in Figure (2.3), then the actual load carrying area is $d\tilde{A}$ rather than

dA . According to equations (2.1) and (2.2) the effective area $d\tilde{A}$ is given by,

$$d\tilde{A} = (1 - D)dA \quad (2.3)$$

The decrease in the load-carrying area increases the effect of stress σ induced by the external force dF . Due to Eq. (2.3), the magnified stress $\tilde{\sigma}$ is given by,

$$\tilde{\sigma} = \frac{dF}{d\tilde{A}} = \frac{\sigma}{1 - D} \quad (2.4)$$

Since the stress $\tilde{\sigma}$ represents the stress magnified by the net area reduction due to damage, it is called *effective stress* (Kachanov, 1986). From equations (2.3) and (2.4) one can postulate that the damaged cylindrical bar of Figure (2.3b) with the cross-sectional area dA subject to force dF is mechanically equivalent to the fictitious undamaged bar of Figure (2.3c), which is subject to force dF , has the cross-sectional area $d\tilde{A}$ and hence stress $\tilde{\sigma}$. (Note - The concept and equations in this section are derived from (Murakami, 2012))

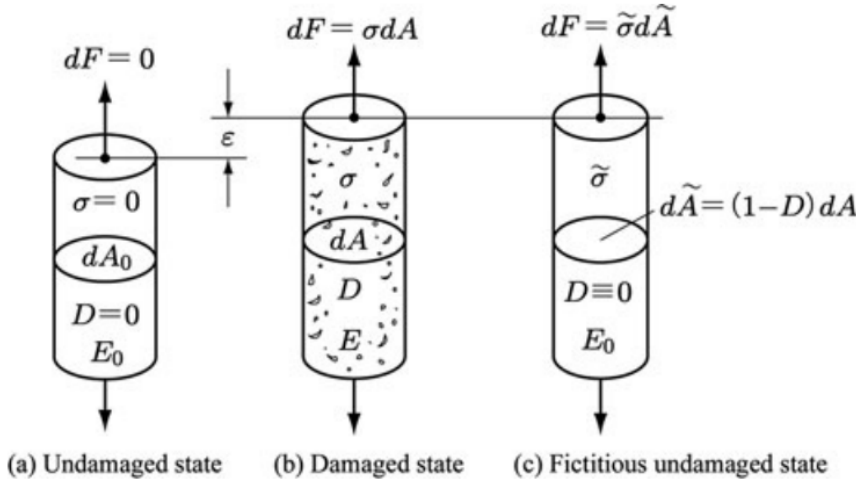


Figure 2.3: Damage of bar under tensile load (Murakami, 2012)

2.3.2 Modelling by variation of elastic modulus

Since the development of microcracks causes the reduction in material stiffness, the damage state can be characterized by variation in elastic modulus (Lemaitre and Chaboche, 1978). Let us consider the bar (b) and (c) of Figure (2.3) that are in the damaged and fictitious undamaged state, respectively. Then the elastic strain ϵ in the bar (c) due to stress $\tilde{\sigma}$ should be equal to the ϵ of the bar (b) under stress σ ; i.e.,

$$\tilde{\sigma} = E_0\epsilon, \quad \sigma = E(D)\epsilon \quad (2.5)$$

$$\epsilon = \frac{\sigma}{E(D)} = \frac{\tilde{\sigma}}{E_0} \quad (2.6)$$

where E_0 and $E(D)$ are the young's moduli of the material in the initial undamaged state and in damaged state after loading, respectively. Therefore, Eq. (2.6) defines another effective stress

$$\tilde{\sigma} = \frac{E_0}{E(D)}\sigma \quad (2.7)$$

Combining equations (2.4) and (2.6),

$$E(D) = (1 - D)E_0 \quad (2.8)$$

$$D = 1 - \frac{E(D)}{E_0} \quad (2.9)$$

Therefore, the damage variable D is characterized by the variation in Young's modulus $E(D)$. The modelling of damage by means of reduction in stiffness can be applied to the anisotropic damage of brittle materials like composite materials, concrete, rocks etc., (Note - The concept and equations in this section are derived from (Murakami, 2012))

2.4 Mechanical representation of the damage state

The deformation of material depends on the direction of applied stress or strain, and hence it is an anisotropic phenomena. Therefore different theories have been developed for modelling 3-D anisotropic damage phenomenon (Murakami, 2012). Some fundamental theories that describe 3-D damage state are given below.

2.4.1 Scalar damage variable

In the case of random or isotropic distribution of microcracks or voids, and when void density is small, the global mechanical properties can be approximated as nearly isotropic. The damage state, in this case, maybe represented using scalar damage variable D . This isotropic damage theory based on the scalar damage variable can be applied to 3-D problems of creep, elastic-plastic, ductile and fatigue damage (Lemaitre, 2012).

2.4.2 Vector damage variable

The damage state can be specified by the decrease in load carrying effective area due to void development. Hence it is easy to postulate a vector damage variable. (Kachanov, 1986) tried to extend the definition of damage to anisotropic damage

by noting a surface element in an arbitrary direction \mathbf{n} , he proposed vector damage variable $\Omega = \Omega_n \mathbf{n}$, where Ω_n is the effective area fraction.

2.4.3 Damage tensor of second order

To describe an anisotropic damage state, a damage variable of second or higher order tensor can be employed. Eq. (2.3) suggests that the damage state (1 - D) is specified by the transformation of the surface element dA of Figure (2.3b) of the damage state into the corresponding surface element $d\tilde{A}$ in the fictitious undamaged state of Figure (2.3c) (Murakami, 2012).

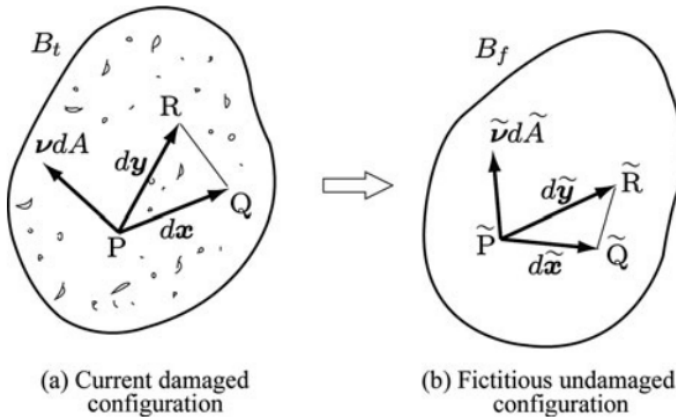


Figure 2.4: Surface element in RVE of a damaged material (Murakami, 2012)

To express damage as a second order tensor, we first consider an arbitrary surface element PQR in RVE in the current damaged configuration B_t of Figure (2.4a). The unit normal vector and area of PQR are denoted by ν and dA . We further postulate the fictitious undamaged configuration B_f of Figure (2.4b) mechanically equivalent to B_t , and the surface element and its area vector are denoted by $\tilde{P}\tilde{Q}\tilde{R}$ and $\tilde{\nu}d\tilde{A}$ respectively. According to Eq. (2.3) the damage variable of second-order tensor D should be defined by linear transformation from area vector νdA in B_t into $\tilde{\nu}d\tilde{A}$ in B_f , i.e.,

$$\tilde{\nu}d\tilde{A} = (\underline{I} - \underline{D})\nu dA \quad (2.10)$$

where \underline{I} is the second order identity tensor. Since the damage tensor \underline{D} is symmetric, it can be expressed by its spectral decomposition

$$D = \sum_{i=1}^3 D_i \mathbf{n}_i \otimes D_i \mathbf{n}_i \quad (2.11)$$

where D_i and n_i are the principal values and principal directions of \underline{D} . (Note - The concept and equations in this section are derived from (Murakami, 2012))

2.5 Effective Stress Tensors

The effective stresses are used to describe the mechanical behaviour of the damaged material. Some of the effective stresses postulated in damage mechanics are given below

2.5.1 Effective stress tensor for isotropic damage (Lemaitre and Chaboche, 1978)

If the damage state is isotropic then the effective stress tensor of three-dimensional state is given by

$$\underline{\tilde{\sigma}} = (1 - D)^{-1} \underline{\sigma} \quad (2.12)$$

where D is the scalar damage variable, and $\underline{\sigma}$ is the Cauchy stress tensor. This effective stress simplifies damage theory and can be applied to a number of damage problems like ductile damage. But this cannot be applied to damage of significant anisotropy, such as brittle damage due to microcrack distribution.

2.5.2 Asymmetric effective stress tensor for anisotropic damage (Murakami, 2012)

The increase in stress caused by the net area reduction in case of anisotropic damage is given by

$$\underline{\tilde{\sigma}} = (\underline{I} - \underline{D})^{-1} \underline{\sigma} \quad (2.13)$$

where \underline{I} and \underline{D} are second-order identity tensor and the second-order damage tensor, respectively. In the actual development of anisotropic damage, the stress-induced in the RVE of damaged material is asymmetric. But asymmetric stress tensors make the numerical analysis complicated, and thus different methods of symmetrization have been proposed. A simple symmetrization of Eq. (2.13) gives,

$$\underline{\tilde{\sigma}} = \frac{1}{2} [(\underline{I} - \underline{D})^{-1} \underline{\sigma} + \underline{\sigma} (\underline{I} - \underline{D})^{-1}] \quad (2.14)$$

2.6 Damage effect tensors

The general form of an effective stress tensor $\underline{\tilde{\sigma}}$ is given by the damage effect tensor \mathbb{M} and the corresponding Cauchy stress tensor $\underline{\sigma}$, i.e.,

$$\underline{\tilde{\sigma}} = \mathbb{M} : \underline{\sigma} \quad (2.15)$$

It is convenient to express the tensors in the form of matrices and then execute the tensor operations as a matrix calculus.. To simplify this procedure, we take

an orthonormal basis n_i with principal directions n_i of the second-order symmetric damage tensor \underline{D} , and represent the tensor in terms of its component to this basis (Murakami, 2012). According to Voigt notation, the second-order symmetric tensor $\underline{\sigma}$ and the related effective stress $\tilde{\underline{\sigma}}$ are expressed by the column vector of six dimensions:

$$[\sigma_P] \equiv [\sigma_{11} \ \sigma_{22} \ \sigma_{33} \ \sigma_{12} \ \sigma_{13} \ \sigma_{23}]^T \quad (2.16)$$

$$[\tilde{\sigma}_P] \equiv [\tilde{\sigma}_{11} \ \tilde{\sigma}_{22} \ \tilde{\sigma}_{33} \ \tilde{\sigma}_{12} \ \tilde{\sigma}_{13} \ \tilde{\sigma}_{23}]^T \quad (2.17)$$

By means of the matrix representation, we have the matrix form

$$[\tilde{\sigma}_P] \equiv [\mathbb{M}_{pq}] : [\sigma_P] \quad (2.18)$$

Matrix representation of the damage effect tensor of Eq. (2.18) is shown below (Wang et al., 2009)

$$[\mathbb{M}_{pq}] \equiv \begin{bmatrix} \frac{1}{\omega_{11}} & 0 & 0 & 0 & 0 & 0 \\ 0 & \frac{1}{\omega_{22}} & 0 & 0 & 0 & 0 \\ 0 & 0 & \frac{1}{\omega_{33}} & 0 & 0 & 0 \\ 0 & 0 & 0 & \frac{1}{\omega_{12}} & 0 & 0 \\ 0 & 0 & 0 & 0 & \frac{1}{\omega_{23}} & 0 \\ 0 & 0 & 0 & 0 & 0 & \frac{1}{\omega_{13}} \end{bmatrix}$$

where

$$\omega_{11} = (1 - d_1); \ \omega_{22} = (1 - d_2); \ \omega_{33} = (1 - d_3);$$

$$\omega_{12} = \sqrt{(1 - d_1)(1 - d_2)}; \ \omega_{23} = \sqrt{(1 - d_2)(1 - d_3)}; \ \omega_{13} = \sqrt{(1 - d_1)(1 - d_3)};$$

2.7 Hypothesis of strain equivalence

The constitutive equation of a damaged material is given by the constitutive equation for an undamaged material by replacing the stress tensor $\underline{\sigma}$ in the equation with the effective stress tensor $\tilde{\underline{\sigma}}$ (Lemaitre and Chaboche, 1978). The stress $\underline{\sigma}$

acting on RVE in the damaged configuration B_t is equivalent to that of the stress $\tilde{\sigma}$ in the fictitious undamaged configuration in Figure (2.5). Therefore the deformation of the damaged material subject to stress $\underline{\sigma}$ should be equal to that of the fictitious undamaged material subject to stress $\tilde{\sigma}$. Suppose the constitutive equation of an undamaged material is given by

$$\epsilon = F_0(\underline{\sigma}, \alpha) \quad (2.19)$$

or

$$\dot{\epsilon} = F_0(\underline{\sigma}, \alpha) \quad (2.20)$$

where α is an internal variable representing the internal change other than damage. and (\cdot) denotes the material time derivative. Then according to hypothesis

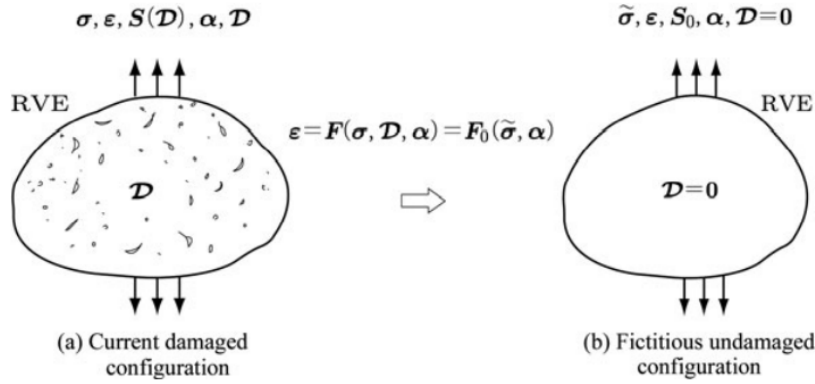


Figure 2.5: Hypothesis of strain equivalence (Murakami, 2012)

of strain equivalence, the inelastic constitutive equation of the damaged material represented by a damage variable D should be given by replacing $\underline{\sigma}$ of Eq. (2.19) with the effective stress $\tilde{\sigma}$ i.e.,

$$\epsilon = F(\sigma, D, \alpha) = F_0(\tilde{\sigma}, \alpha) \quad (2.21)$$

or

$$\dot{\epsilon} = F(\sigma, D, \alpha) = F_0(\tilde{\sigma}, \alpha) \quad (2.22)$$

In case of elastic deformation, constitutive equations for an undamaged and damaged material are given by

$$\underline{\epsilon} = \mathbb{S}_0 : \underline{\sigma}, \quad (2.23)$$

$$\epsilon = \mathbb{S}(D) : \underline{\sigma}, \quad (2.24)$$

where \mathbb{S}_0 and $\mathbb{S}(D)$ are fourth-order elastic compliance tensors of the materials. Therefore, according to the hypothesis of strain equivalence the elastic constitutive equation of the damaged material and the compliance tensor are given by

$$\underline{\epsilon} = \mathbb{S}_0 : \tilde{\sigma} = [\mathbb{S}_0 : \mathbb{M}(D)] : \underline{\sigma} = \mathbb{S}(D) : \underline{\sigma} \quad (2.25)$$

$$\mathbb{S}(\underline{D}) = \mathbb{S}_0 : \mathbb{M}(\underline{D}) \quad (2.26)$$

where $\mathbb{M}(\underline{D})$ is the damage effect tensor which is given by

$$\mathbb{M}(\underline{D}) = \mathbb{S}_0^{-1} : \mathbb{S}(\underline{D}) \quad (2.27)$$

(Note - The concept and equations in this section are derived from (Murakami, 2012))

2.8 Hypothesis of strain energy equivalence

The existence of a strain energy function necessitates the symmetry of the compliance and elastic modulus tensor. But the compliance tensor resulting from the hypothesis of strain equivalence is asymmetric which does not satisfy the requirement. Therefore the hypothesis of strain energy equivalence is used to satisfy the symmetry requirements (Cordebois and Sidoroff, 1982). Let us consider an elastic-plastic material and represent the plastic deformation by an internal state variable α . The complementary strain energy functions of the material at undamaged and damaged state are given, respectively as follows

$$V_0(\underline{\sigma}, \alpha) = \frac{1}{2}\underline{\sigma} : \mathbb{S}_0 : \underline{\sigma} - \phi(\alpha) \quad (2.28)$$

$$V(\underline{\sigma}, \underline{D}, \alpha) = \frac{1}{2}\underline{\sigma} : \mathbb{S}(\underline{D}) : \underline{\sigma} - \phi(\alpha) \quad (2.29)$$

Thus the constitutive equation for the undamaged and damaged material is

$$\epsilon = \frac{\partial V_0}{\partial \underline{\sigma}} = \mathbb{S}_0 : \underline{\sigma} \quad (2.30)$$

$$\epsilon = \frac{\partial V}{\partial \underline{\sigma}} = \mathbb{S}(\underline{D}) : \underline{\sigma} \quad (2.31)$$

Suppose a damaged material of Figure (2.6a) subject to stress $\underline{\sigma}$, and represent the damage and internal state due to inelastic deformation by \underline{D} and α , respectively. Then the strain energy function $V(\underline{\sigma}, \underline{D}, \alpha)$ of the damaged material is given by replacing $\underline{\sigma}$ in the corresponding function $V_0(\underline{\sigma}, \alpha)$ of the undamaged material of Figure (2.6b) with the effective stress $\tilde{\sigma}$

$$V(\underline{\sigma}, \underline{D}, \alpha) = V_0(\tilde{\sigma}, \alpha)$$

By the use of this hypothesis, the elastic strain of Eq. (2.31) leads to

$$\underline{\epsilon} = \frac{\partial V(\underline{\sigma}, \underline{D}, \alpha)}{\partial \underline{\sigma}} = \mathbb{S}(\underline{D}) : \underline{\sigma}$$

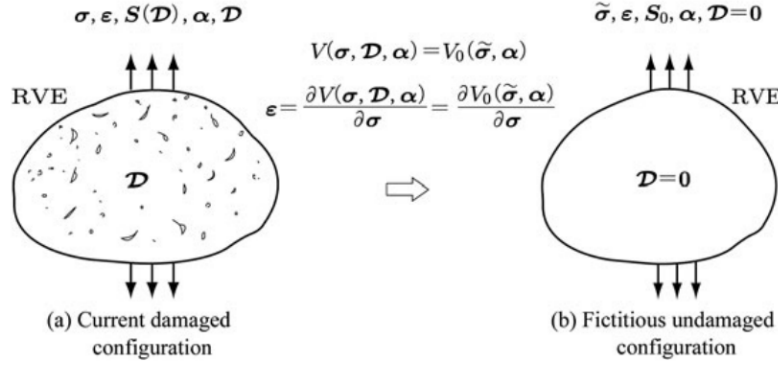


Figure 2.6: Hypothesis of strain energy equivalence (Murakami, 2012)

$$= \frac{\partial V_0(\underline{\sigma}, \alpha)}{\partial \underline{\sigma}} = \frac{\partial}{\partial \underline{\sigma}} \left(\frac{1}{2} \underline{\sigma} : \mathbb{S}_0 : \underline{\sigma} \right)$$

$$= \frac{1}{2} \frac{\partial}{\partial \underline{\sigma}} [(\mathbb{M}(\underline{D}) : \underline{\sigma}) : \mathbb{S}_0 : (\mathbb{M}(\underline{D}) : \underline{\sigma})]$$

$$= [\mathbb{M}^T(\underline{D}) : \mathbb{S}_0 : \mathbb{M}(\underline{D})] \quad (2.32)$$

From Eq. (2.32), the elastic compliance tensor of the damaged material is given as follows

$$\mathbb{S}(\underline{D}) = \mathbb{M}^T(\underline{D}) : \mathbb{S}_0 : \mathbb{M}(\underline{D}) \quad (2.33)$$

If the damage effect tensor $\mathbb{M}(\underline{D})$ can be expressed as a fourth-order symmetric tensor, then the elastic compliance tensor $\mathbb{S}(\underline{D})$ becomes a fourth-order symmetric tensor which satisfies the symmetry requirement. (Note - The concept and equations in this section are derived from (Murakami, 2012))

2.9 Elastic constitutive equation and elastic modulus tensor of orthotropic material

Orthotropic materials are a special form of anisotropic materials because their properties change when measured from different directions. They exhibit different material properties in mutually perpendicular directions. Some examples of orthotropic materials are wood, composite materials etc. Orthotropic materials require nine independent variables to express their constitutive matrix. The 9 elastic

constants are three Young's moduli E_1, E_2, E_3 , the three Poisson's ratios $\nu_{12}, \nu_{23}, \nu_{13}$, and three shear moduli G_{12}, G_{23}, G_{13} . The constitutive equation and elastic stiffness matrix of orthotropic material (Lemiere, 1968) has the form,

$$\underline{\sigma} = \mathbb{C}_0 : \underline{\epsilon} \quad \text{or} \quad \sigma_{ij} = C_{ijkl}^0 \epsilon_{kl}, \quad (2.34)$$

$$[C_{pq}^0] = \begin{bmatrix} \frac{1 - \nu_{23}\nu_{32}}{E_2 E_3 \Delta} & \frac{\nu_{12} + \nu_{13}\nu_{32}}{E_2 E_3 \Delta} & \frac{\nu_{13} + \nu_{12}\nu_{23}}{E_2 E_3 \Delta} & 0 & 0 & 0 \\ \frac{\nu_{21} + \nu_{23}\nu_{31}}{E_1 E_3 \Delta} & \frac{1 - \nu_{13}\nu_{31}}{E_1 E_3 \Delta} & \frac{\nu_{23} + \nu_{21}\nu_{13}}{E_1 E_3 \Delta} & 0 & 0 & 0 \\ \frac{\nu_{31} + \nu_{21}\nu_{32}}{E_1 E_2 \Delta} & \frac{\nu_{32} + \nu_{12}\nu_{31}}{E_1 E_2 \Delta} & \frac{1 - \nu_{12}\nu_{21}}{E_1 E_2 \Delta} & 0 & 0 & 0 \\ 0 & 0 & 0 & G_{12} & 0 & 0 \\ 0 & 0 & 0 & 0 & G_{23} & 0 \\ 0 & 0 & 0 & 0 & 0 & G_{13} \end{bmatrix}$$

where

$$\Delta = (1 - \nu_{12}\nu_{21} - \nu_{23}\nu_{32} - \nu_{31}\nu_{13} - 2\nu_{12}\nu_{23}\nu_{31})/E_1 E_2 E_3$$

$$\text{and } \frac{\nu_{12}}{E_2} = \frac{\nu_{21}}{E_1}, \frac{\nu_{23}}{E_3} = \frac{\nu_{32}}{E_2}, \frac{\nu_{13}}{E_3} = \frac{\nu_{31}}{E_1}$$

Chapter 3

Working environment

The material models necessary for simulating damage must be programmed first using a programming language, compiled, and then tested in a commercial FEM software. The programming language of choice for most commercial FEM software (e.g., ANSYS, ABAQUS) is FORTRAN because it is fast and efficient. To program the material model, an integrated development environment (IDE) and a compiler compatible with the version of the FEM software are required. This chapter describes the tools required for developing and testing the damage models and instructions on how to use them in detail.

3.1 Software tools required

- **GNU Octave**

GNU Octave is software which uses a high-level programming language primarily intended for numerical computations. Initially, the damage models are developed on Octave and tested using simple loading cases like uniaxial tension with the help of constitutive driver routines (B.Kiefer) before implementing them as user material routine (USERMAT) in ANSYS.

- **Microsoft Visual Studio**

Microsoft Visual Studio is the IDE used for programming the damage models as user material routines using the FORTRAN programming language.

- **Intel parallel studio**

The compiler available in Intel parallel studio is used for compiling the USERMAT before testing them in a FEM software.

- **ANSYS**

ANSYS is the commercial FEM software chosen for creating FE models of specimens and analyzing damage models under different loading conditions.

The following sections provide the reader with a detailed description, starting from developing the user material routine to implementing and analysing the results

in the ANSYS environment. The flowchart below shows the steps involved in the whole process

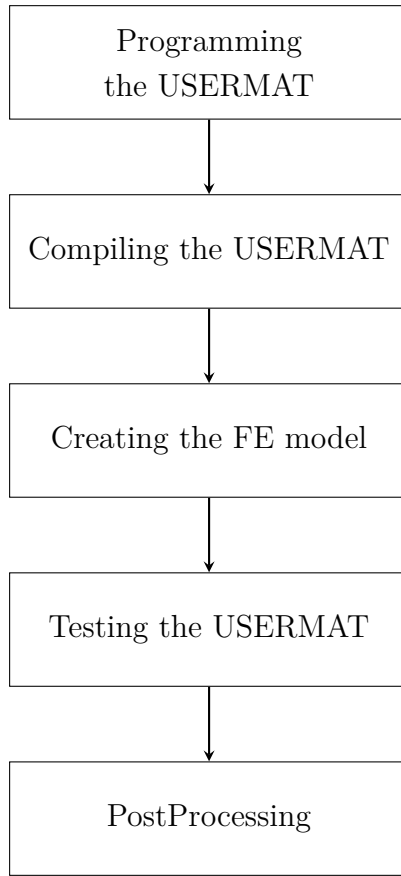


Figure 3.1: Steps involved in developing and testing damage models

3.2 Programming the USERMAT

The user material routine (USERMAT) is an ANSYS programmable feature which allows users to write their own material constitutive equations within a newly developed general material framework (Lin, 1999). The USERMAT is called at all integration points of the finite element during the solution phase. ANSYS demands the necessary variables declared in a certain way so that the USERMAT developed can work compatibly with ANSYS when it is called at each integration point. The guidelines for declaring input and output arguments can be found on ANSYS' user-mat guide. The following image shows the USERMAT interface with the set of possible input arguments that USERMAT can access from ANSYS. For every Newton raphson iteration, the USERMAT is called at every material integration point, and ANSYS passes in strains, stresses and state variables at the beginning of the time increment and the current strain increment. The USERMAT then computes and updates the necessary output arguments like stresses, state variables and the material tangent stiffness matrix $\frac{\partial \sigma}{\partial \epsilon}$ at the end of the increment.

```

subroutine usermat(
& matId, elemId,kDomIntPt, kLayer, kSectPt,
& ldstep,isubst,keycut,
& nDirect,nShear,ncomp,nStatev,nProp,
& Time,dTime,Temp,dTemp,
& stress,statev,dsdePl,sedEl,sedPl,epseq,
& Strain,dStrain, epsPl, prop, coords,
& tsstif, epsZZ,
& var1, var2, var3, var4, var5,
& var6, var7, var8)

INTEGER
& matId, elemId,
& kDomIntPt, kLayer, kSectPt,
& ldstep,isubst,keycut,
& nDirect,nShear,ncomp,nStatev,nProp
DOUBLE PRECISION
& Time, dTime, Temp, dTemp,
& sedEl, sedPl, epseq, epsZZ
DOUBLE PRECISION
& stress (ncomp ), statev (nStatev),
& dsdePl (ncomp,ncomp),
& Strain (ncomp ), dStrain (ncomp ),
& epsPl (ncomp ), prop (nProp ),
& coords (3), rotateM (3,3),
& defGrad_t(3,3), defGrad(3,3),
& tsstif (2)

```

Figure 3.2: USERMAT interface (Lin, 1999)

3.3 Compiling the USERMAT

The USERMAT must be compiled before testing them in ANSYS environment. The compilation process checks for errors in the source code and converts it into ANSYS executable files (.dll files). The compiler present in Intel parallel studio is suitable for this purpose. The step by step process of compiling the USERMAT is given below

- Create an empty directory and copy the USERMAT file to be compiled (.f files) into the empty directory.
- Change the name of the USERMAT file to *usermat*
- Go to "Control Panel>Search System>Edit the system environment variables >Environment variables" and click New in the user variables for the PC, which opens a window
- In that window, type ANS_USER_PATH as variable name and copy and paste the path to your working directory as variable value.
- Go to folder "C:\ Program Files\ ANSYS Inc\ v(version)\ ansys\ custom\ user\ win64" and copy the ANSUSERSHARED.bat file and paste it in the working directory
- Open command prompt and navigate to the working directory
- Type ANSUSERSHARED.bat and press enter. This opens the Intel compiler and asks for USERMAT file name

- Type *usermat* without extension and press Enter.
- If there is no error in the *usermat* file the compiler will show the message "usermatLib.dll has been successfully build."
- For ANSYS to access these .dll files, open ANSYS Mechanical APDL product launcher and in the file management section browse to the current working directory
- By clicking run, one should see the message "Note - This ANSYS version was linked by Licensee" in the Mechanical APDL output window. This indicates that ANSYS is using the shared library with the USERMAT and the developed models can now be tested

3.4 Creating the FE model

The preprocessor section of ANSYS mechanical APDL is used to create and mesh the FE model. The ANSYS user-programmable feature can be used with 18x family elements, which include LINK180, PLANE 182, PLANE 183, SOLID 185, SOLID 186 (Lin, 1999). The type of element required for creating FE models can be chosen from the element type menu in the preprocessor section. Once the element type is chosen, the material model, and the material properties can be entered in the *Material props* section. The *Modelling* section can be utilised to create the geometry and then can be meshed using the *Meshing* option.

To use the same FE model repetitively, to test different material models with different material properties the FE model can be saved in the form of an APDL script. An APDL script is a simple text file containing the commands required to create and solve the FE model. A simple way to create an APDL script for an FE model is to copy the log of commands automatically created in the log file during the construction of the model and pasting it to a new text file. This log file can be accessed by going to *List > Files > Logfile*. The created APDL script can then be accessed via *File > Read input from*.

3.5 Testing the USERMAT

To access the user material option, the TB,USER command must be included in the APDL script. The table command for USER material option is

TB,USER,matId,NTEMPS,NPTS (Lin, 1999)

matId - material reference number

NTEMPS - Number of temperature points

NPTS - Number of material constants at a given temperature

If state variables are used in the USERMAT, the number of state variables need to be defined in the APDL script by the command TB,STATE

TB,STATE,matId,,NPTS (Lin, 1999)

matId - material reference number

NPTS - Number of state variables to be used in USERMAT

A simple example for defining a user material and two state variables is given in the Figure.(3.3) below

```
!*
YOUNG = 210e3
POISSON = 0.33
T1 = 1

TB,USER,1,1,2,
TBTEMP,T1
TBDATA,,YOUNG,POISSON
TB,STATE,1,,2
```

Figure 3.3: Table (TB) commands

Before defining boundary conditions (BCs), the entities required for solving the FE model, such as time at the end of the load step, the number of substeps, the results to be stored etc., must be defined. This can be done using *Sol'n Controls* option in the solution menu. Once the BCs are defined, the model can be solved by giving the command *SOLVE*.

3.6 PostProcessing

Once the simulation completes, the results can be analyzed using the 'General Postprocessor' option. The nodal and element solutions for components like stress, strain, displacement etc., can be plotted using the 'contour plot' option, found on Plot results. By default, this option plots the results at the last substep. To plot the solution at the substep of choice one must navigate to *Read results > By pick* and select the substep to be plotted. Since the postprocessor of ANSYS does not have GUI option for plotting state variables the following command must be given: *plnsol, svar, n* where *n* is the number of the state variable to be plotted. The time history of a certain variable, such as stress, reaction force, strain etc., at a node or an element can be plotted using *TimeHist Postpro* option. On clicking the *TimeHist Postpro* option a *Variable List* window opens up (See Figure. (3.4)).

To add the variables to plot, click the green add symbol on the top-left corner which opens a window with the list of variables that can be added to the *Variable List* window. Once the variables have been added, the variables can be plotted against each other or against time. Figure.(3.4) shows the *Variable List* window with X-component of force and displacement of node 3 selected and plotted against each other.

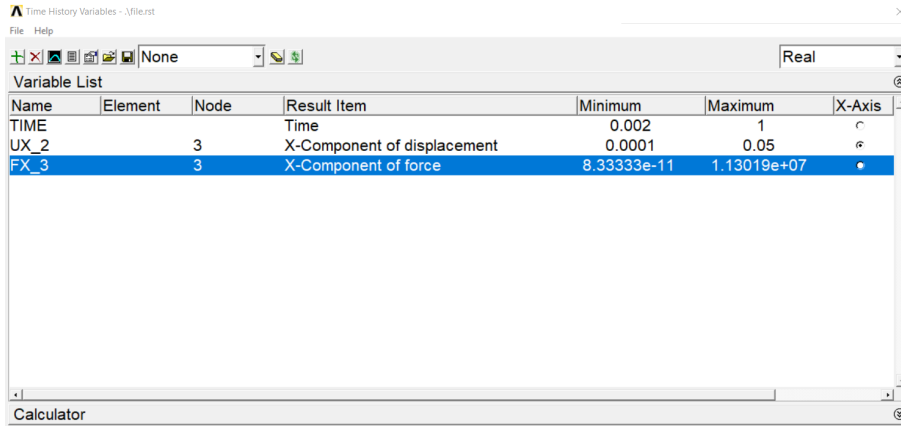


Figure 3.4: Time history post processor window

The time history results of each variable at a node or an element can also be saved as a text file using *List Data* option in the *Variable List* window.

Chapter 4

Progressive failure analysis of orthotropic composite materials

4.1 Fibre-reinforced Composites

Fibre-reinforced composites is a term for a large family of materials ranging from short fibre reinforced polyamides to unidirectional graphite fibre epoxies. They are usually orthotropic in nature i.e., their material properties differ in mutually perpendicular directions. Fibre-reinforced composites consist of three components 1) the fibres as the discontinuous or dispersed phase, 2) the matrix as the continuous phase, and 3) the fine interphase region, also known as the interface (Wikipedia). The failure in fibre reinforced composites happens mainly due to matrix cracking or fibre failure. Therefore the failure can be divided mainly into two types, namely 1) Longitudinal failure and 2) Transverse failure (Maimí et al., 2007). The mechanism of both failure in a unidirectional fibre-reinforced composite material, their causes and their effects on material behaviour are discussed in detail below

4.1.1 Longitudinal failure

In fibre-reinforced plastics, the most significant portion of the load is carried by fibres. When the fibres fail, the load must distribute to other areas of the structure and cause structural collapse. Longitudinal tensile failure occurs as a fracture along a plane whose normal is parallel to the fibre direction. Longitudinal compressive failure occurs from the collapse of the fibres due to shear kinking and damage of the supporting matrix. Fibre misalignment causes shear stress between fibres that rotate fibres, which increases shear stress further and leads to instability (Maimí et al., 2007).

4.1.2 Transverse failure

Transverse failure happens due to matrix cracking and fibre-matrix debonding. Under the presence of in-plane shear stress and transverse tensile stress, the combined effects of defects such as resin-rich regions, fibre-resin debonds etc., trigger a crack that extends through the thickness. The transverse cracks are formed at the fibre-resin interface without affecting the fibres. When a unidirectional fibre composite is loaded in shear, a non-linear stress-strain behaviour is observed before the material fails by through-thickness matrix cracking (Maimí et al., 2007).

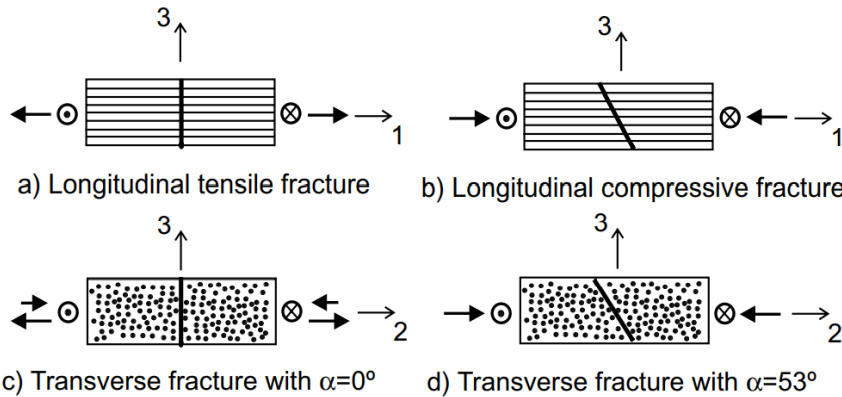


Figure 4.1: Fracture planes in FRP material (Maimí et al., 2007)

4.2 Failure criteria

Failure criteria refer to the onset of damage at a material point. Since the properties of the orthotropic composite materials are different in the mutually perpendicular directions, three failure mode indices, F_l , F_t , F_z , are used for failure modes in three principal material directions. Since the failure due to tension and compression in each direction cannot happen at the same integration point and at the same time, the failure mode index must be calculated based on whether the material direction is under tension or compression (Wang et al., 2009). Some of the damage initiation criteria are given as follows

4.2.1 3D Hashin's quadratic strain criteria

Hashin's quadratic strain criteria (Wang et al., 2009) includes shear strain components in addition to the normal strain components. The criteria for each material direction is given below

i) Longitudinal direction 1 ,

$$F_l^2 = \begin{cases} \left(\frac{\epsilon_{11}}{\epsilon_{11}^{f,t}} \right)^2 + \left(\frac{\epsilon_{12}}{\epsilon_{12}^f} \right)^2 + \left(\frac{\epsilon_{13}}{\epsilon_{13}^f} \right)^2 \geq 1 & (\epsilon_{11} > 0) \\ \left(\frac{\epsilon_{11}}{\epsilon_{11}^{f,c}} \right)^2 \geq 1 & (\epsilon_{11} < 0) \end{cases} \quad (4.1)$$

ii) Transverse direction 2,

$$F_t^2 = \begin{cases} \frac{(\epsilon_{22} + \epsilon_{33})^2}{\epsilon_{22}^{f,t} \epsilon_{33}^{f,t}} - \frac{\epsilon_{22} \epsilon_{33}}{(\epsilon_{23}^f)^2} + \left(\frac{\epsilon_{12}}{\epsilon_{12}^f} \right)^2 + \left(\frac{\epsilon_{13}}{\epsilon_{13}^f} \right)^2 + \left(\frac{\epsilon_{23}}{\epsilon_{23}^f} \right)^2 \geq 1 & (\epsilon_{22} > 0) \\ \frac{(\epsilon_{22} + \epsilon_{33})^2}{\epsilon_{22}^{f,c} \epsilon_{33}^{f,c}} + \frac{\epsilon_{22} + \epsilon_{33}}{\epsilon_{22}^{f,c}} \left(\frac{\epsilon_{22}^{f,c}}{2\epsilon_{12}^f} - 1 \right) - \frac{\epsilon_{22} \epsilon_{33}}{(\epsilon_{23}^f)^2} + \left(\frac{\epsilon_{12}}{\epsilon_{12}^f} \right)^2 \\ + \left(\frac{\epsilon_{13}}{\epsilon_{13}^f} \right)^2 + \left(\frac{\epsilon_{23}}{\epsilon_{23}^f} \right)^2 \geq 1 & (\epsilon_{22} > 0) \end{cases} \quad (4.2)$$

iii) Transverse direction 3,

$$F_z^2 = \begin{cases} \left(\frac{\epsilon_{33}}{\epsilon_{33}^{f,t}} \right)^2 + \left(\frac{\epsilon_{13}}{\epsilon_{13}^f} \right)^2 + \left(\frac{\epsilon_{23}}{\epsilon_{23}^f} \right)^2 \geq 1 & (\epsilon_{33} > 0) \\ \left(\frac{\epsilon_{33}}{\epsilon_{33}^{f,c}} \right)^2 + \left(\frac{\epsilon_{13}}{\epsilon_{13}^f} \right)^2 + \left(\frac{\epsilon_{23}}{\epsilon_{23}^f} \right)^2 \geq 1 & (\epsilon_{33} > 0) \end{cases} \quad (4.3)$$

in which $\epsilon_{ii}^{f,t} = \frac{\sigma_i^{f,t}}{C_{ii}}$, $\epsilon_{ii}^{f,c} = \frac{\sigma_i^{f,c}}{C_{ii}}$ ($i = 1, 2, 3$), $\epsilon_{12}^f = \frac{\sigma_{12}^f}{C_{44}}$, $\epsilon_{13}^f = \frac{\sigma_{13}^f}{C_{55}}$, $\epsilon_{23}^f = \frac{\sigma_{23}^f}{C_{66}}$

4.2.2 Maximum stress criteria

Since the load-carrying area decreases due to increase in damage, the effect of stress gets magnified in the damaged material. Therefore, in the case of maximum stress criteria, normal stress components of the effective stress ($\tilde{\sigma}$) are checked against the failure strength in each principal material direction. The maximum stress criteria (Jiang et al., 2018) for each material direction are given in the table below

Damage direction	Tension	Compression
Longitudinal direction 1 (F_l)	$\frac{\tilde{\sigma}_{11}}{X_t} \leq 1$	$\frac{\tilde{\sigma}_{11}}{-X_c} \leq 1$
Transverse direction 2 (F_t)	$\frac{\tilde{\sigma}_{22}}{Y_t} \leq 1$	$\frac{\tilde{\sigma}_{22}}{-Y_c} \leq 1$
Transverse direction 3 (F_z)	$\frac{\tilde{\sigma}_{33}}{Z_t} \leq 1$	$\frac{\tilde{\sigma}_{33}}{-Z_c} \leq 1$

Table 4.1: Maximum stress criterion

where X_t, Y_t and Z_t are failure strength in tension and X_c, Y_c and Z_c are failure strength in compression in each principal material direction respectively.

4.2.3 Modified Hashin's failure criterion

Modified Hashin's failure criterion (Jiang et al., 2018) for plane stress condition is given below

i) Longitudinal direction 1,

$$F_l = \begin{cases} \left[\left(\frac{\tilde{\sigma}_{11}}{X_t} \right)^2 + \alpha \left(\frac{\tilde{\sigma}_{12}}{S} \right)^2 \right]^{\frac{1}{2}} \geq 1 & (\tilde{\sigma}_{11} > 0) \\ \left[\left(\frac{\tilde{\sigma}_{11}}{X_c} \right)^2 + \alpha \left(\frac{\tilde{\sigma}_{12}}{S} \right)^2 \right]^{\frac{1}{2}} \geq 1 & (\tilde{\sigma}_{11} < 0) \end{cases} \quad (4.4)$$

i) Transverse direction 2,

$$F_t = \begin{cases} \left[\left(\frac{\tilde{\sigma}_{22}}{Y_t} \right)^2 + \alpha \left(\frac{\tilde{\sigma}_{12}}{S} \right)^2 \right]^{\frac{1}{2}} \geq 1 & (\tilde{\sigma}_{22} > 0) \\ \left[\left(\frac{\tilde{\sigma}_{22}}{Y_c} \right)^2 + \alpha \left(\frac{\tilde{\sigma}_{12}}{S} \right)^2 \right]^{\frac{1}{2}} \geq 1 & (\tilde{\sigma}_{22} < 0) \end{cases} \quad (4.5)$$

where the shear contribution factor α ranges from 0 to 1.

4.3 Types of damage evolution

Once the damage has initiated in a material point of the composite material, the stiffness must be degraded. This results in strain-softening of the composite materials rather than strain hardening, which is observed in metals. Several post-damage models have been proposed for progressive failure analysis, and most of them belong to one of the following categories (Sleight, 1999): instantaneous unloading, gradual loading, or constant stress at failure material point, as shown in Figure (4.2).

Since continuum damage mechanics is a methodology to predict the progressive failure behaviour of composites (Wang et al., 2009), non-linear gradual unloading of the composite material is adopted and simulated in this work. Therefore non-linear material properties degradation model is implemented. Based on the type of damage variable chosen, i.e., scalar, vector or second-order tensor, the damage modelling can be classified into isotropic or anisotropic damage modelling (Murakami, 2012). A brief description of the types of damage modelling, damage evolution equation used and material tangent stiffness is given below

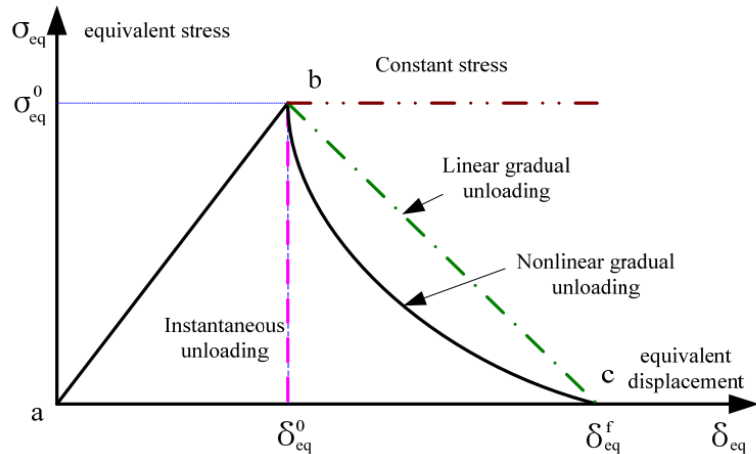


Figure 4.2: Types of degradation behaviour in damaged composite materials (Wang et al., 2009)

4.3.1 Isotropic damage

In the case of isotropic distribution of cracks, the damage state is usually considered isotropic (Lemaitre, 2012), and only a scalar variable D is required to represent the damage state of the material. A simple exponential law for calculating damage evolution is given in the Eq. (4.6) (Peerlings, 1999)

$$D = 1 - e^{-P(\tilde{\epsilon} - k)} \quad (4.6)$$

where P is the softening parameter which determines the slope of the damage evolution, $\tilde{\epsilon}$ is the 1D equivalent strain and k is the threshold value. Since the Eq. (4.6) is of exponential type, the damage D evolves exponentially from 0 to 1, and the strain-softening will be an exponential decay function. Once the damage starts to evolve, the stiffness of the material must be degraded (Murakami, 2012). Therefore the elastic stiffness matrix of the damaged material is given by,

$$\mathbb{C}(D) = (1 - D)\mathbb{C}_0 \quad (4.7)$$

where \mathbb{C}_0 is the material stiffness matrix of the undamaged material. Therefore the stress-strain relation for a strain softening model is given by,

$$\underline{\sigma} = \mathbb{C}(D) : \underline{\epsilon} \quad (4.8)$$

The finite element equations obtained for the strain-softening model are non-linear. Therefore Newton-Raphson technique is used to solve the resulting system of non-linear equations. To ensure the robustness of the Newton-Raphson method, it is important to compute the material tangent constitutive tensor \mathbb{C}_T (Lapczyk and Hurtado, 2007). It can be derived as follows,

$$\begin{aligned} \mathbb{C}_T &= \frac{\partial \underline{\sigma}}{\partial \underline{\epsilon}} \\ \underline{\sigma} &= f(\underline{\epsilon}, D) \\ \mathbb{C}_T &= \mathbb{C}(D) + \underline{\epsilon} : \left(\frac{\partial \underline{\sigma}}{\partial D} \otimes \frac{\partial D}{\partial \underline{\epsilon}} \right) \end{aligned} \quad (4.9)$$

In the above equation, the first term $\mathbb{C}(D)$ is the damaged elasticity matrix and second term is due increased damage. In the absence of damage propagation in an increment (e.g., during unloading), the material tangent is equal to the damaged elasticity matrix, so the response is linearly elastic.

4.3.2 Anisotropic damage

In the case of orthotropic materials, the material property differs in the mutually perpendicular directions. Therefore it is more appropriate to choose a second-order damage tensor (Murakami, 2012). In this work, an orthotropic second-order damage tensor \underline{D} is chosen, whose principal directions are assumed to coincide with

the principal material directions. The eigenvalues of the damage tensor \underline{D} have a simple physical interpretation, i.e., the i^{th} eigenvalue d_i represents the effective fractional reduction in load carrying area on planes that are perpendicular to i^{th} principal material direction (Wang et al., 2009). The damage tensor \underline{D} can be represented as,

$$\underline{D} = \begin{bmatrix} d_1 & 0 & 0 \\ 0 & d_2 & 0 \\ 0 & 0 & d_3 \end{bmatrix}$$

A simple exponential damage evolution law (Wang et al., 2009) for each principal material direction in case of anisotropic damage is given as follows,

$$d_i = 1 - \frac{e^{-P(F_I-1)}}{F_I} \quad (4.10)$$

where d_i ($i = 1,2,3$) and F_I ($I = l,t,z$) are damage evolution and failure index in each principal material direction respectively. The material tangent stiffness tensor for anisotropic damage (Lapczyk and Hurtado, 2007) can also be derived in the same way as isotropic damage and it is given as follows

$$\begin{aligned} \mathbb{C}_T &= \frac{\partial \sigma}{\partial \underline{\epsilon}} \\ \sigma &= f(\underline{\epsilon}, \underline{D}) \\ \mathbb{C}_T &= \mathbb{C}(\underline{D}) + \underline{\epsilon} : \sum_{i=1}^3 \left(\frac{\partial \sigma}{\partial d_i} \otimes \frac{\partial d_i}{\partial \underline{\epsilon}} \right) \end{aligned} \quad (4.11)$$

In the above equation, the first term $\mathbb{C}(D)$ is the degraded stiffness matrix and the second term (i.e., due to increased damage) must be computed only if the corresponding failure mode is active. Since the damage evolution equation d_i depends on the failure index, the term $\frac{\partial d_i}{\partial \underline{\epsilon}}$ must be computed based on whether the corresponding damage happened during tension or compression. The matrix representation of degraded stiffness for plane-stress(2D) and 3D, and the explicit results of the derivatives for the second term are presented in the Appendix () and ()

4.4 Localisation and Mesh Regularisation

Finite element simulations which use continuum damage mechanics based models are prone to mesh dependency. Because of the strain-softening behaviour of the material, the strain tends to localize, resulting in a strong mesh dependency, i.e., the solution is non-objective with respect to mesh refinement, and the energy

dissipated decreases with the decrease in finite element size (Lapczyk and Hurtado, 2007). Merely improving the numerical solution schemes cannot alleviate the problem associated with mesh dependency and localization. Even if the convergence to the actual solution is improved, the solution may not even make sense from a physical point of view (Peerlings, 1999). Therefore the so-called fracture energy regularization is used to reduce the mesh sensitivity. In this technique, the softening law (damage evolution law) is modified so that the amount of energy dissipated over a fully degraded finite element depends on the fracture energy of the material and the finite element size (Cervera and Chiumenti, 2006). Therefore the fracture energy G_f of the material and characteristic length L_c of the finite element must be included in the damage evolution equations. The damage evolution equations based on fracture energy regularization technique for each principal direction is given below (Wang et al., 2009),

In longitudinal direction 1,

$$d_1 = 1 - \frac{e^{P_1(F_l-1)}}{F_l} \quad (4.12)$$

In transverse direction 2,

$$d_2 = 1 - \frac{e^{P_2(F_t-1)}}{F_t} \quad (4.13)$$

In transverse direction 3,

$$d_3 = 1 - \frac{e^{P_3(F_z-1)}}{F_z} \quad (4.14)$$

where $P_1 = \frac{-\sigma_{11}^f \epsilon_{11}^f L_c}{G_{f,1}}$, $P_2 = \frac{-\sigma_{22}^f \epsilon_{22}^f L_c}{G_{f,2}}$ and $P_3 = \frac{-\sigma_{33}^f \epsilon_{33}^f L_c}{G_{f,3}}$

$G_{f,i}$ - is the fracture energy in each principal direction ($i = 1,2,3$)

σ_{ii}^f - failure strength in each principal direction ($i = 1,2,3$)

ϵ_{ii}^f - failure strain in each principal direction ($i = 1,2,3$)

L_c - Characteristic length

4.5 Numerical implementation of the damage model in ANSYS

As discussed before, the material models necessary for simulating progressive damage failure are implemented using the ANSYS user-programmable feature

called USERMAT. The damage model implemented using USERMAT computes and updates the current stress and consistent tangent stiffness. The following sections deal with the numerical implementation of the damage model based on two different methods or types of failure criteria used to predict the damage initiation.

- Strain based damage model
- Stress based damage model

4.5.1 Strain based damage model

In the case of the strain-based damage model, the damage initiation is predicted using current strain $\underline{\epsilon}_{n+1}$ (Wang et al., 2009). The USERMAT receives strains, stresses and state variables at the beginning of the time increment and the current strain increment. The following steps describe the process of implementing the damage model

- Calculate current strain

$$\underline{\epsilon}_{n+1} = \underline{\epsilon}_n + \Delta \underline{\epsilon}$$

- Calculate the current degraded material stiffness matrix $\mathbb{C}(\underline{D}_n)$
- Calculate the failure indices $F_I(\underline{\epsilon})$ (Refer to Section (4.2.1))

Check if $F_I \geq F_{I\max}$

- if $F_I(\underline{\epsilon}) < 1$

$$\underline{\sigma}_{n+1} = \mathbb{C}(\underline{D}_n) : \underline{\epsilon}_{n+1}$$

$$\mathbb{C}_T = \mathbb{C}(\underline{D}_n)$$

- else

Calculate the damage variables using damage evolution law, (Refer to Eq. (4.12) to (4.14))

$$d_1(F_l), d_2(F_t), d_3(F_z)$$

Check if $d_i \geq 0$

Calculate the updated degraded stiffness based on damage variables

$$\mathbb{C}(\underline{D}_{n+1})$$

Calculate current stress

$$\underline{\sigma}_{n+1} = \mathbb{C}(\underline{D}_{n+1}) : \underline{\epsilon}_{n+1}$$

Calculate tangent stiffness

$$\mathbb{C}_T = \mathbb{C}(\underline{D}_{n+1}) + \sum_{i=1}^3 \left(\frac{\partial \mathbb{C}(\underline{D}_{n+1})}{\partial d_i} : \underline{\epsilon}_{n+1} \otimes \frac{\partial d_i}{\partial \underline{\epsilon}_{n+1}} \right)$$

4.5.2 Stress based damage model

In the case of stress-based damage model, the damage initiation is predicted using effective stress ($\tilde{\sigma}_{n+1}$) (Jiang et al., 2018). The USERMAT receives strains, stresses and state variables at the beginning of the time increment and the current strain increment. The following steps describe the process of implementing the damage model.

- Calculate the elastic stiffness matrix $\mathbb{C}(\underline{D}_n)$
- Calculate effective stress

$$\tilde{\sigma}_{n+1} = \mathbb{C}_0 : \underline{\epsilon}_{n+1}$$

- Calculate the failure indices $F_I(\underline{\sigma})$, (Refer to Section (4.2.2) and (4.2.3))

Check if $F_I \geq F_{I\max}$

- if $F_I(\underline{\sigma}) < 1$

$$\underline{\sigma}_{n+1} = \tilde{\sigma}_{n+1}$$

$$\mathbb{C}_T = \mathbb{C}(\underline{D}_n)$$

- else

Calculate the damage variables using damage evolution law, (Refer to Eq. (4.12) to (4.14))

$$d_1(F_l), d_2(F_t), d_3(F_z)$$

Check if $d_i \geq 0$

Calculate the updated degraded stiffness based on damage variables

$$\mathbb{C}(\underline{D}_{n+1})$$

Calculate current stress

$$\underline{\sigma}_{n+1} = \mathbb{M}(\underline{D}_{n+1})^{-1} : \tilde{\sigma}_{n+1}$$

Calculate tangent stiffness

$$\mathbb{C}_T = \mathbb{C}(\underline{D}_{n+1}) + \sum_{i=1}^3 \left(\frac{\partial \underline{\sigma}_{n+1}}{\partial d_i} : \underline{\epsilon}_{n+1} \otimes \frac{\partial d_i}{\partial \underline{\epsilon}_{n+1}} \right)$$

4.6 Schematic of USERMAT implementation

The flowchart below (4.6) shows the schematic of the user material routine (USERMAT) implementation for both and strain and stress based damage model and how the USERMAT interacts with the ANSYS environment.

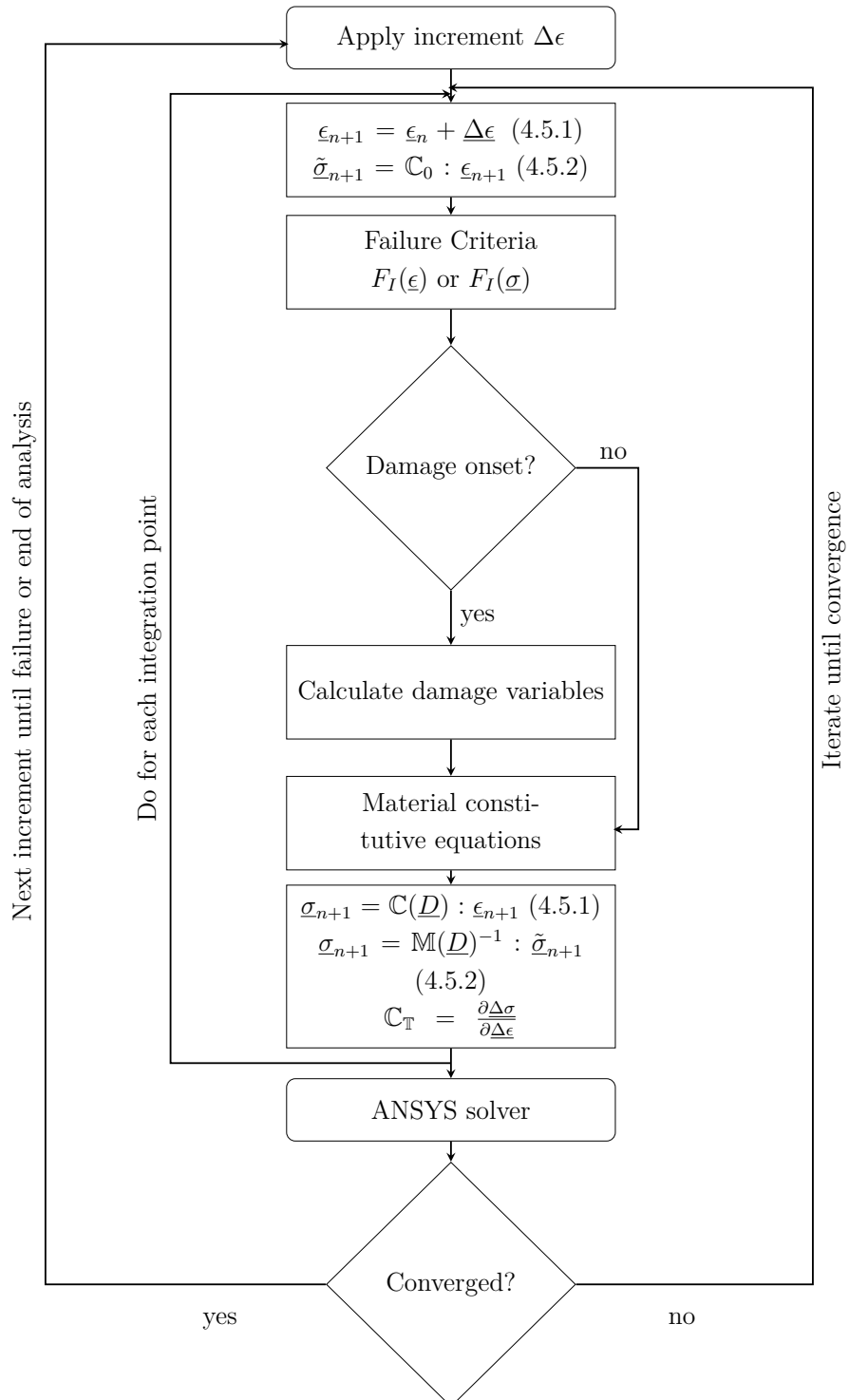


Figure 4.3: Schematic of USERMAT implementation

Chapter 5

Results and Discussion

5.1 Modelling linear elastic behaviour of orthotropic materials

Before implementing the damage behaviour in orthotropic materials, their linear elastic behaviour must be implemented which describes the phenomena before the damage initiation. As mentioned before orthotropic materials require 9 independent material constants to model their elastic behaviour. Table (5.1) summarises the utilised material parameters. The material parameters presented in table (5.1) belongs to an unidirectional glass fiber-reinforced epoxy material obtained from (Lapczyk and Hurtado, 2007). In this material, the strength in the longitudinal direction (X_t and X_c) is very high compared to the transverse directions (Y_t and Y_c) because the fibers are aligned parallel to the longitudinal direction.

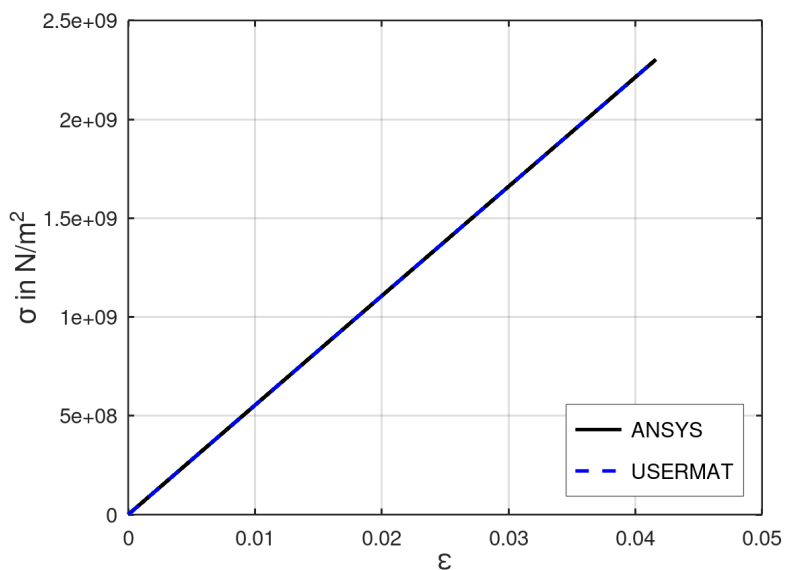


Figure 5.1: Stress-Strain relation (Standard vs user-defined material routine)

Symbol	Material Parameter	Value
E_1	Elastic modulus in longitudinal (1) direction	55000e6 N/m ²
$E_2 = E_3$	Elastic modulus in transverse (2 and 3) directions	9500e6 N/m ²
$\nu_{12} = \nu_{13}$	Poisson's ratio (in-plane)	0.33
ν_{23}	Poisson's ratio (Planes 2-3)	0.27
$G_{12} = G_{13}$	In-plane shear modulus	5500e6 N/m ²
G_{23}	Shear modulus (Planes 2-3)	3000e6 N/m ²
X_t	Tensile strength in longitudinal (1) direction	2500e6 N/m ²
X_c	Compressive strength in longitudinal (1) direction	2000e6 N/m ²
Y_t	Tensile strength in transverse (2 and 3) directions	50e6 N/m ²
Y_c	Compressive strength in transverse (2 and 3) directions	200e6 N/m ²
S_{12}	In-plane shear strength	50e6 N/m ²

Table 5.1: Material parameters (Integration point studies)

The constitutive matrix given in the section (2.9) and Hooke's law help us model the elastic behaviour of the orthotropic materials. The linear elastic behaviour of the orthotropic material is implemented as USERMAT in ANSYS, and in this section, the USERMAT is compared against the standard orthotropic material routine present in ANSYS using a structural example. A bar of length 10 mm and area 1 mm² ($b = 1$ mm, $t = 1$ mm) fixed at one end is chosen for the analysis. The bar is constructed using 8 node SOLID 185 elements, and full integration has been used (see Figure (5.2)). A displacement of 1 mm is applied at the free end, and the Figure (5.1) compares the stress-strain relation between standard material routine and the implemented USERMAT

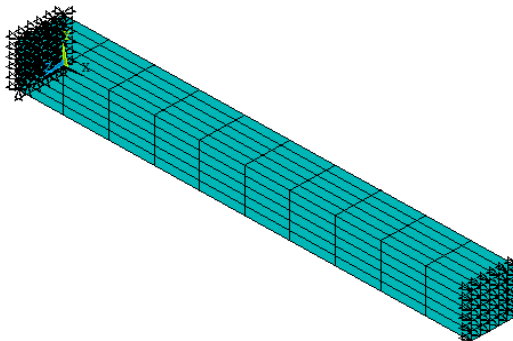


Figure 5.2: Bar used for analysis: Mesh and BCs

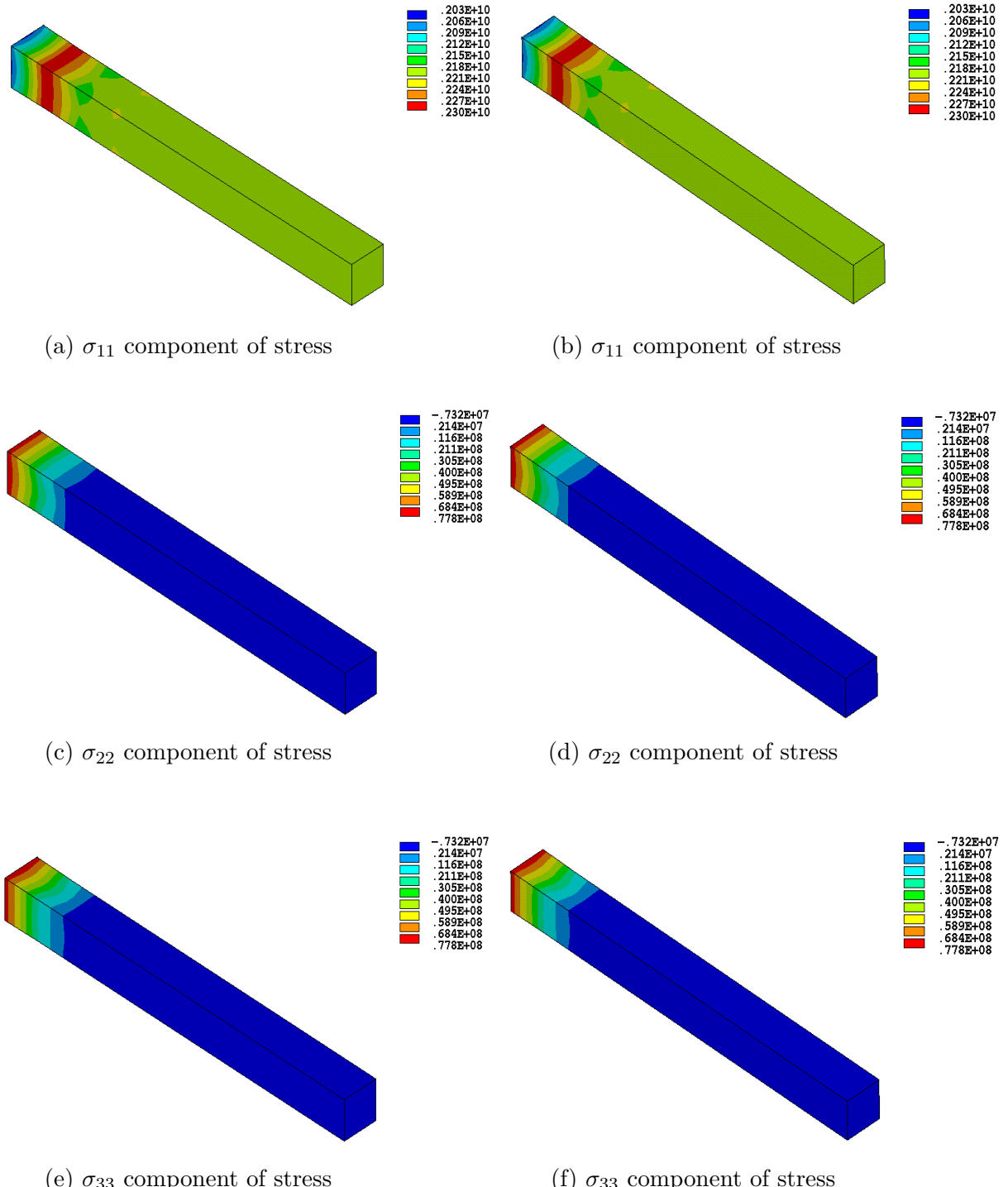


Figure 5.3: Contour plots of the stress components σ_{11} , σ_{22} and σ_{33} of the bar obtained using standard material routine (Figures a, c, e on the left) and (Figures b, d, f on the right)

Figure (5.3) shows the contour plots of the normal stresses (σ_{11} , σ_{22} and σ_{33}) computed using standard material routine and USERMAT respectively. The comparison of the stress-strain relation and contour plots between the both the routines confirm that the results obtained are similar and therefore further damage-initiation and evolution processes can now be implemented.

5.2 Damage behaviour at integration point level

The damage models are first developed on the octave and tested using constitutive driver routines (B.Kiefer), enabling us to understand the phenomenon at the integration point level and the possibility to test the material tangent. To demonstrate the evolution of damage after damage initiation and the strain-softening, following simple loading cases are investigated at the integration point level.

- Uniaxial tension
- Biaxial tension
- Triaxial tension.

After that, the damage models are implemented as USERMAT and tested in the ANSYS environment using a 3D finite element of unit length. The finite element is subjected to the above loading cases, and the results are compared against the Octave implementation

5.2.1 Uniaxial tension

In the case of uniaxial tension, the normal stress is present only in one direction, and all the shear stresses are zero. In the ANSYS environment, uniaxial tension is achieved by applying a displacement on the finite element in a normal direction (e.g: longitudinal), which increases the strain ϵ_{11} linearly over time, and the lateral (transverse) contraction is not constrained. 3D Hashin's quadratic strain criteria (Section(4.2.1)) are used to predict the damage initiation, and the exponential evolution law Eq. (4.10) is used to calculate the damage evolution.

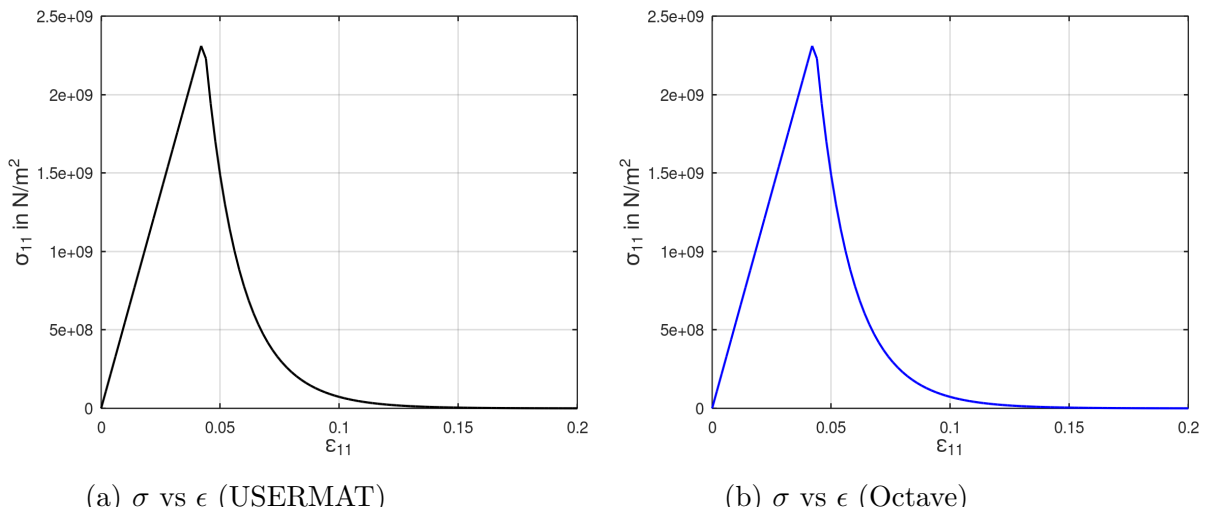


Figure 5.4: Evolution of stress for uniaxial tension test in 11 direction

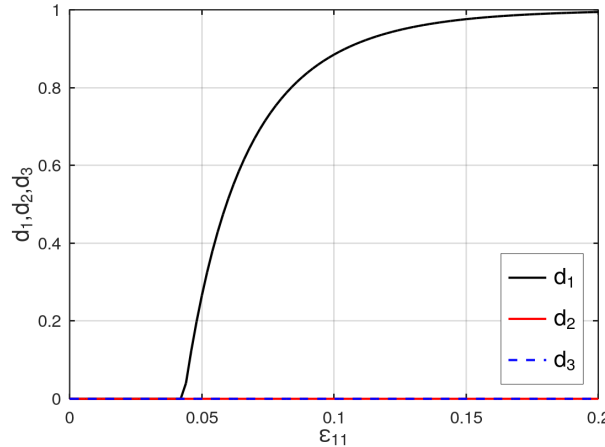


Figure 5.5: Evolution of damage components for uniaxial tension test in 11 direction

The stress-strain behaviour obtained from USERMAT and Octave are presented in Figures (5.4a) and (5.4b) respectively. Figure (5.5) shows the evolution of damage variables. The system is linearly elastic until the failure strain, and the damage is zero. Once the strain ϵ_{11} exceeds the failure strain, the damage d_1 starts to evolve exponentially, and the stress starts to drop due to the reduction in stiffness in 1 direction. The damage variables d_2 and d_3 are zero. The comparison between the Figures (5.4a) and (5.4b) suggests that the damage model implemented in octave and as USERMAT in ANSYS are numerically similar.

Drawbacks of strain based failure criteria

Since the lateral contraction is not constrained during uniaxial tension, the transverse directions experience negative strain due to Poisson's effect, i.e., ϵ_{22} and ϵ_{33} will be negative. If the compressive strength in the transverse directions 2 and 3 are sufficiently low, the strains ϵ_{22} and ϵ_{33} will exceed the failure strain. This leads to damage evolution without the presence of stress in transverse directions. This phenomenon causes convergence issues and the computation stops when the damage evolves without the presence of stress. Figure (5.6) shows the norm of the residual stress, which does not reach zero (or a below a tolerance value) after 100 iterations of the Newton-Raphson-algorithm, which indicates the failure of the model to converge to a solution when using low compressive strength in the transverse direction ($Y_c = -180$ MPa).

This problem can be rectified by using stress-based failure criteria. Since damage evolution depends on failure index F , the transverse failure indices F_t and F_z will be zero during uniaxial tension if the stress-based failure criteria are used. This results in zero damage in the transverse direction. The next section presents the results obtained using stress-based damage model and the use of mesh regularization in the damage evolution law.

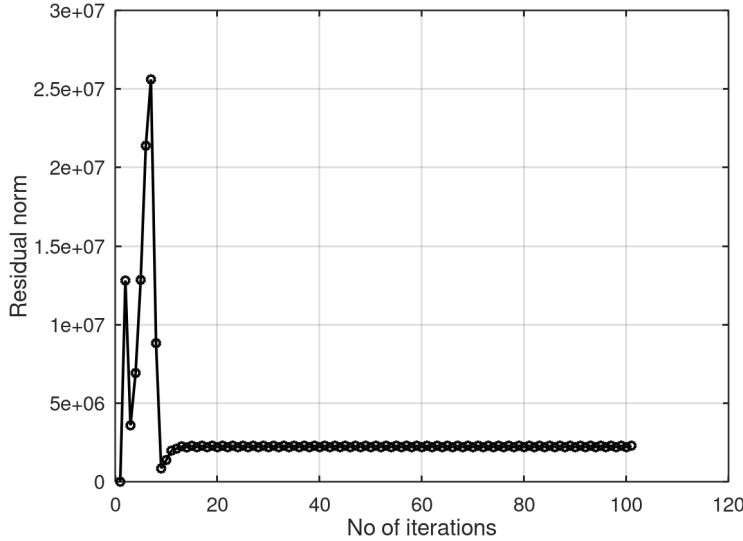


Figure 5.6: Convergence issue: Residual norm of the stress *vs* no of Newton-Raphson iterations

Stress-based damage models and mesh regularization

As mentioned in section (4.4), the strain localisation problems result in strong mesh dependency, so fracture energy G_f and characteristic length L_c of the element have been included in the damage evolution law in order to alleviate the problem. So the damage model is modified by changing the failure criteria to maximum stress criteria (4.1) and including the damage evolution equations from (4.12) to (4.14). The uniaxial tension is conducted again with the changes mentioned above and with very low transverse compression strength ($Y_c = -180$ MPa), and the results are presented below.

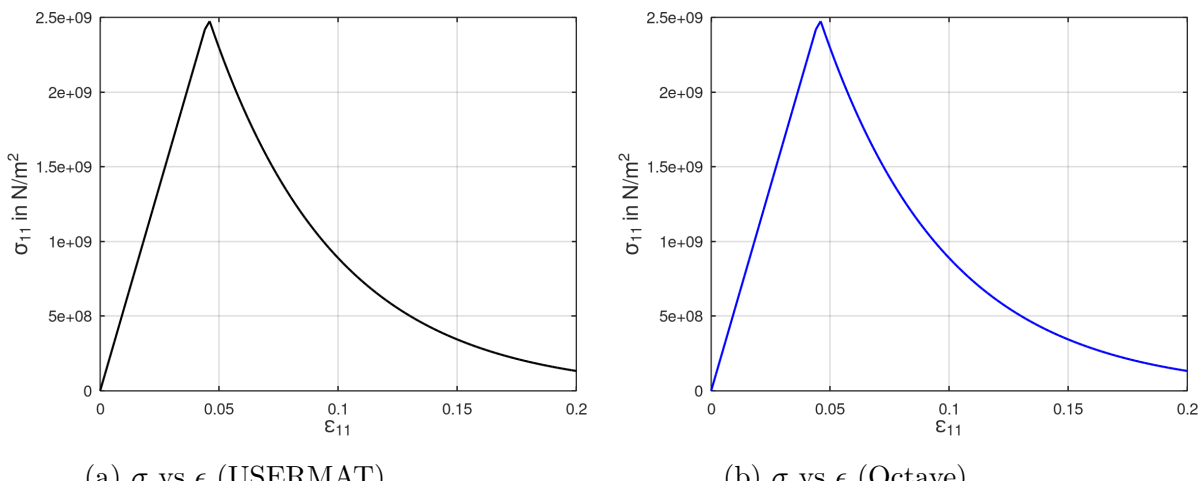


Figure 5.7: Evolution of stress components (Stress-based damage model)

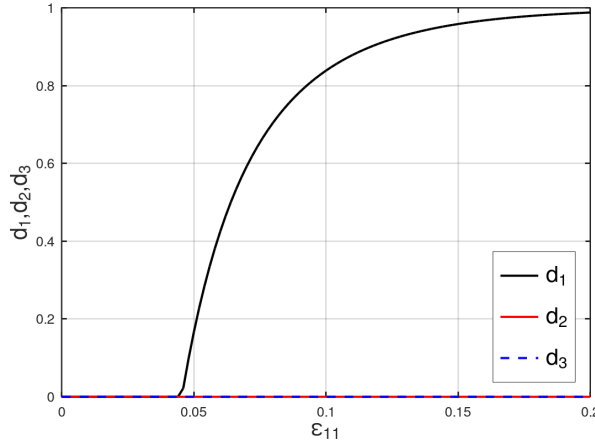


Figure 5.7: Evolution of damage components (Stress-based damage model)

From Figure (5.7) it is evident that the damage d_2 and d_3 are zero as a result of stress-based damage failure criteria because the stress components σ_{22} and σ_{33} are zero under uniaxial tension. While using mesh regularization, the slope of the damage curve is determined by the characteristic length L_c . The following Figure (5.8) shows how the damage evolution is affected by the characteristic length L_c ,

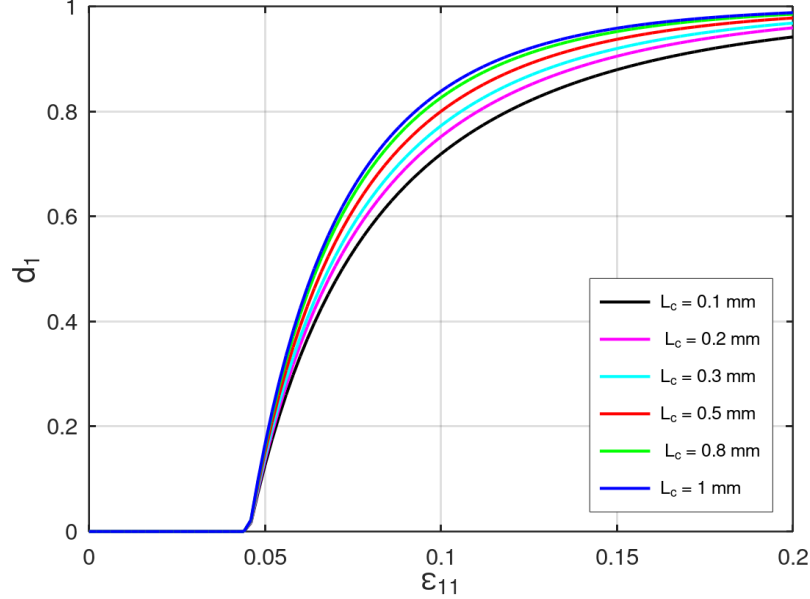


Figure 5.8: Influence of characteristic length L_c on the damage evolution

Discussion of tangent stiffness

In the case of uniaxial tension, the components of the stress tensor other than σ_{11} are zero. Since stress conditions are enforced, the Octave driver routine

(B.Kiefer) uses the Newton-Raphson method to determine the input strain components other than ϵ_{11} iteratively. The Newton-Raphson method requires a tangent stiffness for computation which can be derived using the Eq. (4.11) for anisotropic damage. This enables us to test the derived algorithmic tangent stiffness (ATS) before implementing them as USERMAT in ANSYS. The derived algorithmic tangent stiffness is verified by comparing it with the numerical tangent stiffness computed using numerical perturbation. In numerical perturbation, the coefficients of the strain tensor are perturbed by a very small value, i.e., $\Delta\epsilon_{kl}^{n+1} = \delta_m$ (where $\delta_m \ll 1$) and the resulting stress perturbations are calculated (B.Kiefer).

$$\Delta\sigma_{ij}^{n+1} = \sigma_{ij}^{n+1}(\epsilon_{kl}^{n+1} + \delta_m) - \sigma_{ij}^{n+1}(\epsilon_{kl}^{n+1}) \quad (5.1)$$

Then the components of the tangent stiffness tensor can be estimated as

$$C_T = \frac{\Delta\sigma_{ij}^{n+1}}{\Delta\epsilon_{kl}^{n+1}} \quad (5.2)$$

Since the material routine must be evaluated for every perturbation of ϵ_{kl} the routine has to be called six time recursively per load-step iteration. The Figures (5.9a) and (5.9b) shows the strain components ϵ_{22} and ϵ_{33} computed using algorithmic and numerical tangent stiffness which are plotted against ϵ_{11} respectively.

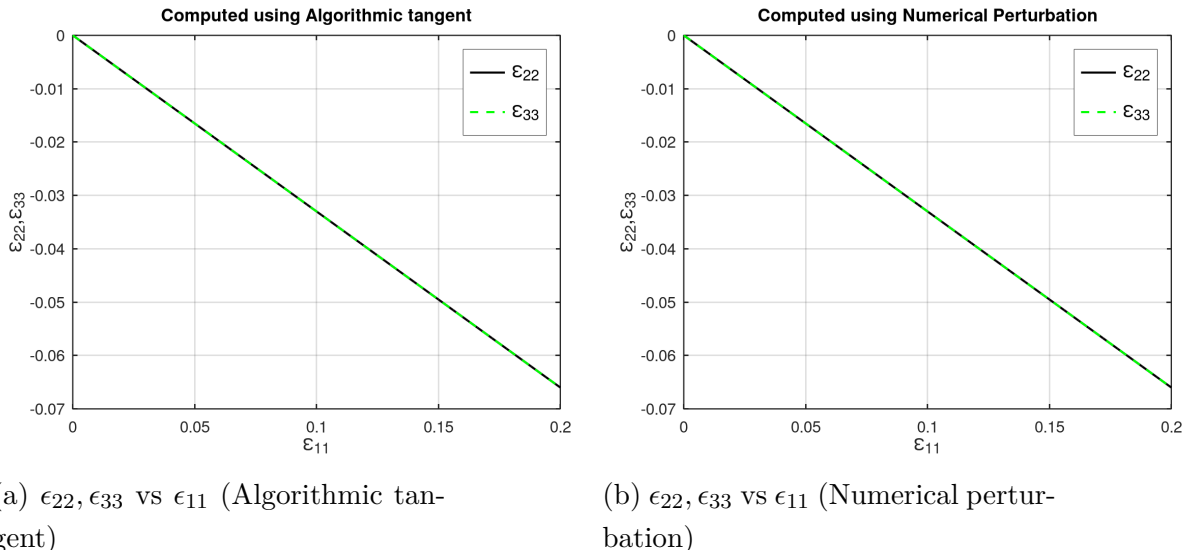


Figure 5.9: The strain components ϵ_{22} and ϵ_{33} computed using algorithmic (a) and numerical tangent stiffness (b) under uniaxial tension

The algorithmic tangent took less time than the numerical tangent to complete the simulation and provided the same results. This indicates that the derived algorithmic tangent is well suited for the computation.

5.2.2 Biaxial tension

In the case of biaxial tension, normal stresses are present only in two normal directions, and all the shear stresses are zero, i.e., only two non-zero components presented located on the main diagonal of the stress tensor. In ANSYS, biaxial tension is achieved by applying the same displacements in two normal directions of the finite element (1 and 2 direction), and the contraction in the third direction (3) is unconstrained. The following figures show the corresponding stress and damage components obtained from the test.

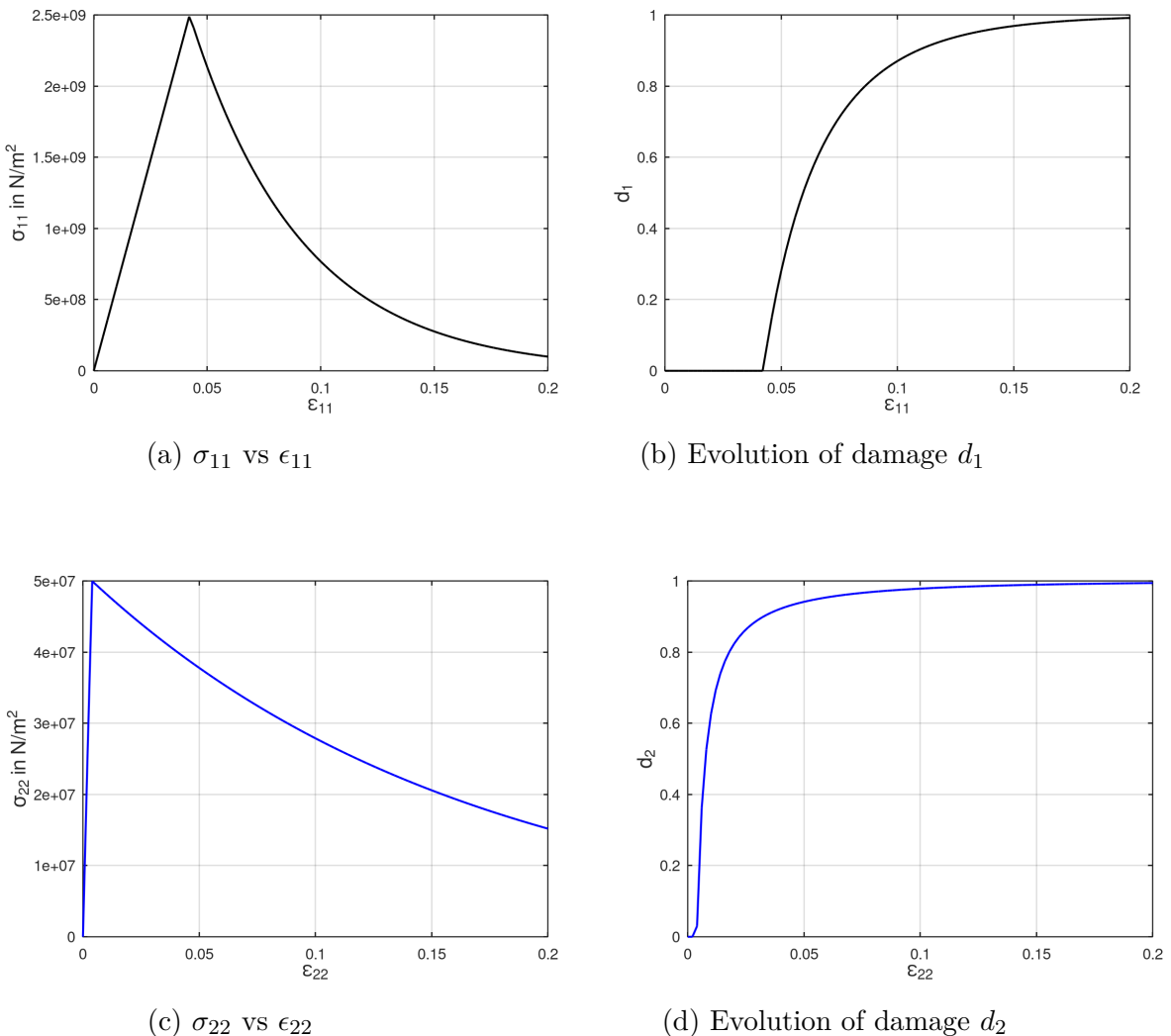
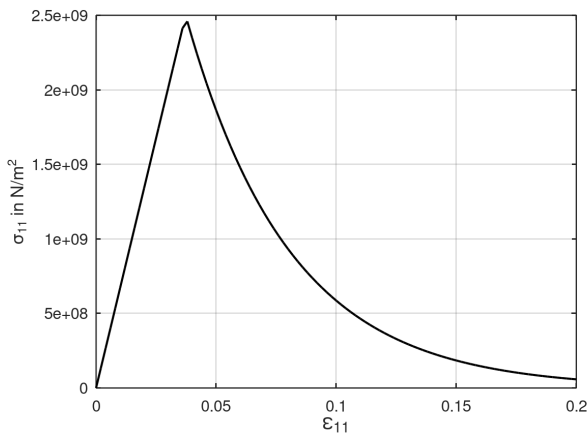
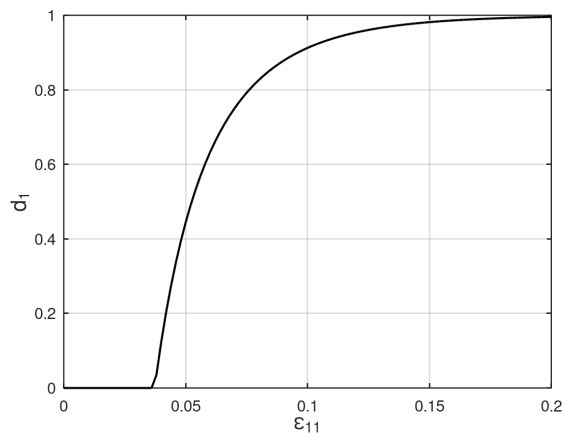
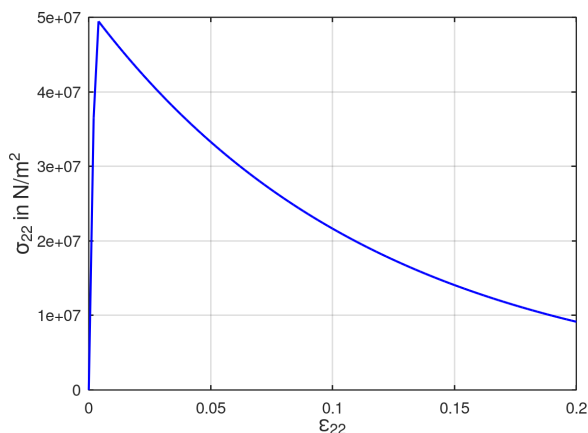
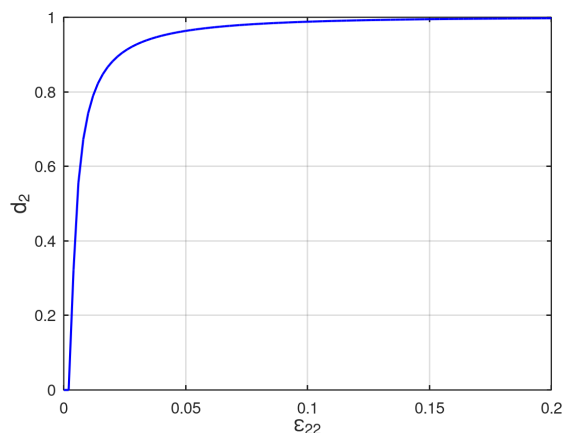


Figure 5.10: Evolution of stress (Figures a, c on the left) and corresponding damage (Figure b, d on the right) components under biaxial tension

Since the tensile strength in transverse direction is very low compared to the longitudinal direction, evolution of damage (d_2) begins very soon and simultaneously the stress component (σ_{22}) drops as seen in Figures (5.10c) and (5.10d). The damage d_1 and d_2 at the end of the loading are 0.9916 and 0.9941 and the residual stress σ_{11} and σ_{22} at the end of the loading are 9.94×10^7 and 1.51×10^7 respectively.

5.2.3 Triaxial tension

In the case of triaxial tension, the normal stresses are present in all three normal directions, and all the shear stresses are zero, i.e., only diagonal components of the stress tensor are non-zero. In Ansys, triaxial tension is achieved by applying the same displacement in all three normal directions (1, 2 and 3 direction). The following Figure (5.11) shows the corresponding stress and damage components obtained from the test.

(a) σ_{11} vs ϵ_{11} (b) Evolution of damage d_1 (c) σ_{22} vs ϵ_{22} (d) Evolution of damage d_2

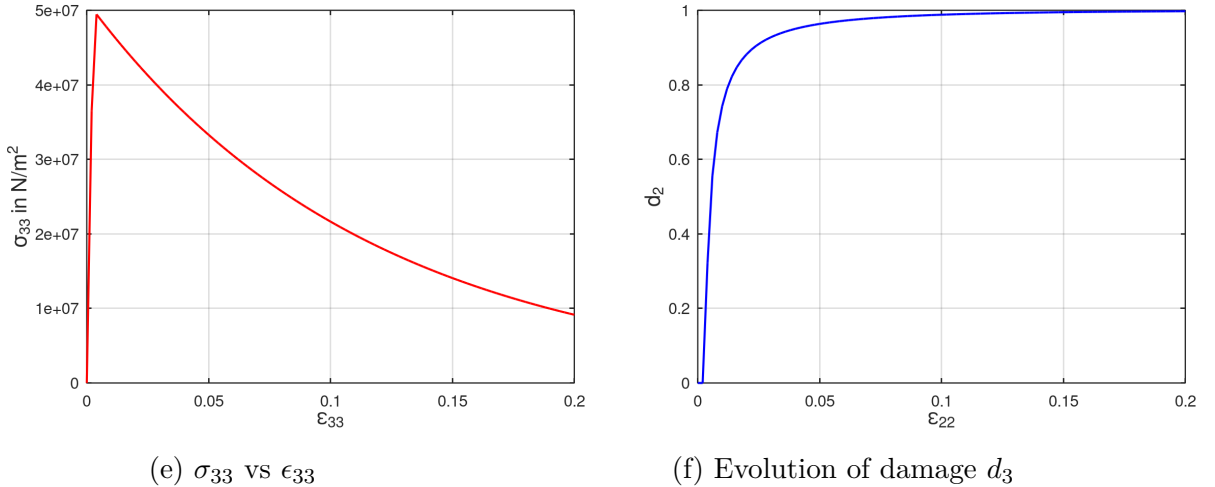


Figure 5.11: Evolution of stress (Figures a, c, e on the left) and corresponding (Figures b ,d, f on the right) damage components under triaxial tension

Since the material properties are the same in transverse 2 and 3 direction and the tensile strength is very low compared to the longitudinal 1 direction, the damage d_2 and d_3 evolves simultaneously (Figures (5.11d) and (5.11f)) and very soon as expected. Therefore the stress components σ_{22} and σ_{33} drop very soon as shown in Figures (5.11c) and (5.11e)

5.3 Representative structural examples

The following structural examples are used to test the damage model implemented as a USERMAT in the ANSYS environment

- Notched tensile specimen (2D - Plane stress)
- Compact tension (CT) specimen (2D - Plane stress)
- Plate with hole (3D)

Each example is chosen to demonstrate specific features of the damage model. These features include, at first, the capability of the model to represent damage initiation and propagation and secondly, the calculation of multiple damage variables, i.e., the ability to show anisotropic damage development in the composite material when a load is applied, both in 2D and 3D setting. Furthermore, mesh convergence studies are performed to show that the regularization scheme employed gives better results than the model with no regularization. For all the finite element simulations of the above models, linear quadrilateral elements are used (both 2D and 3D) with full Gauss integration. The material used for the finite element simulations is T700/2510 carbon fiber/epoxy fabric. The material has a high modulus and strength in the longitudinal direction compared to the transverse direction. The material properties

are obtained from (Jiang et al., 2018) and a summary of the material properties are given in the Table (5.2).

Symbol	Material Parameter	Value
E_{11}	Modulus in longitudinal (1) direction	55.8 GPa
$E_{22} = E_{33}$	Modulus in transverse (2 and 3) directions	54.9 GPa
ν_{12}	Poisson's ratio	0.043
$G_{12} = G_{23} = G_{13}$	Shear modulus	4.2 GPa
X_t	Tensile strength in longitudinal (1) direction	910.1 MPa
X_c	Compressive strength in longitudinal (1) direction	-710.2 MPa
Y_t	Tensile strength in (2 and 3) directions	772.2 MPa
Y_c	Compressive strength in (2 and 3) directions	-703.3 MPa
S_{12}	In-plane strength	131 MPa
G_f^{lt}	Tensile fracture energy along longitudinal (1) direction	125 KJ/m ²
G_f^{lc}	Compressive fracture energy along longitudinal (1) direction	250 KJ/m ²
G_f^{tt}	Tensile fracture energy along (2 and 3) directions	95 KJ/m ²
G_f^{tc}	Compressive fracture energy along (2 and 3) directions	254 KJ/m ²

Table 5.2: Material parameters (Representative structural examples)

5.3.1 Notched tensile specimen

The first example demonstrates the model's capability to represent damage initiation and propagation. A notched tensile specimen is widely used for analysis of stress concentration, fatigue etc. Because of the symmetry, only one-quarter of the specimen is modelled in the finite element analysis and the geometry and boundary conditions (BCs) are shown in the Figure (5.12). The meshes consist of plane-stress elements (PLANE 182) with bilinear interpolations for displacements, and 2×2 Gauss integration has been utilized. Three different finite element meshes have been used in the fracture zone with the elements of $h = 1$ mm, 0.5 mm, 0.25 mm and a total of 500, 840, 1460 elements respectively for the convergence studies (see Figure (5.13)). At first, the longitudinal direction is kept parallel to the loading direction, and the behaviour of the model is analyzed by applying a displacement controlled load (U_x) in the longitudinal direction (X-direction). The maximum stress

criterion (section 4.2.2) has been used to predict the damage initiation.

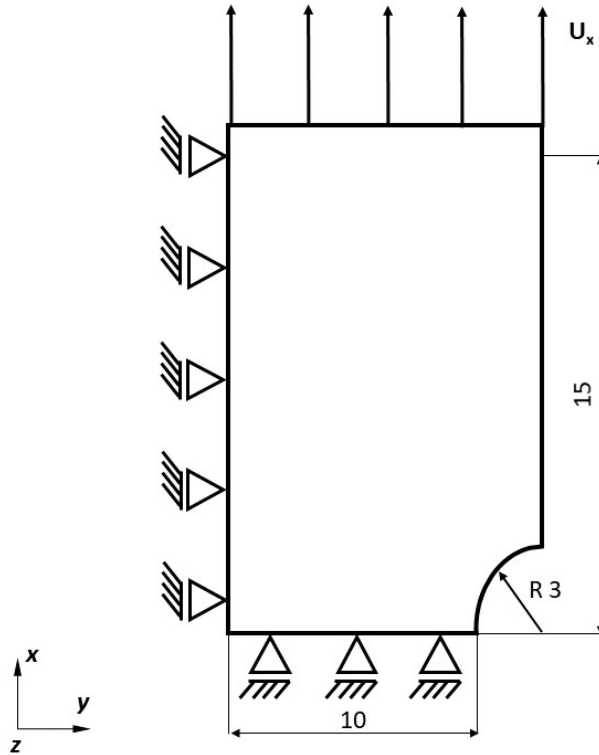


Figure 5.12: Specimen geometry and boundary conditions. Dimensions are given in mm. Displacement controlled loading U_x is applied.

The global force-displacement response for the three different meshes with and without the regularization schemes (see section(4.4)) have been plotted in Figures (5.14a) and (5.14b) respectively. The force-displacement response is characterized by a large linear regime followed by a gradual drop of the load (because of the softening) or a sudden drop in the case of no regularization. From Figure (5.14), it is evident that the model with regularization gives a more stable force-displacement response compared to the model without regularization, where the maximum load capacity is very low, and the load drops significantly with the decrease in mesh size (i.e., increase in the number of elements) compared to the regularized model. The regularization scheme employed cannot fully alleviate the mesh dependency problem but it improves the solution significantly compared to the material model without regularization. For numerical reasons the maximum damage is limited to a threshold value of $d_{max} = 0.999$. The improvement in the global response by using regularization schemes has been illustrated by the damage distributions at the end of the loading process. The damage distributions at the end of the process have been plotted for the three different meshes in the Figure (5.15).

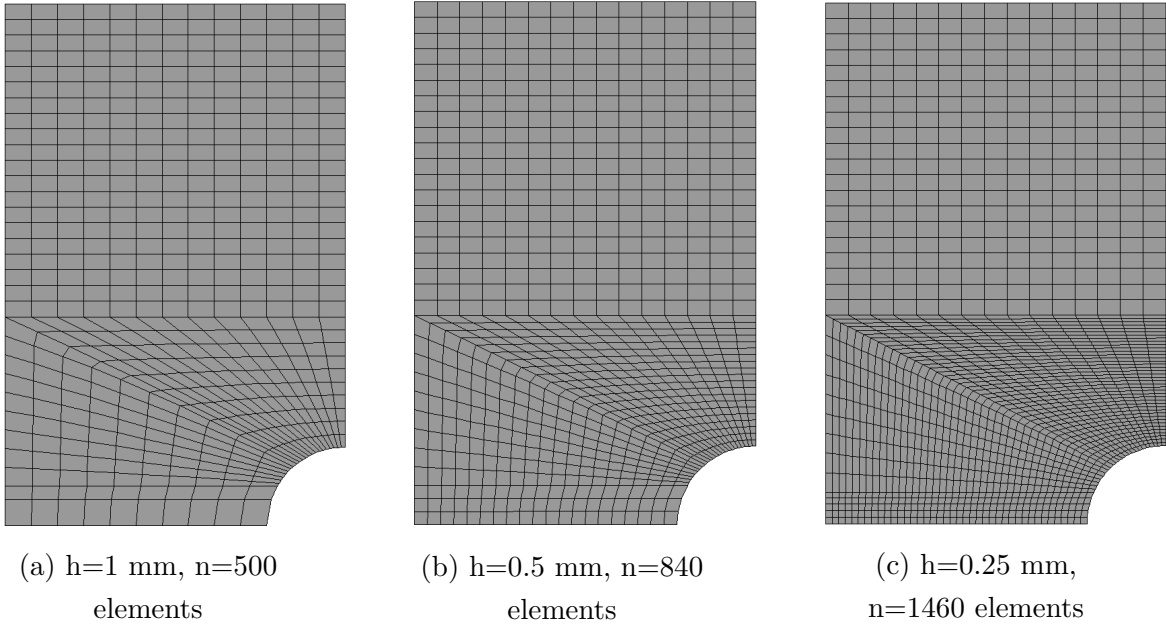


Figure 5.13: Considered meshes (h is the length of the element along fracture zone and n the total number of elements)

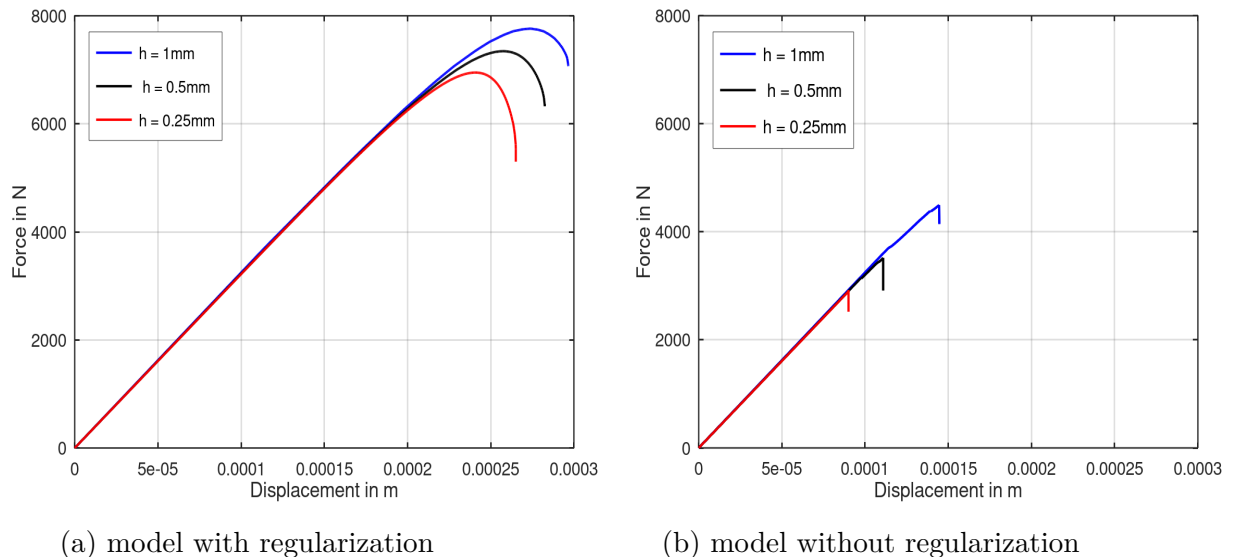


Figure 5.14: Convergence study: Global force-displacement response for model with regularization (Figure a on the left) and without regularization (Figure b the right)

A relatively large portion of the fracture zone takes part in the damage process instead of very few elements (one or two elements) in the case of no regularization. In the case of regularized models, damage initiates at the tip of the blunt notch and propagates perpendicular to the loading direction. The width of the damage zone is approximately the same in the three discretizations, but the number of elements that reach a critical damage value (red) increases with the increase in the number of elements along the fracture zone.

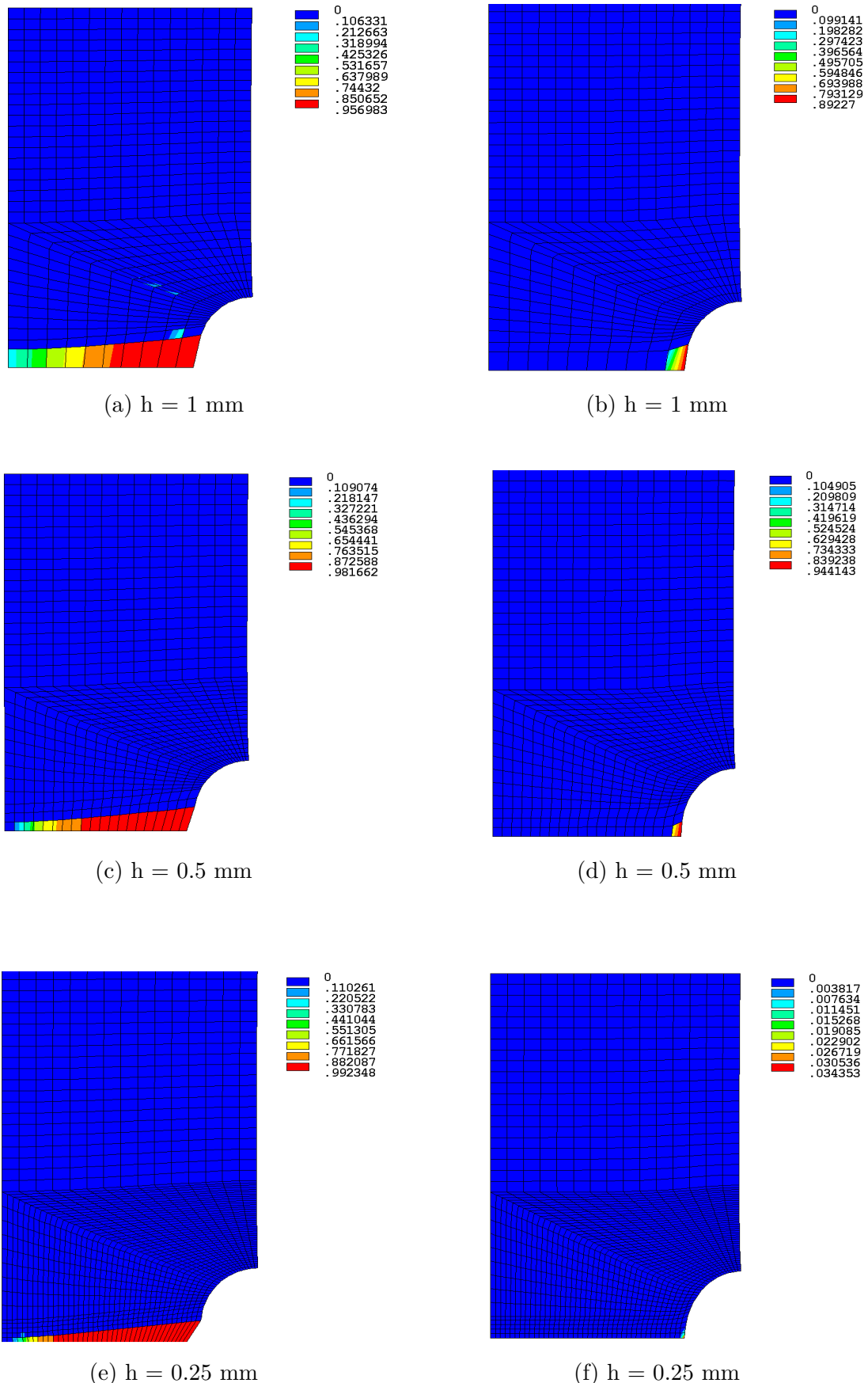


Figure 5.15: Convergence study for model with (Figures a, c, e) and without(b, d, f) regularization: Damage contour plots d_1 at the end of the loading

Now the transverse direction is kept parallel to the loading direction, and the behaviour of the damage model, i.e., initiation and propagation of damage d_2 , is analysed by applying a tensile load in the transverse direction. The damage d_2 at the end of the loading process is shown in the Figure (5.17)

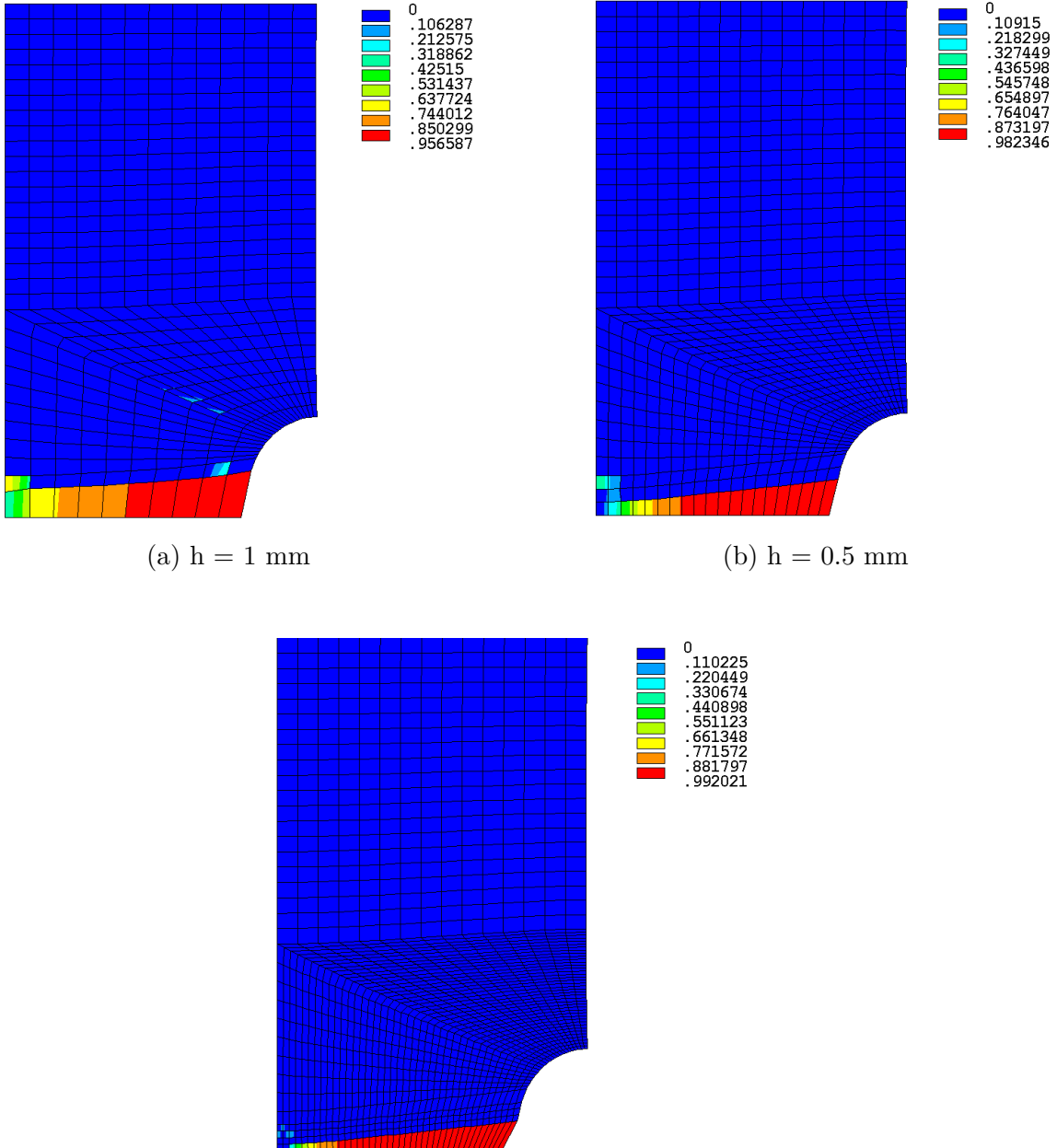


Figure 5.16: $h = 0.25 \text{ mm}$

Figure 5.17: Damage contour plots d_2 at the end of the loading (Loading in transverse direction)

The damage pattern looks similar to the distribution of damage d_1 at the end of loading. The force-displacement response of both longitudinal and transverse

loading for a single mesh type ($h = 0.5\text{mm}$) is compared in the Figure (5.18). As expected, the maximum load capacity is high in the longitudinal direction because of the high tensile strength compared to transverse direction.

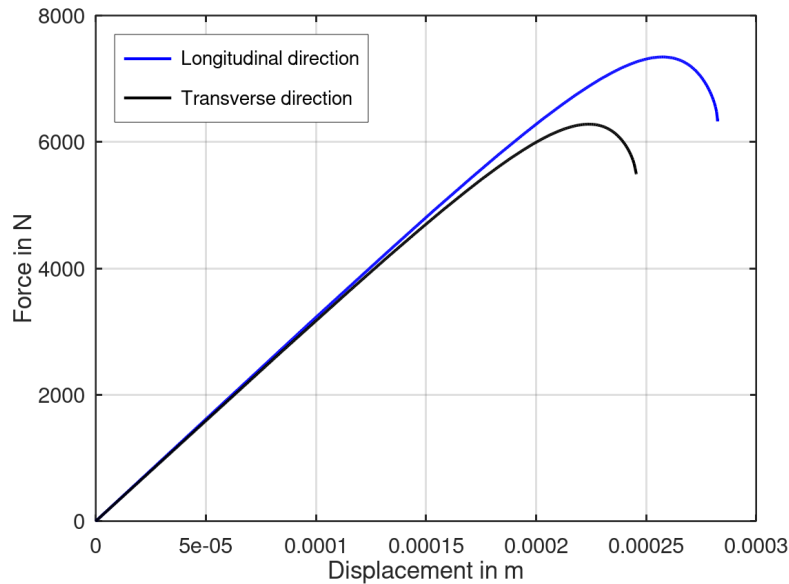


Figure 5.18: Comparison of force-displacement response in longitudinal and transverse direction for $h = 0.5\text{mm}$ discretization

5.3.2 Compact Tension (CT) Specimen

The compact tension test is a standard test for plane fracture of materials and the measurement of fatigue crack growths. In the plane stress (2D) setting, two damage variables (d_1 and d_2), one in each principal direction, are employed to represent the anisotropic damage development. Because of the symmetry, only one half of the specimen is modelled, and the geometry and appropriate boundary conditions (Peerlings, 1999) are given in Figure (5.19). The mesh consists of plane stress (PLANE 182) elements with bilinear interpolations for displacements, and 2×2 Gauss integration has been utilized. Just like the notched tensile specimen, three different finite element meshes have been used in the fracture zone with the elements of size $h = 1$ mm, 0.5 mm and 0.25 mm and a total of 509, 1409, 4811 elements, respectively for the convergence studies (Figure 5.20). A node is created at the centre of the pinhole, and the innermost nodes of the pinhole contour are connected to this node by rigid coupling option in ANSYS. A displacement controlled load (U_x) is applied at the central node, and the global force-displacement response can be obtained from this central node. At first, the longitudinal direction is kept parallel to the loading direction, and the behaviour of the model is analyzed.

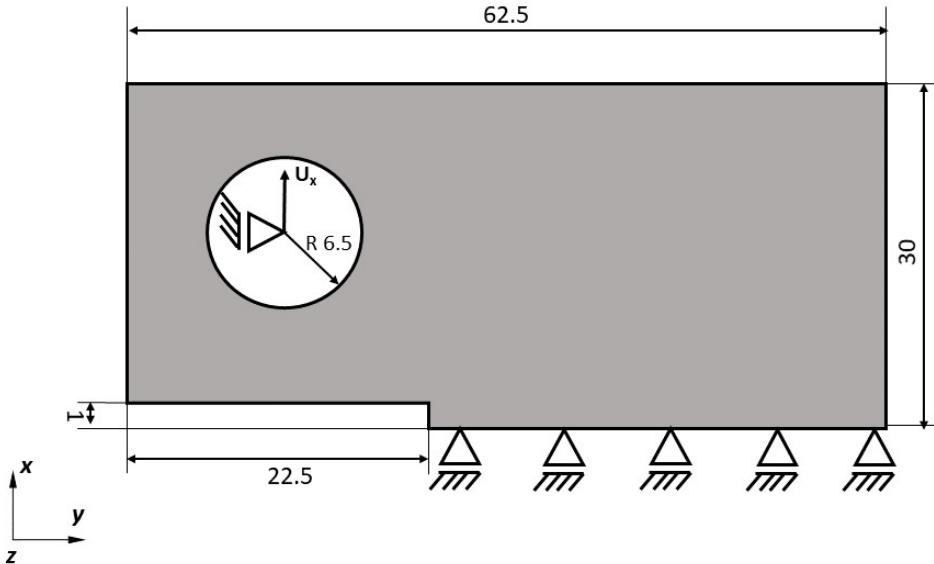


Figure 5.19: Specimen geometry and boundary conditions. Dimensions are given in mm. Displacement controlled loading U_x is applied

The distributions of the damage variables d_1 and d_2 at the end of the loading process for the three different meshes have been plotted in Figure (5.21). The damage d_1 is caused by tension in the longitudinal direction and d_2 by tension in the transverse direction. The width of the damage zone for d_1 is approximately the same in all three discretizations. When the damage d_1 reaches the maximum

threshold value in almost all the distorted elements, the simulations terminates; therefore, the maximum value and distribution of the damage variable d_2 depends on the size of the elements. From Figures (5.21b), (5.21d) and (5.21f) it is clearly evident that the maximum value and the width of the damage zone for d_2 increases with decrease in mesh size.

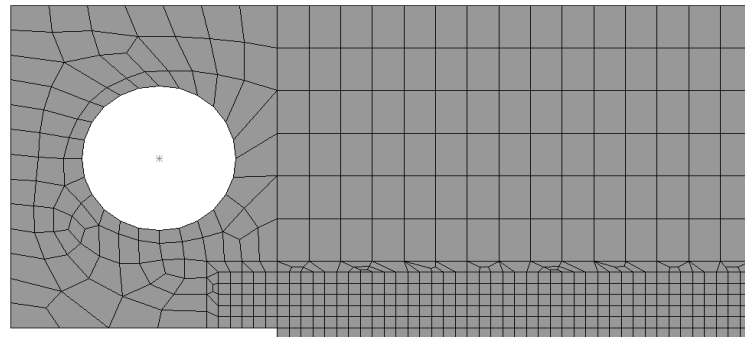
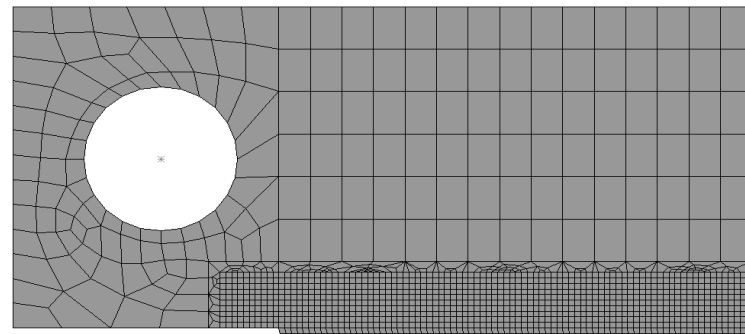
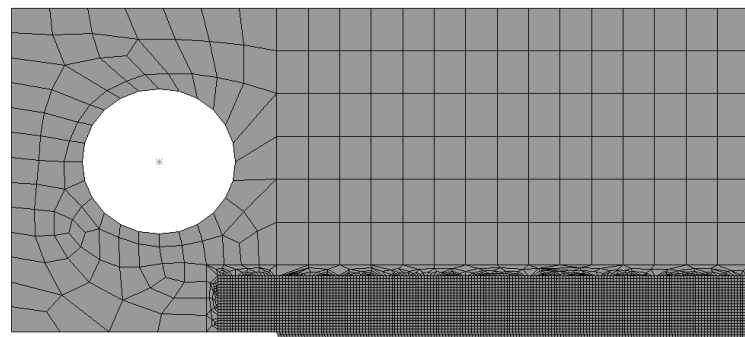
(a) $h = 1 \text{ mm}$ (b) $h = 0.5 \text{ mm}$ (c) $h = 0.25 \text{ mm}$

Figure 5.20: Considered meshes (h is the length of the element along fracture zone and n the total number of elements)

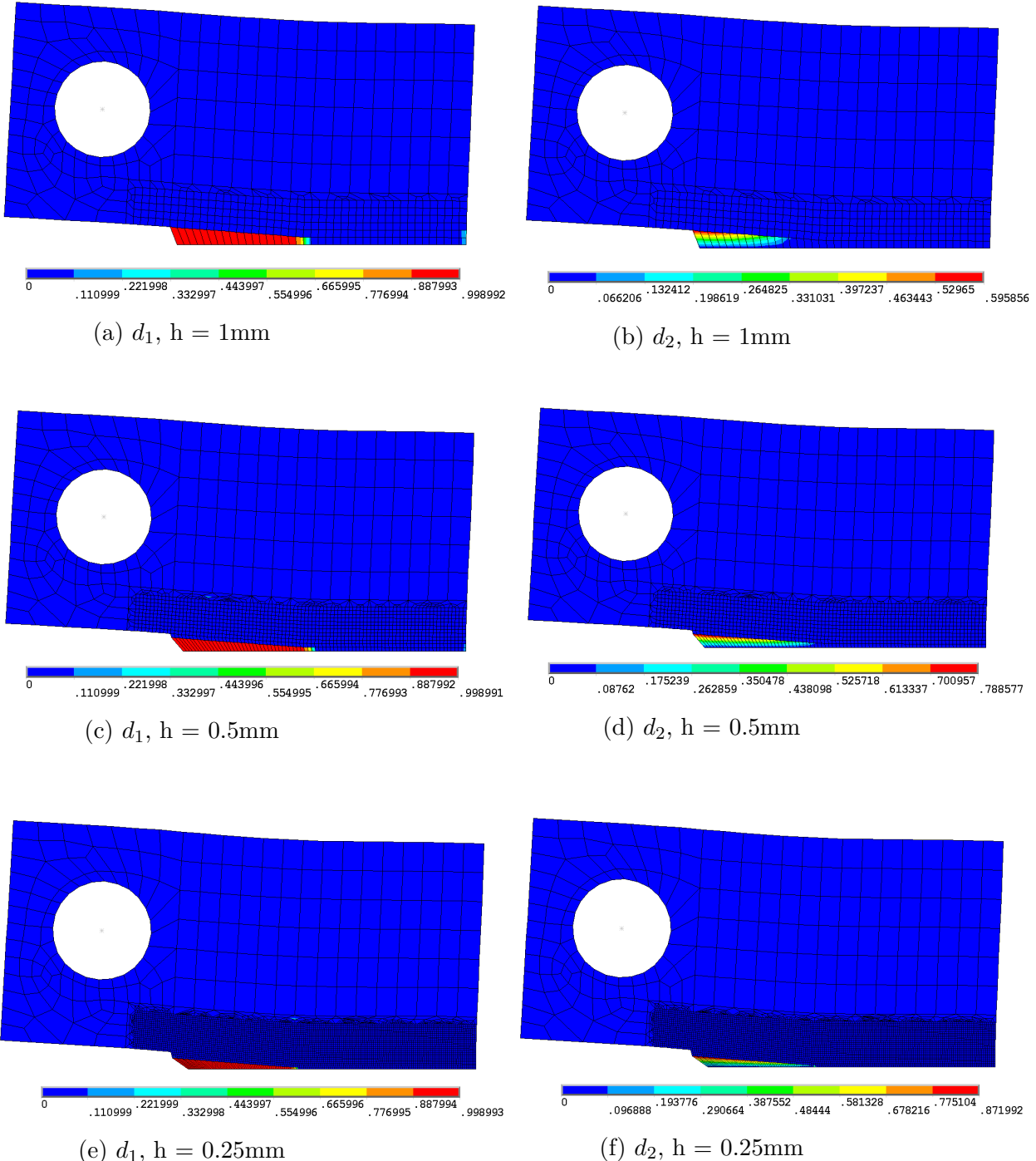


Figure 5.21: Damage distributions at the end of loading in longitudinal direction:
Damage contour plots d_1 and d_2

Now the transverse direction is kept parallel to the loading direction, and the anisotropic development of damage d_1 and d_2 is analysed. In this case, damage d_2 is the primary damage variable and damage d_1 is dependent on the mesh size. The damage distributions (d_1 and d_2) for loading in transverse direction and force-displacement comparison of longitudinal and transverse loading for $h = 1\text{mm}$ discretization are shown in Figure (5.22) and (5.23) respectively.

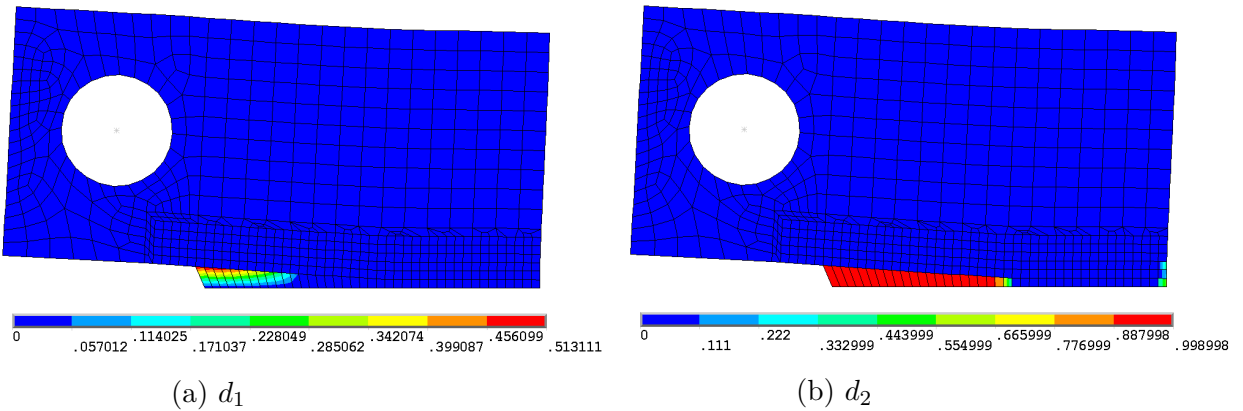


Figure 5.22: Damage distributions at the end of loading in transverse direction:
 Damage contour plots d_1 and d_2 ($h = 1\text{mm}$ discretization)

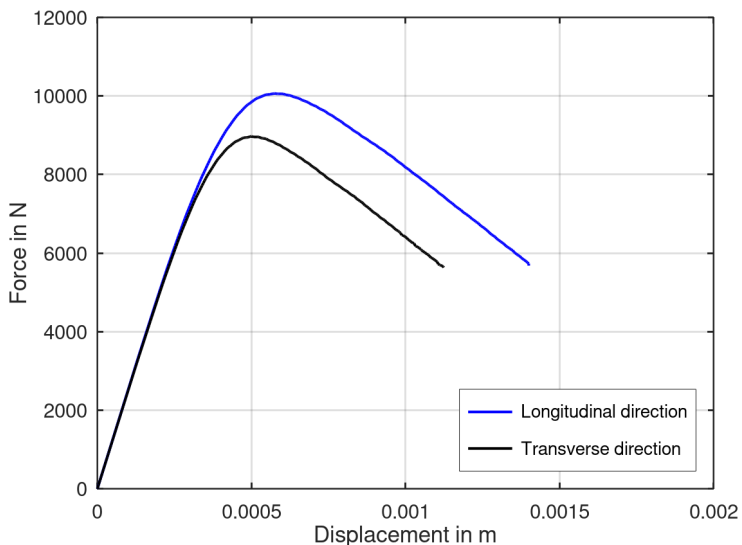


Figure 5.23: Comparison of force-displacement response in longitudinal and transverse direction for $h = 1$ mm discretization

Effect of shear in damage development

the effect of shear on damage initiation and propagation is studied by introducing the modified Hashin's failure criterion (section (4.2.3)) where α is the shear contribution factor which ranges from 0 to 1. The effect of shear can be studied by varying this shear contribution factor α . The maximum value of α is chosen to be 0.5 to avoid the damage development only due to shear because the shear strength is low compared to other strengths. The global force-displacement response obtained for different α by loading the CT-Specimen in the longitudinal direction is shown in Figure (5.24). It is evident that by increasing α , the failure index increases, which reduces the maximum load capacity of the CT specimen.

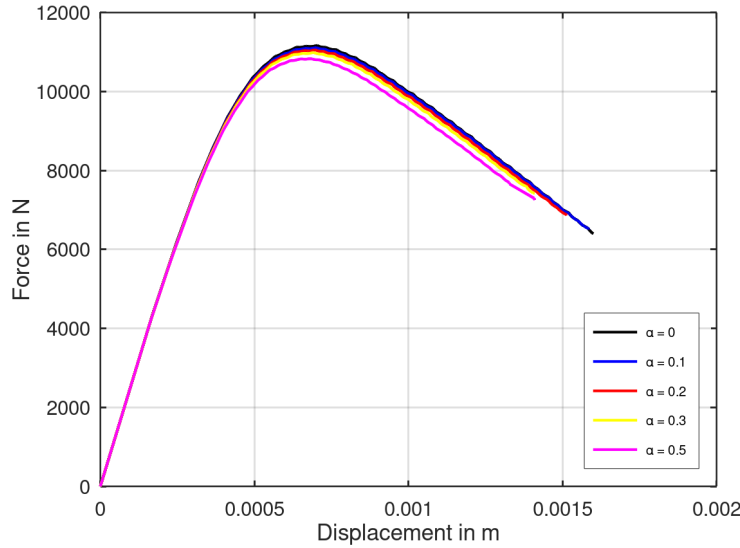


Figure 5.24: Comparison of force-displacement response for different shear coefficient (α) ($h = 1\text{mm}$ discretization)

From Figure (5.25), it is clear that the increase in shear contribution has little to no effect in the initiation and distribution of the damage d_1 because the shear stress component (σ_{12}) is very low compared to the stress component (σ_{11}) which is responsible for damage d_1 . However, the shear stress (σ_{12}) affects the damage d_2 because its magnitude is significant compared to the stress component (σ_{22}) which was the only component responsible for damage d_2 in the case of the maximum stress criterion.

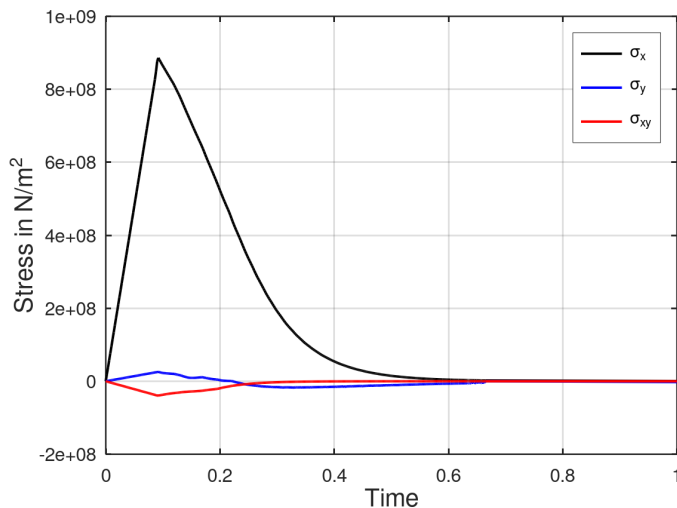


Figure 5.25: Evolution of stress components during longitudinal tensile loading ($h = 1\text{mm}$ discretization)

The contour plots of damage d_2 for increasing shear contribution are plotted in Figure (5.26). Compared to no shear effect ($\alpha = 0$), the model with the presence of shear effect has more realistic damage propagation of (d_2), and the width of the damage zone is significantly larger. For the model with shear effect, the width of the damage zone is almost similar in all the cases, but the maximum damage value and the number of elements reaching critical damage value increase with the increase in α .

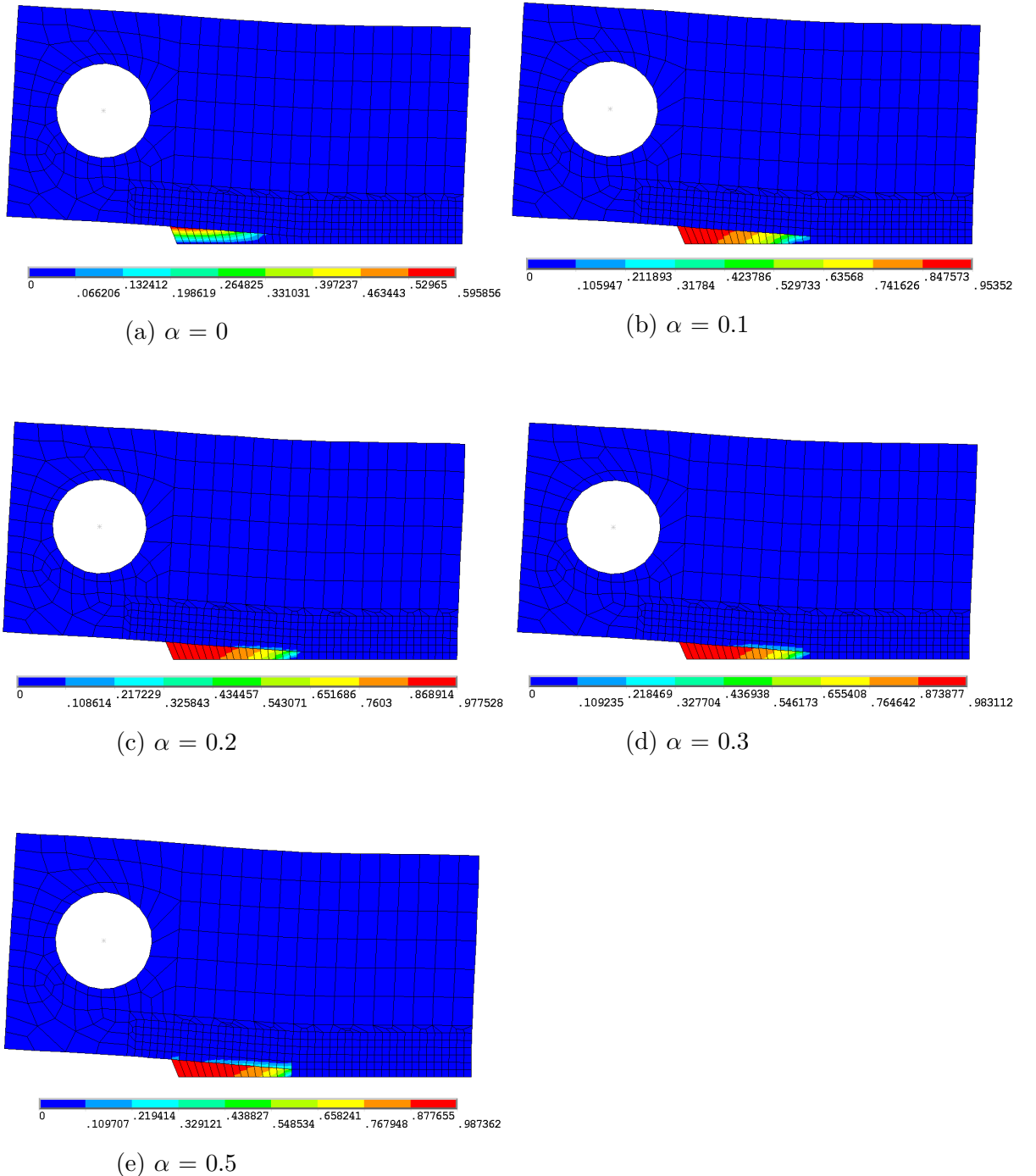


Figure 5.26: Damage distributions at the end of longitudinal loading: Damage contour plots d_2 for different shear co-efficients (α)

In the case of transverse loading, the damage d_2 is unaffected because the magnitude of the shear stress (σ_{12}) is very low compared to the stress (σ_{22}). However, the damage d_1 is affected because the magnitude of the shear stress component (σ_{12}) is similar compared to (σ_{11}).

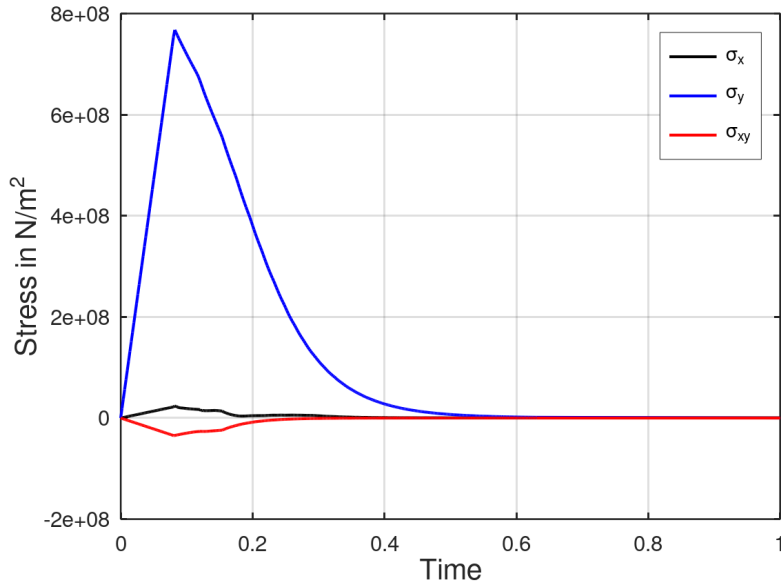


Figure 5.27: Evolution of stress components during transverse tensile loading (h=1mm discretization)

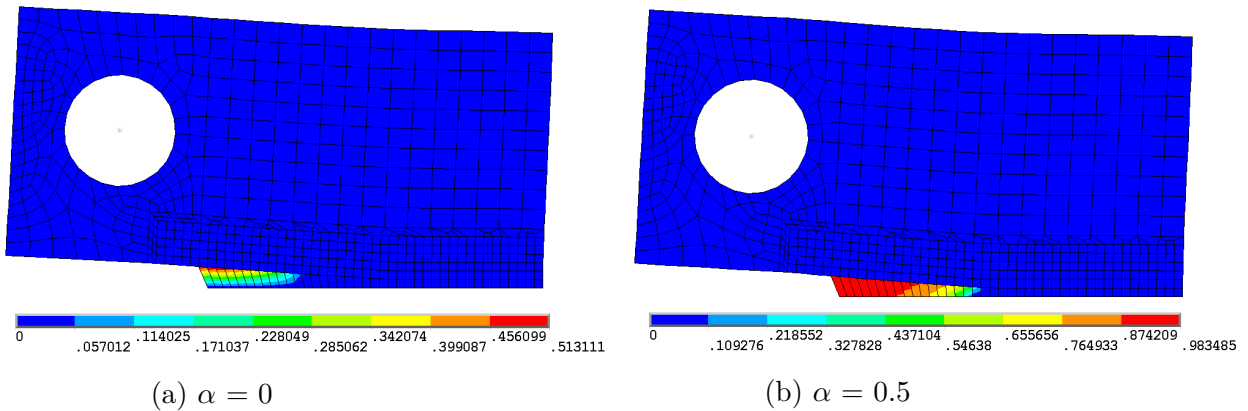


Figure 5.28: Damage distributions at the end of transverse loading: Damage contour plots d_1 for different shear co-efficient (α)

5.3.3 Plate with hole (3D)

This third example demonstrates the model's ability to show the anisotropic damage development for three dimensional (3D) problems. In 3D, three damage variables (d_1 , d_2 and d_3) are employed to represent the anisotropic damage development, i.e., one damage variable for each principal material direction. Because of symmetry, only one-eighth of the specimen has been modelled. The geometry and the appropriate boundary conditions are given in Figure (5.29). Eight node solid elements (SOLID 185) with trilinear interpolations of the displacements and full integration has been used to perform the FE modelling. The thickness has been divided into four elements, and a fine mesh has been used in the region closer to the fracture zone shown in the Figure (5.30).

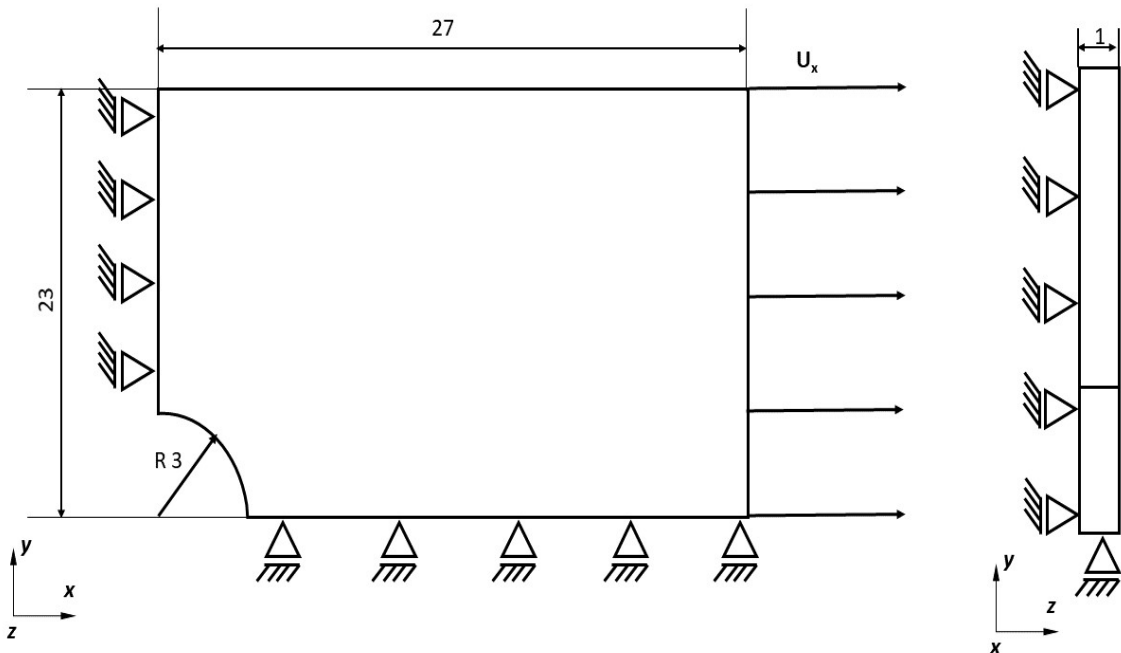


Figure 5.29: Specimen geometry and boundary conditions. Dimensions are given in mm. Displacement controlled loading U_x is applied

The longitudinal direction is kept parallel to the loading direction, and the behaviour of the model is analyzed by applying displacement controlled load (U_x) in the longitudinal direction (X-direction). The strength in transverse directions (2 and 3) are large enough so that damage variables d_2 and d_3 does not initiate when a longitudinal tensile load is applied. So to demonstrate the model's capability to show anisotropic damage development the strength in transverse directions (2 and 3) has been reduced (For both tension and compression). The material properties considered for 3D damage model (Jiang et al., 2018) are given in the Table (5.3). The maximum stress criterion (see Section(4.2.2)) has been used to predict the damage initiation in the three principal material directions.

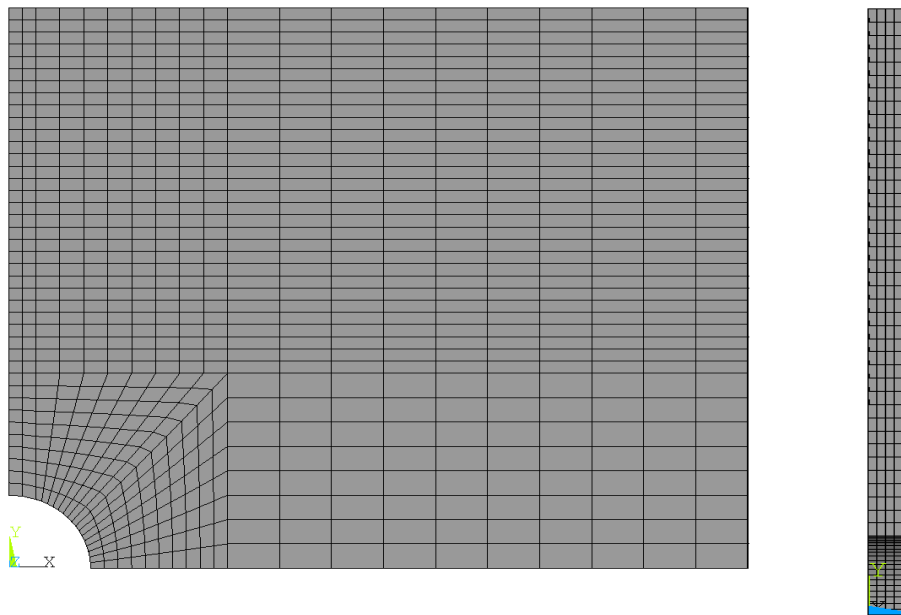


Figure 5.30: Finite element discretization used for 3D damage study

Symbol	Material Parameter	Value
E_{11}	Modulus in longitudinal (1) direction	55.8 GPa
$E_{22} = E_{33}$	Modulus in transverse (2 and 3) directions	54.9 GPa
$\nu_{12} = \nu_{13}$	Poisson's ratio	0.043
$G_{12} = G_{23} = G_{13}$	Shear modulus	4.2 GPa
X_t	Tensile strength in longitudinal (1) direction	910.1 MPa
X_c	Compressive strength in longitudinal (1) direction	-710.2 MPa
Y_t	Tensile strength in (2 and 3) directions	150 MPa
Y_c	Compressive strength in (2 and 3) directions	-200 MPa
S_{12}	In-plane strength	131 MPa
G_f^{lt}	Tensile fracture energy along longitudinal (1) direction	125 KJ/m ²
G_f^{lc}	Compressive fracture energy along longitudinal (1) direction	250 KJ/m ²
G_f^{tt}	Tensile fracture energy along (2 and 3) directions	95 KJ/m ²
G_f^{tc}	Compressive fracture energy along (2 and 3) directions	254 KJ/m ²

Table 5.3: Material parameters (3D Damage model)

The global force-displacement response has been plotted for this longitudinal tensile loading in Figure (5.31). The response is similar to the longitudinal loading in the notched tensile specimen, being characterized by a linear regime followed by a gradual drop of the load because of the softening. The softening is observed to initiate when the damage happens in critical number of elements in the fracture zone.

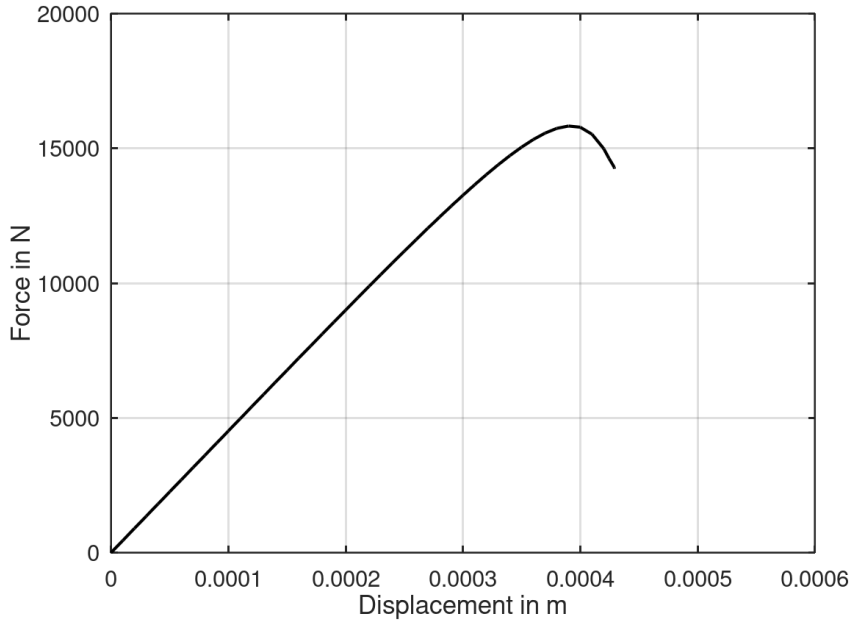
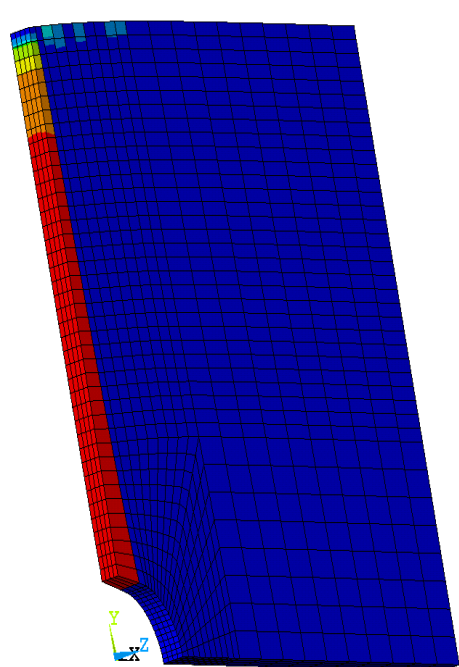
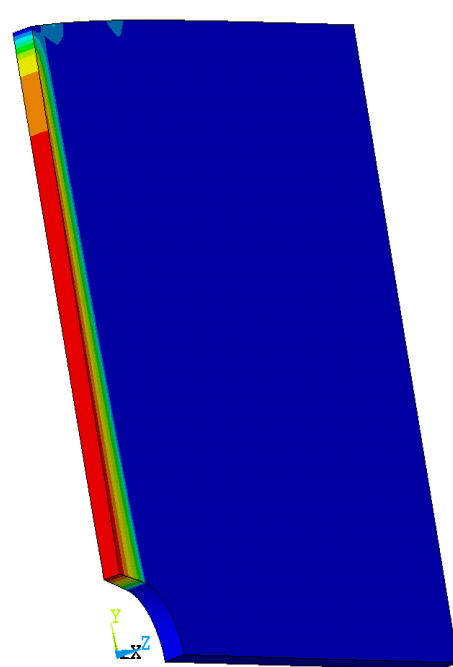
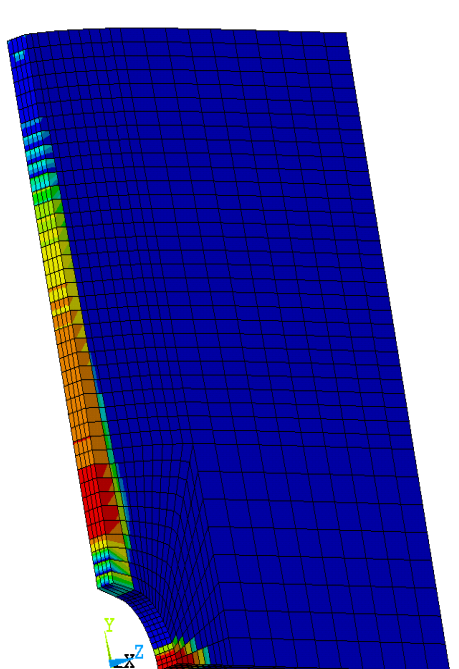
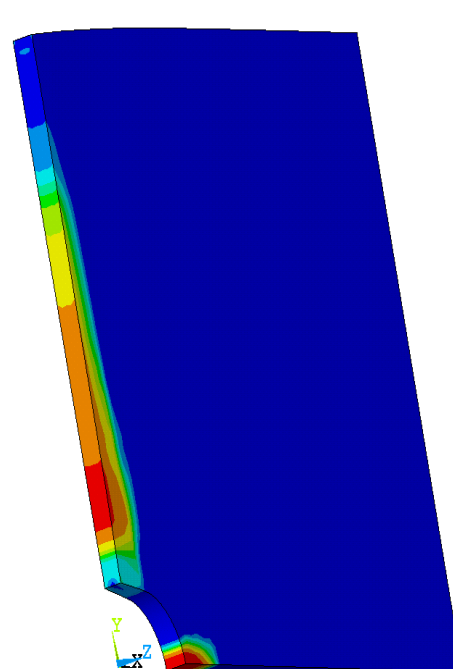


Figure 5.31: Global force-displacement response for the longitudinal tensile loading

The damage distribution (d_1 , d_2 and d_3) at the end of the tensile loading is shown in the Figure (5.32). In order to get a good visualization and understanding both element and nodal solution values of the damage are plotted. The initiation and evolution of damage d_1 is caused by the normal stress component σ_{11} in the longitudinal direction. The damage d_1 initiates at the tip of the blunt notch and then propagates perpendicular to the loading direction.

From Figures (5.32c) and (5.32d) it is evident that the damage d_2 happens at two separate regions, i) perpendicular to the loading direction where damage d_1 already propagated ii) right at the blunt notch at the bottom edge of the plate. It has been observed that the damage d_2 in the region (i) happens because of tension in the transverse direction, and in the region (ii) the damage is caused by the compression in the transverse direction. The propagation of damage d_3 is caused by the normal stress component σ_{33} in the thickness direction. The damage d_2 and d_3 has much lesser influence on the strength of the specimen compared to the damage d_1 during longitudinal tensile loading.

(a) Damage d_1 - element solution(b) Damage d_1 - nodal solution(c) Damage d_2 - element solution(d) Damage d_2 - nodal solution

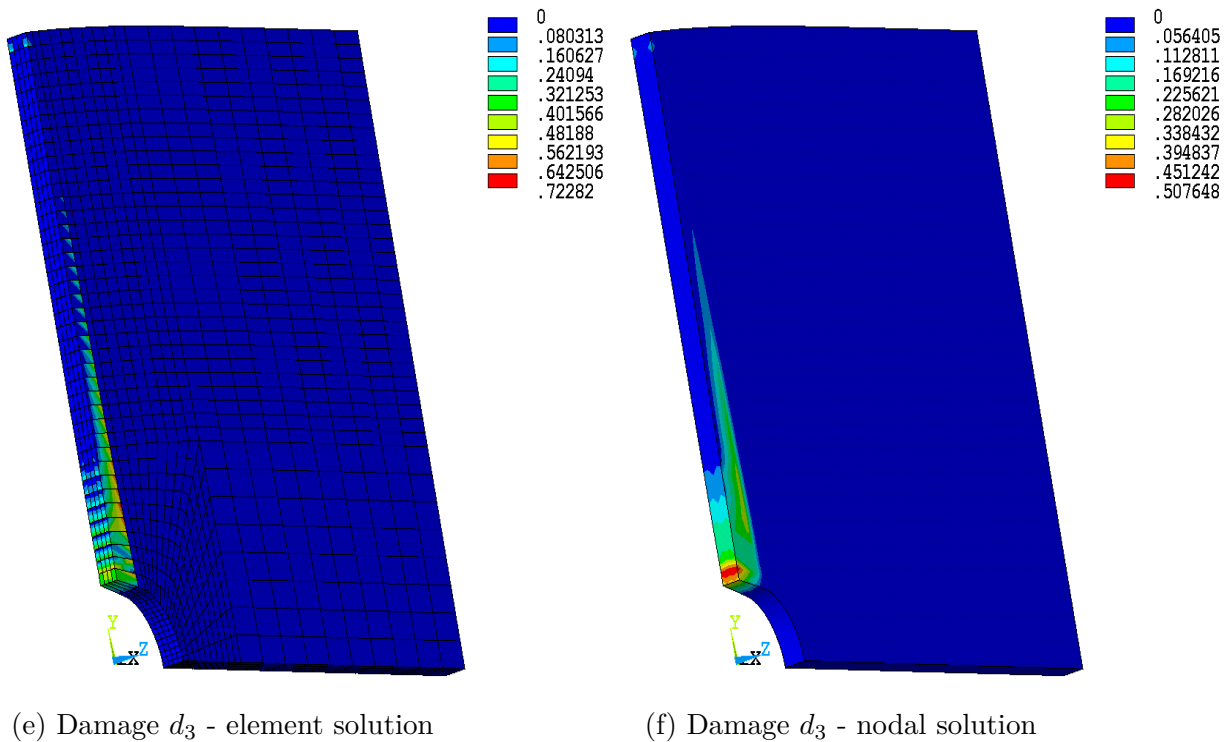


Figure 5.32: Contour plots of the damage distribution d_1 , d_2 and d_3 at the end of longitudinal tensile loading

These damage contour plots clearly indicate that the developed 3D model has the ability to show not only the damage development in three principal material directions but also both tension and compression damage happening simultaneously in a specimen when a load is applied.

Chapter 6

Summary and Conclusion

The main aim of this thesis is to develop progressive damage models which can describe the effect of damage in composite materials when subject to various loading conditions. The models are developed using the framework of continuum damage mechanics (CDM). A second-order orthotropic damage tensor is employed to show the anisotropic damage development. A key issue in damage modelling is the convergence issue that arises due to the mesh dependent behaviour of the strain-softening models. A fracture energy regularization technique has been employed to reduce the mesh sensitivity, by adjusting dissipated energy to each finite element. At first, the damage models are implemented in Octave and tested using constitutive driver routines for simple loading cases to verify the numerical implementation and understand the damage behaviour at integration point level, i.e., damage-evolution and strain-softening. During the integration point studies, it is been observed that the failure criteria, which use strain to predict the damage initiation, cause convergence issues when damage evolves without the presence of stress in the given material direction, i.e. when transverse strength is very low, and a uniaxial tension is applied in the longitudinal direction. So the damage models implemented as user-defined material routines (USERMAT) in ANSYS employ stress-based failure criteria.

The user-defined material routines (USERMAT) are tested using a finite element of unit length in ANSYS to compare against the results from the Octave implementation. Once verified, representative structural examples (2D and 3D) are used to test the damage models in ANSYS to see how they predict the initiation and evolution of damage under various circumstances. Finite elements of varying sizes are used in the area prone to damage to analyze the mesh sensitivity of the damage models. It has been observed that the employed regularization scheme significantly improves the global response, but it does not fully alleviate the mesh dependency problems which arise due to strain-softening. Therefore a drop in maximum load capacity, i.e., reduction in energy dissipation, is observed in the global force-displacement response when the mesh is refined. Different failure criteria have

been employed to see how the damage initiation and failure indices affect the model. It has been observed that the inclusion of the shear effect naturally reduces the maximum load capacity because of the increase in failure index for the same load. In some cases, the shear effect improves the damage behaviour when the magnitude of shear stress is significant compared to the normal stresses in the given material direction. Finally, the implemented damage models employing exponential damage evolution laws have the ability to represent the anisotropic damage development with the help of a second-order damage tensor and the strain-softening, which results from the stiffness degradation in 2D and 3D cases. This work provides a better understanding of the numerical implementation of the anisotropic damage models, which can predict the damage behaviour of complex composite materials.

The following changes and developments can be made in the future to make this anisotropic damage model an excellent tool to analyze the complex damage phenomena in composite materials used in real-life applications

- By incorporating complex failure criteria like Linde's failure criteria, Hashin's quadratic failure criteria (Jiang et al., 2018) etc., the damage initiation and propagation can be predicted more accurately because of the inclusion of shear effects and quadratic terms.
- From section (5.3.2) (CT-specimen), it is evident that when most of the distorted elements reach a critical value, the simulation terminates. This has been the case in most of the work done before For e.g., (Lapczyk and Hurtado, 2007), (El-Sisi et al., 2015) etc.,. But in very few works (Jiang et al., 2018), (Sokolinsky et al., 2011) an option called element deletion (available in the FEM software Abaqus) is employed to delete a particular failed element when the damage reaches a critical threshold value. This option can be included in the future to avoid the premature termination of analyses, and the whole crack propagation in the case of the CT-specimen can be simulated.
- Non-local gradient-enhanced damage formulations can be incorporated into the anisotropic damage models to eliminate the mesh dependency problems encountered in this work. These non-local models use weighted volume averages of the state variables to create spatial interactions, which induces a smoothening effect on the deformation and damage. Gradient enhanced formulations use higher-order deformation gradients of internal variables to create spatial discretization, eliminating the mesh dependency. In order to incorporate these gradient-enhanced formulations, a user element routine (USERELEM) must be developed in addition to the user material routine (USRMAT). Some of the works based on non-local damage models are (Peerlings, 1999), (Fassin et al., 2019), (Geers, 1998), (Seupel et al., 2018)

Bibliography

- B.Kiefer. Constitutive driver routines. Driver routines provided during the plasticity course (CMS) for testing the implemented material models. [coded by: B. Kiefer 15 Nov 2011, analytical solution added: S. Prueger 10 Dec 2018].
- Brainkart. Uni, Bi and Triaxial tension. https://www.brainkart.com/article/Triaxial-Stress,-Biaxial-Stress,-and-Uniaxial-Stress_5991/#:~:text=A%20two%2Ddimensional%20state%20of,called%20a%20uniaxial%20stress%20state. [Online; accessed 20-August-2021].
- Miguel Cervera and Michele Chiumenti. Smeared crack approach: back to the original track. *International journal for numerical and analytical methods in geomechanics*, 30(12):1173–1199, 2006.
- JP Cordebois and F Sidoroff. Damage induced elastic anisotropy. In *Mechanical Behavior of Anisotropic Solids/Comportement Méchanique des Solides Anisotropes*, pages 761–774. Springer, 1982.
- Alaa El-Din A El-Sisi, Hesham M El-Emam, Hani A Salim, and Hossam El-Din M Sallam. Efficient 3d modeling of damage in composite materials. *Journal of Composite Materials*, 49(7):817–828, 2015.
- BG Falzon and Paola Apruzzese. Numerical analysis of intralaminar failure mechanisms in composite structures. part i: Fe implementation. *Composite Structures*, 93(2):1039–1046, 2011.
- Marek Fassin, Robert Eggersmann, Stephan Wulffinghoff, and Stefanie Reese. Gradient-extended anisotropic brittle damage modeling using a second order damage tensor-theory, implementation and numerical examples. *International Journal of Solids and Structures*, 167:93–126, 2019.
- Marc Georges Denis Geers. Experimental analysis and computational modelling of damage and fracture. 1998.
- Zvi Hashin. Analysis of composite materials—a survey. 1983.
- Rodney Hill. Elastic properties of reinforced solids: some theoretical principles. *Journal of the Mechanics and Physics of Solids*, 11(5):357–372, 1963.

Hongyong Jiang, Yiru Ren, Zhihui Liu, Songjun Zhang, and Xiaoqing Wang. Evaluations of failure initiation criteria for predicting damages of composite structures under crushing loading. *Journal of Reinforced Plastics and Composites*, 37(21): 1279–1303, 2018.

Lasar Kachanov. *Introduction to continuum damage mechanics*, volume 10. Springer Science & Business Media, 1986.

LM Kachanov. On the rupture time under the condition of creep. *Izv. Akad. Nauk SSSR, Otd. Tekh. Nauk*, 8:26, 1958.

Ireneusz Lapczyk and Juan A Hurtado. Progressive damage modeling in fiber-reinforced materials. *Composites Part A: Applied Science and Manufacturing*, 38 (11):2333–2341, 2007.

J Lemaitre and Jean-Louis Chaboche. Aspect phénoménologique de la rupture par endommagement. *J Méc Appl*, 2(3), 1978.

Jean Lemaitre. *A course on damage mechanics*. Springer Science & Business Media, 2012.

BM Lempriere. Poisson’s ratio in orthotropic materials. *Aiaa Journal*, 6(11):2226–2227, 1968.

G Lin. Ansys user material subroutine usermat. *ANSYS, Canonsburg, PA*, 1999.

P Maimí, Pedro Ponces Camanho, JA Mayugo, and CG Dávila. A continuum damage model for composite laminates: Part i—constitutive model. *Mechanics of materials*, 39(10):897–908, 2007.

Sumio Murakami. *Continuum damage mechanics: a continuum mechanics approach to the analysis of damage and fracture*, volume 185. Springer Science & Business Media, 2012.

Ronnie Henricus Johannes Peerlings. Enhanced damage modelling for fracture and fatigue. 1999.

P.Nikethan. Composite materials in a Boeing 787 'Dreamliner'. <https://www.slideshare.net/nagababutallam/composite-materials-in-aerospace-industry>, 2016. [Online; accessed 5-August-2021].

Muhammad Masood Rafi, Ali Nadjai, and Faris Ali. Analytical modeling of concrete beams reinforced with carbon frp bars. *Journal of Composite Materials*, 41(22): 2675–2690, 2007.

- Andreas Seupel, Geralf Hütter, and Meinhard Kuna. An efficient fe-implementation of implicit gradient-enhanced damage models to simulate ductile failure. *Engineering Fracture Mechanics*, 199:41–60, 2018.
- David W Sleight. *Progressive failure analysis methodology for laminated composite structures*. Citeseer, 1999.
- Vladimir S Sokolinsky, Kyle C Indermuehle, and Juan A Hurtado. Numerical simulation of the crushing process of a corrugated composite plate. *Composites Part A: Applied Science and Manufacturing*, 42(9):1119–1126, 2011.
- TWI. Composite materials. <https://www.twi-global.com/technical-knowledge/faqs/what-is-a-composite-material#:~:text=A%20composite%20material%20is%20a,also%20improve%20strength%20and%20stiffness.>, 2016. [Online; accessed 15-July-2021].
- Yuequan Wang, Mingbo Tong, and Shuhua Zhu. Three dimensional continuum damage mechanics model of progressive failure analysis in fibre-reinforced composite laminates. In *50th AIAA/ASME/ASCE/AHS/ASC Structures, Structural Dynamics, and Materials Conference 17th AIAA/ASME/AHS Adaptive Structures Conference 11th AIAA No*, page 2629, 2009.
- Wikipedia. Fibre-reinforced composite. https://en.wikipedia.org/wiki/Fiber-reinforced_composite. [Online; accessed 10-June-2021].

Appendix

A Stiffness matrix of the damaged material

Plane stress (2D)

The stiffness matrix of the damage material for plane-stress problems has the form

$$\mathbb{C}(D) = \frac{1}{D} \begin{bmatrix} C_{11}(1-d_1) & C_{12}(1-d_1)(1-d_2) & 0 \\ C_{21}(1-d_2)(1-d_1) & C_{22}(1-d_2) & 0 \\ 0 & 0 & D(1-d_3)G_{12} \end{bmatrix}$$

where $D = 1 - (1-d_1)(1-d_2)\nu_{12}\nu_{21}$ and $d_3 = 1 - (1-d_1)(1-d_2)$

3D

The stiffness matrix of the damage material for 3D problems has the form

$$\mathbb{C}(D) = \begin{bmatrix} C_{11}^d & C_{12}^d & C_{13}^d & 0 & 0 & 0 \\ C_{21}^d & C_{22}^d & C_{23}^d & 0 & 0 & 0 \\ C_{31}^d & C_{32}^d & C_{33}^d & 0 & 0 & 0 \\ 0 & 0 & 0 & C_{44}^d & 0 & 0 \\ 0 & 0 & 0 & 0 & C_{55}^d & 0 \\ 0 & 0 & 0 & 0 & 0 & C_{66}^d \end{bmatrix}$$

where $C_{ij}^d = (1-d_i)(1-d_j)$, $i, j = 1, 2, 3$

$$\begin{aligned} C_{44}^d &= (1 - d_1)(1 - d_2), \\ C_{55}^d &= (1 - d_1)(1 - d_3), \\ C_{66}^d &= (1 - d_2)(1 - d_3) \end{aligned}$$

B Second term of the tangent stiffness

The explicit results of the derivatives of the second term in tangent stiffness for material model using maximum stress criteria (see section(4.2.2)) and the damage evolution equations (4.12) to (4.14) is presented below

From Eq. (2.15) we get,

$$\underline{\sigma} = \begin{bmatrix} \omega_{11}\tilde{\sigma}_{11} & \omega_{22}\tilde{\sigma}_{22} & \omega_{33}\tilde{\sigma}_{33} & \omega_{12}\tilde{\sigma}_{12} & \omega_{23}\tilde{\sigma}_{23} & \omega_{13}\tilde{\sigma}_{13} \end{bmatrix}$$

where

$$\omega_{11} = (1 - d_1); \quad \omega_{22} = (1 - d_2); \quad \omega_{33} = (1 - d_3);$$

$$\omega_{12} = \sqrt{(1 - d_1)(1 - d_2)}; \quad \omega_{23} = \sqrt{(1 - d_2)(1 - d_3)}; \quad \omega_{13} = \sqrt{(1 - d_1)(1 - d_3)};$$

Therefore,

$$\frac{\partial \underline{\sigma}}{\partial d_1} = \begin{bmatrix} -\tilde{\sigma}_{11} \\ 0 \\ 0 \\ \frac{(d_2 - 1)\tilde{\sigma}_{12}}{2\omega_{12}} \\ 0 \\ \frac{(d_3 - 1)\tilde{\sigma}_{13}}{2\omega_{13}} \end{bmatrix} \quad \frac{\partial \underline{\sigma}}{\partial d_2} = \begin{bmatrix} 0 \\ -\tilde{\sigma}_{22} \\ 0 \\ \frac{(d_1 - 1)\tilde{\sigma}_{12}}{2\omega_{12}} \\ \frac{(d_3 - 1)\tilde{\sigma}_{13}}{2\omega_{13}} \\ 0 \end{bmatrix} \quad \frac{\partial \underline{\sigma}}{\partial d_3} = \begin{bmatrix} 0 \\ 0 \\ -\tilde{\sigma}_{33} \\ 0 \\ \frac{(d_2 - 1)\tilde{\sigma}_{12}}{2\omega_{12}} \\ \frac{(d_1 - 1)\tilde{\sigma}_{13}}{2\omega_{13}} \end{bmatrix}$$

Now,

$$\frac{\partial d_i(F_I)}{\partial \underline{\epsilon}} = \frac{\partial d_i}{\partial F_I} \frac{\partial F_I}{\partial \underline{\epsilon}}$$

$$\frac{\partial d_1}{\partial F_l} = \frac{1 - P_1 F_l * e^{P_1(F_l-1)}}{F_l^2}$$

if ($\tilde{\sigma}_{11} > 0$)

$$\frac{\partial F_l}{\partial \underline{\epsilon}} = \begin{bmatrix} \frac{C_{11}}{X_t} & \frac{C_{12}}{X_t} & \frac{C_{13}}{X_t} & 0 & 0 & 0 \end{bmatrix}$$

if ($\tilde{\sigma}_{11} < 0$)

$$\frac{\partial F_l}{\partial \underline{\epsilon}} = \begin{bmatrix} \frac{C_{11}}{X_c} & \frac{C_{12}}{X_c} & \frac{C_{13}}{X_c} & 0 & 0 & 0 \end{bmatrix}$$

Now,

$$\frac{\partial d_2}{\partial F_t} = \frac{1 - P_2 F_t * e^{P_2(F_t-1)}}{F_t^2}$$

if ($\tilde{\sigma}_{22} > 0$)

$$\frac{\partial F_t}{\partial \underline{\epsilon}} = \begin{bmatrix} \frac{C_{21}}{Y_t} & \frac{C_{22}}{Y_t} & \frac{C_{23}}{Y_t} & 0 & 0 & 0 \end{bmatrix}$$

if ($\tilde{\sigma}_{22} < 0$)

$$\frac{\partial F_t}{\partial \underline{\epsilon}} = \begin{bmatrix} \frac{C_{21}}{Y_c} & \frac{C_{22}}{Y_c} & \frac{C_{23}}{Y_c} & 0 & 0 & 0 \end{bmatrix}$$

Now,

$$\frac{\partial d_3}{\partial F_z} = \frac{1 - P_3 F_z * e^{P_3(F_z-1)}}{F_z^2}$$

if ($\tilde{\sigma}_{33} > 0$)

$$\frac{\partial F_z}{\partial \underline{\epsilon}} = \begin{bmatrix} \frac{C_{31}}{Z_t} & \frac{C_{32}}{Z_t} & \frac{C_{33}}{Z_t} & 0 & 0 & 0 \end{bmatrix}$$

if ($\tilde{\sigma}_{33} < 0$)

$$\frac{\partial F_z}{\partial \underline{\epsilon}} = \begin{bmatrix} \frac{C_{31}}{Z_c} & \frac{C_{32}}{Z_c} & \frac{C_{33}}{Z_c} & 0 & 0 & 0 \end{bmatrix}$$

C APDL Script

The APDL script for simulating uniaxial tension in a unit cube is presented below

```

1 /CLEAR
2
3 L = 1
4
5 STRETCH =0.2
6
7 /PREP7

```

```
8 !*
9
10 ERESX,NO
11 ET,1 ,SOLID185
12 !*
13 KEYOPT,1 ,2 ,0
14 KEYOPT,1 ,3 ,0
15 KEYOPT,1 ,6 ,0
16 KEYOPT,1 ,8 ,0
17 !*
18
19 T1 = 1
20 TB,USER,1 ,1 ,9 ,9
21 TBTEMP,T1
22 TBDATA, ,55000e6 ,9500e6 ,9500e6 ,0.33 ,0.27 ,0.33 ,5500e6 ,3000e6 ,5500e6
23 TB,STATE,1 , ,7
24
25 MAT,1
26 TYPE,1
27
28 BLC4,0 ,0 ,L,L,L
29 ESIZE , ,L
30 VMESH,1
31
32 NSEL,S ,LOC,X,0
33 D,ALL,UX
34 NSEL,ALL
35
36 NSEL,S ,LOC,Y,0
37 D,ALL,UY
38 NSEL,ALL
39
40 NSEL,S ,LOC,Z,0
41 D,ALL,UZ
42 NSEL,ALL
43
44 /SOL
45 !*
46 ANTYPE,0
47 NSUBST,100 ,10000 ,100
48 OUTRES,ERASE
49 OUTRES,ALL,ALL
50 OUTRES,SVAR,ALL, ,NSVAR
51 TIME,1
52
53 NSEL,S ,LOC,X,L
54 D,ALL,UX,STRETCH
55 NSEL,ALL
56
```

```
57 /SOL  
58 /STATUS,SOLU  
59 SOLVE  
60  
61  
62 FINISH
```

D Source code for USERMAT

The source code for the anisotropic damage model (in 3D) implemented as user material routine in ANSYS is given below

```

1
2
3      subroutine usermat(
4          matId, elemId, kDomIntPt, kLayer, kSectPt,
5          & ldstep, isubst, keycut,
6          & nDirect, nShear, ncomp, nStatev, nProp,
7          & Time, dTime, Temp, dTemp,
8          & stress, ustatev, dsdePl, sedEl, sedPl, epseq,
9          & Strain, dStrain, epsPl, prop, coords,
10         & var0, defGrad_t, defGrad,
11         & tsstif, epsZZ,
12         & var1, var2, var3, var4, var5,
13         & var6, var7, var8)
14
15
16 #include "impcom.inc"
17 #include "ansysdef.inc"
18     integer :: matId, elemId, kDomIntPt, kLayer, kSectPt, ldstep,
19     & isubst, keycut, nDirect, nShear, ncomp, nStatev, nProp
20
21
22     double precision :: Time,      dTime,      Temp,      dTemp,
23     &             sedEl,      sedPl,      epseq,      epsZZ
24
25     double precision :: stress (ncomp), ustatev (nStatev),
26     &             dsdePl (ncomp,ncomp), Strain (ncomp),
27     &             dStrain (ncomp), epsPl (ncomp),
28     &             prop   (nProp), coords (3),
29     &             defGrad (3,3),    defGrad_t(3,3),
30     &             tsstif (2)
31
32
33     EXTERNAL        usermat3d
34     EXTERNAL        myuserfunc
35     integer :: myvar
36
37
38
39     double precision :: var0, var1, var2, var3, var4, var5,
40     &             var6, var7, var8
41
42     integer :: iott, wrinqr
43     external wrinqr
44 C ****

```

```

46 c
47     iott = wrinqr(WR_OUTPUT)
48     write(iott,*)'*****'
49     write(iott,*)'* #DEBUG# UserMatLib.d11 USERMAT      *'
50     write(iott,*)'*****'
51     myvar = 99
52     call myuserfunc(myvar)
53
54
55
56 if (ncomp >= 4) then
57
58
59 call usermat3d (
60     & matId, elemId, kDomIntPt, kLayer, kSectPt,
61     & ldstep, isubst, keycut,
62     & nDirect, nShear, ncomp, nStatev, nProp,
63     & Time, dTime, Temp, dTemp,
64     & stress, ustatev, dsdePl, sedEl, sedPl, epseq,
65     & Strain, dStrain, epsPl, prop, coords,
66     & var0, defGrad_t, defGrad,
67     & tsstif, epsZZ,
68     & var1, var2, var3, var4, var5,
69     & var6, var7, var8)
70
71
72 end if
73 return
74 end
75
76
77 ***** Subroutine for 3d elements (Linear elastic isotropic model) ****
78 subroutine usermat3d(
79     & matId, elemId, kDomIntPt, kLayer, kSectPt,
80     & ldstep, isubst, keycut,
81     & nDirect, nShear, ncomp, nStatev, nProp,
82     & Time, dTime, Temp, dTemp,
83     & stress, ustatev, dsdePl, sedEl, sedPl, epseq,
84     & Strain, dStrain, epsPl, prop, coords,
85     & var0, defGrad_t, defGrad,
86     & tsstif, epsZZ,
87     & var1, var2, var3, var4, var5,
88     & var6, var7, var8)
89
90
91 #include "impcom.inc"
92 #include "ansysdef.inc"
93 c
94     integer :: matId, elemId, kDomIntPt, kLayer, kSectPt, ldstep,

```

```

95      &           isubst , keycut , nDirect , nShear , ncomp , nStatev , nProp
96
97
98      double precision :: Time,       dTime,       Temp,       dTemp,
99      &                   sedEl ,      sedPl ,      epseq ,      epsZZ
100
101     double precision :: stress (ncomp ), ustatev (nStatev),
102     &                   dsdePl (ncomp ,ncomp ), Strain (ncomp ),
103     &                   dStrain (ncomp ), epsPl (ncomp ),
104     &                   prop (nProp ), coords (3),
105     &                   defGrad (3,3),      defGrad_t (3,3),
106     &                   tsstif (2)
107
108
109
110
111 ***** USER DEFINED VARIABLES (FOR CALCULATION PURPOSE) *****
112
113      integer :: mcomp, twenty
114      double precision :: HALF, ONE, TWO, ZERO,
115      &                   THREE
116
117      PARAMETER (ZERO      = 0.d0 ,
118      &             HALF      = 0.5d0 ,
119      &             ONE      = 1.d0 ,
120      &             TWO      = 2.d0 ,
121      &             THREE     = 3.d0 ,
122      &             mcomp    = 6
123      &             )
124
125      EXTERNAL      vzero , vmove
126
127      double precision dsdeEl(mcomp,mcomp) , sigma(mcomp) ,
128      &             sigi (mcomp) , C_T(mcomp,mcomp) ,
129      &             dsdeEl_d (mcomp,mcomp) , T_strain (mcomp) ,
130      &             id (3,3) , C_T_1(mcomp,mcomp) , M_inv (mcomp,mcomp) ,
131      &             C_T_1_a(mcomp) , C_T_0(mcomp,mcomp) ,
132      &             C_T_1_b(mcomp) , C_T_2(mcomp,mcomp) ,
133      &             C_T_2_a(mcomp) ,
134      &             C_T_2_b(mcomp) , C_T_3(mcomp,mcomp) ,
135      &             C_T_3_a(mcomp) ,
136      &             C_T_3_b(mcomp) , sigma_eff (mcomp)
137
138
139
140      integer          i ,j ,k ,l ,n ,P ,ielem ,iiter ,key
141      double precision young_x , young_y , young_z ,
142      &             pr_xy , pr_yz , pr_xz , L_c , k1 , k2 , k3 , d1_max ,
143      &             xK , yield , G_c_1_t , G_c_1_c , G_c_2_t , G_c_2_c ,

```

```

144      &           eps_11_f_t ,eps_11_f_c ,eps_22_f_t ,d2_max ,
145      &           eps_22_f_c ,eps_33_f_t ,eps_33_f_c ,d3_max ,
146      &           eps_12_f ,eps_13_f ,eps_23_f ,sig_11_f_t ,
147      &           sig_22_f_t ,sig_33_f_t ,d1 ,d2 ,d3 ,d1_new ,d2_new
148
149      double precision d3_new ,F_f,F_m,F_z ,term1 ,term2 ,g_xy , g_yz ,
150      &           g_xz ,delta ,pr_yx , pr_zy , pr_zx ,xy_yx , yz_zy ,
151      &           zx_xz ,xyz , E_xyz , sig_11_f_c , sig_22_f_c ,
152      &           sig_33_f_c ,sig_12_f ,sig_23_f ,sig_13_f ,F_f_new ,
153      &           F_m_new ,F_z_new ,V ,term3 ,G_c_3_t ,G_c_3_c
154
155
156
157      double precision var0 , var1 , var2 , var3 , var4 , var5 ,
158      &           var6 , var7 , var8
159
160
161      V      = ustatev(1)
162      d1     = ustatev(2)
163      d2     = ustatev(3)
164      d3     = ustatev(4)
165      F_f    = ustatev(5)
166      F_m    = ustatev(6)
167      F_z    = ustatev(7)
168
169 c *** get Young's modulus and Poisson's ratio , initial yield stress and others
170      young_x = prop(1)
171      young_y = prop(2)
172      young_z = prop(3)
173      pr_xy   = prop(4)
174      pr_yz   = prop(5)
175      pr_xz   = prop(6)
176      g_xy    = prop(7)
177      g_yz    = prop(8)
178      g_xz    = prop(9)
179
180
181      sig_11_f_t = 910.1e6
182      sig_11_f_c = -710.2e6
183      sig_22_f_t = 150e6
184      sig_22_f_c = -200e6
185      sig_33_f_t = 150e6
186      sig_33_f_c = -200e6
187      sig_12_f   = 131e6
188      sig_13_f   = 131e6
189      sig_23_f   = 131e6
190      G_c_1_t    = 12.5e4
191      G_c_1_c    = 25e4
192      G_c_2_t    = 9.5e4

```

```

193      G_c_2_c      = 25.4e4
194      G_c_3_t      = 9.5e4
195      G_c_3_c      = 25.4e4
196      L_c          = V** (1.0/3.0)
197
198
199
200      pr_yx = (young_y * pr_xy) / young_x
201      pr_zy = (young_z * pr_yz) / young_y
202      pr_zx = (young_z * pr_xz) / young_x
203
204
205      xy_yx = pr_xy*pr_yx
206      yz_zy = pr_yz*pr_zy
207      zx_xz = pr_zx*pr_xz
208      xyz     = TWO*pr_xy*pr_yz*pr_zx
209      E_xyz   = young_x*young_y*young_z
210
211      delta = (ONE - (xy_yx) - (yz_zy) - (zx_xz) - (xyz)) / E_xyz
212
213      tsstif(1) = g_xz
214      tsstif(2) = g_yz
215
216
217
218
219
220 ***** ELASTIC STIFFNESS MATRIX *****
221
222      dsdeEl(1,1) = (ONE -yz_zy) / (young_y*young_z*delta)
223      dsdeEl(1,2) = (pr_yx + pr_zx*pr_yz) / (young_y*young_z*delta)
224      dsdeEl(1,3) = (pr_zx + pr_yx*pr_zy)/(young_y*young_z*delta)
225      dsdeEl(1,4) = 0
226      dsdeEl(1,5) = 0
227      dsdeEl(1,6) = 0
228      dsdeEl(2,1) = (pr_yx + pr_zx*pr_yz) /(young_y*young_z*delta)
229      dsdeEl(2,2) = (ONE -zx_xz)/(young_x*young_z*delta)
230      dsdeEl(2,3) = (pr_zy + pr_zx*pr_xy) /(young_x*young_z*delta)
231      dsdeEl(2,4) = 0
232      dsdeEl(2,5) = 0
233      dsdeEl(2,6) = 0
234      dsdeEl(3,1) = (pr_zx + pr_yx*pr_zy) /(young_y*young_z*delta)
235      dsdeEl(3,2) = (pr_zy + pr_zx*pr_xy) / (young_x*young_z*delta)
236      dsdeEl(3,3) = (ONE -xy_yx)/(young_x*young_y*delta)
237      dsdeEl(3,4) = 0
238      dsdeEl(3,5) = 0
239      dsdeEl(3,6) = 0
240      dsdeEl(4,1) = 0
241      dsdeEl(4,2) = 0

```

```

242 dsdeEl(4,3) = 0
243 dsdeEl(4,4) = g_xy
244 dsdeEl(4,5) = 0
245 dsdeEl(4,6) = 0
246 dsdeEl(5,1) = 0
247 dsdeEl(5,2) = 0
248 dsdeEl(5,3) = 0
249 dsdeEl(5,4) = 0
250 dsdeEl(5,5) = g_yz
251 dsdeEl(5,6) = 0
252 dsdeEl(6,1) = 0
253 dsdeEl(6,2) = 0
254 dsdeEl(6,3) = 0
255 dsdeEl(6,4) = 0
256 dsdeEl(6,5) = 0
257 dsdeEl(6,6) = g_xz
258
259
260
261     eps_11_f_t = sig_11_f_t / ((ONE -yz_zy) / (young_y*young_z*delta))
262     eps_11_f_c = sig_11_f_c / ((ONE -yz_zy) / (young_y*young_z*delta))
263     eps_22_f_t = sig_22_f_t / ((ONE -zx_xz) / (young_x*young_z*delta))
264     eps_22_f_c = sig_22_f_c / ((ONE -zx_xz) / (young_x*young_z*delta))
265     eps_33_f_t = sig_33_f_t / ((ONE -xy_yx) / (young_x*young_y*delta))
266     eps_33_f_c = sig_33_f_c / ((ONE -xy_yx) / (young_x*young_y*delta))
267     eps_12_f   = sig_12_f / g_xy
268     eps_13_f   = sig_13_f / g_xz
269     eps_23_f   = sig_23_f / g_yz
270
271 c *** Calculate current strain
272 do i=1,ncomp
273     T_strain(i) = Strain(i) + dStrain(i)
274 end do
275
276
277 c**** Compute effective stress
278 call vzero(sigma_eff, 6)
279 do i=1,ncomp
280     do j=1,ncomp
281         sigma_eff(i) = sigma_eff(i) + (dsdeEl(i,j)*T_strain(j))
282     end do
283 end do
284
285
286
287
288 c****Damage initiation criteria
289
290 if (sigma_eff(1) >= 0) then

```

```

291     F_f_new = sigma_eff(1)/sig_11_f_t
292 else
293     F_f_new = sigma_eff(1)/sig_11_f_c
294 endif
295
296
297 if (sigma_eff(2)>= 0) then
298   F_m_new = sigma_eff(2)/sig_22_f_t
299 else
300   F_m_new = sigma_eff(2)/sig_22_f_c
301 endif
302
303
304 if (sigma_eff(3) >= 0 )then
305   F_z_new = sigma_eff(3)/sig_33_f_t
306 else
307   F_z_new = sigma_eff(3)/sig_33_f_c
308 endif
309
310
311 c***** To make sure damage initiation criteria is greater than or equal to previous s
312
313 if (F_f_new >= F_f) then
314   F_f = F_f_new
315 else
316   F_f = F_f
317 endif
318
319 if (F_m_new >= F_m) then
320   F_m = F_m_new
321 else
322   F_m = F_m
323 endif
324
325 if (F_z_new >= F_z) then
326   F_z = F_z_new
327 else
328   F_z = F_z
329 endif
330
331
332
333 call vzero(sigma ,6)
334 call vzero(C_T_1_a, 6)
335 call vzero(C_T_2_a, 6)
336 call vzero(C_T_3_a, 6)
337 if ((F_f <= 1) .AND. (F_m <= 1) .AND. (F_z <= 1)) then
338
339 c***** Update stress

```

```

340      do i=1,ncomp
341          sigma( i ) = sigma_eff( i )
342      end do
343
344
345
346      else
347
348 c***** Terms in damage evolution equations *****
349      if ( sigma_eff(1) >= 0) then
350          k1 = (-sig_11_f_t*eps_11_f_t*L_c)/G_c_1_t
351      else
352          k1 = (-sig_11_f_c*eps_11_f_c*L_c)/G_c_1_c
353      endif
354
355
356      if ( sigma_eff(2) >= 0) then
357          k2 = (-sig_22_f_t*eps_22_f_t*L_c)/G_c_2_t
358      else
359          k2 = (-sig_22_f_c*eps_22_f_c*L_c)/G_c_2_c
360      endif
361
362
363      if ( sigma_eff(3) >= 0) then
364          k3 = (-sig_33_f_t*eps_33_f_t*L_c)/G_c_3_t
365      else
366          k3 = (-sig_33_f_c*eps_33_f_c*L_c)/G_c_3_c
367      endif
368
369      d1_max = 0.999
370      d2_max = 0.999
371      d3_max = 0.999
372
373 c***** Damage evolution equations *****
374      if (F_f > 1) then
375
376          d1_new = d1_max*(ONE - (exp(k1*(F_f - ONE)))/F_f)
377
378          if (d1_new > d1) then
379              d1 = d1_new
380          else
381              d1 = d1
382          endif
383
384      endif
385
386
387      if (F_m > 1) then
388

```

```

389      d2_new = d2_max*(ONE - (exp(k2*(F_m- ONE)))/F_m)
390
391      if (d2_new > d2) then
392          d2 = d2_new
393      else
394          d2 = d2
395      endif
396
397      endif
398
399
400      if (F_z > 1) then
401
402          d3_new = d3_max*(ONE - (exp(k3*(F_z - ONE)))/F_z)
403
404          if (d3_new > d3) then
405              d3 = d3_new
406          else
407              d3 = d3
408          endif
409
410      endif
411
412
413
414
415 c*****      Inverse of the damage effect tensor *****
416
417      do i = 1,ncomp
418          do j= 1,ncomp
419              M_inv(i,j) = ZERO
420          end do
421      end do
422
423      M_inv(1,1) = (1 - d1)
424      M_inv(2,2) = (1 - d2)
425      M_inv(3,3) = (1 - d3)
426      M_inv(4,4) = sqrt((1 - d1)*(1 - d2))
427      M_inv(5,5) = sqrt((1 - d3)*(1 - d2))
428      M_inv(6,6) = sqrt((1 - d1)*(1 - d3))
429
430 c*****      Find nominal stress from effective stress *****
431      do i=1,ncomp
432          do j=1,ncomp
433              sigma(i) = sigma(i) + (M_inv(i,j)*sigma_eff(j))
434          end do
435      end do
436
437

```

```

438 c***** Degraded stiffness *****
439      dsdeEl_d(1,1)=(ONE-yz_zy)/(young_y*young_z*delta)*(ONE
440      & -d1)**2
441      dsdeEl_d(1,2) = (pr_yx + pr_zx*pr_yz) / (young_y*young_z*delta)
442      & *(ONE - d1)*(ONE - d2)
443      dsdeEl_d(1,3) = (pr_zx + pr_yx*pr_zy) / (young_y*young_z*delta)*
444      & (ONE - d1)*(ONE - d3)
445      dsdeEl_d(1,4) = 0
446      dsdeEl_d(1,5) = 0
447      dsdeEl_d(1,6) = 0
448      dsdeEl_d(2,1) = (pr_yx + pr_zx*pr_yz) / (young_y*young_z*delta)*
449      & (ONE - d1)*(ONE - d2)
450      dsdeEl_d(2,2)=(ONE-zx_xz)/(young_x*young_z*delta)*(ONE - d2)**2
451      dsdeEl_d(2,3) = (pr_zy + pr_zx*pr_xy)/(young_x*young_z*delta)*
452      & (ONE - d3)*(ONE - d2)
453      dsdeEl_d(2,4) = 0
454      dsdeEl_d(2,5) = 0
455      dsdeEl_d(2,6) = 0
456      dsdeEl_d(3,1) = (pr_zx + pr_yx*pr_zy) /(young_y*young_z*delta)*
457      & (ONE - d3)*(ONE - d1)
458      dsdeEl_d(3,2) = (pr_zy + pr_zx*pr_xy) / (young_x*young_z*delta)*
459      & (ONE - d3)*(ONE- d2)
460      dsdeEl_d(3,3) = (ONE-xy_yx)/(young_x*young_y*delta)*(ONE
461      & -d3)**2
462      dsdeEl_d(3,4) = 0
463      dsdeEl_d(3,5) = 0
464      dsdeEl_d(3,6) = 0
465      dsdeEl_d(4,1) = 0
466      dsdeEl_d(4,2) = 0
467      dsdeEl_d(4,3) = 0
468      dsdeEl_d(4,4) = g_xy*(ONE - d1)*(ONE - d2)
469      dsdeEl_d(4,5) = 0
470      dsdeEl_d(4,6) = 0
471      dsdeEl_d(5,1) = 0
472      dsdeEl_d(5,2) = 0
473      dsdeEl_d(5,3) = 0
474      dsdeEl_d(5,4) = 0
475      dsdeEl_d(5,5) = g_yz*(ONE - d2)*(ONE - d3)
476      dsdeEl_d(5,6) = 0
477      dsdeEl_d(6,1) = 0
478      dsdeEl_d(6,2) = 0
479      dsdeEl_d(6,3) = 0
480      dsdeEl_d(6,4) = 0
481      dsdeEl_d(6,5) = 0
482      dsdeEl_d(6,6) = g_xz*(ONE - d3)*(ONE - d1)
483
484      if ((d1 == ZERO)) then
485
486          do i=1,mcomp

```

```

487      do j=1,mcomp
488         C_T_1(i,j) = 0
489      end do
490   end do
491
492   else
493
494      C_T_1_a =(-sigma_eff(1),ZERO,ZERO,(HALF*(d2-1)*sigma_eff(4))
495      & /M_inv(4,4),ZERO,(HALF*(d3-1)*sigma_eff(6))/M_inv(6,6)/)
496
497
498 c***** Derivative of d1 with respect to strain (d_d1/d_epsilon) *****
499
500 c** For Tension
501 if (sigma_eff(1)> 0) then
502
503   term1 = d1_max*((ONE-k1*F_f)*exp(k1*(F_f - ONE)))/(F_f**2)
504
505   C_T_1_b = (/ (term1*dsdeE1(1,1))/sig_11_f_t ,
506   & (term1*dsdeE1(1,2))/sig_11_f_t ,(term1*dsdeE1(1,3))
507   & /sig_11_f_t ,ZERO,ZERO,ZERO/)
508
509
510 c** For Compression
511 else
512
513   term1 = d1_max*((ONE-k1*F_f)*exp(k1*(F_f - ONE)))/(F_f**2)
514
515   C_T_1_b = (/ (term1*dsdeE1(1,1))/sig_11_f_c ,
516   & (term1*dsdeE1(1,2))/sig_11_f_c ,(term1*dsdeE1(1,3))
517   & /sig_11_f_c ,ZERO,ZERO,ZERO/)
518
519 endif
520
521 do i = 1,mcomp
522   do j = 1,mcomp
523     C_T_1(i,j) = C_T_1_a(i)*C_T_1_b(j)
524   end do
525 end do
526
527 endif
528
529
530
531 if ((d2 == ZERO)) then
532
533   do i=1,mcomp
534     do j=1,mcomp
535       C_T_2(i,j) = 0

```

```

536         end do
537     end do
538
539     else
540
541         C_T_2_a =(/ZERO,-sigma_eff(2),ZERO,(HALF*(d1- 1)*sigma_eff(4))
542         & /M_inv(4,4),(HALF*(d3 - 1)*sigma_eff(5))/M_inv(5,5),ZERO /)
543
544 c*****      Derivative of d2 with respect to strain (d_d2/d_epsilon)
545
546 c****      For Tension
547     if (sigma_eff(2)> 0)  then
548
549         term2 = d2_max*((ONE-k2*F_m)*exp(k2*(F_m - ONE)))/(F_m**2))
550
551         C_T_2_b = (/ (term2*dsdeEl(2,1))/sig_22_f_t ,
552         & (term2*dsdeEl(2,2))/sig_22_f_t ,(term2*dsdeEl(2,3))
553         & /sig_22_f_t ,ZERO,ZERO,ZERO/)
554
555 c**      For Compression
556     else
557
558         term2 = d2_max*((ONE-k2*F_m)*exp(k2*(F_m - ONE)))/(F_m**2))
559
560         C_T_2_b = (/ (term2*dsdeEl(2,1))/sig_22_f_c ,
561         & (term2*dsdeEl(2,2))/sig_22_f_c ,(term2*dsdeEl(2,3))
562         & /sig_22_f_c ,ZERO,ZERO,ZERO/)
563
564     endif
565
566
567     do i = 1,mcomp
568         do j = 1,mcomp
569             C_T_2(i,j) = C_T_2_a(i)*C_T_2_b(j)
570         end do
571     end do
572
573     endif
574
575     if ((d3 == ZERO))then
576
577         do i=1,ncomp
578             do j=1,ncomp
579                 C_T_3(i,j) = 0
580             end do
581         end do
582
583     else

```

```

585
586      C_T_3_a = (/ZERO,ZERO,-sigma_eff(3), ZERO,
587      & (HALF*(d2 - 1)*sigma_eff(5))/M_inv(5,5),(HALF*(d1 - 1)
588      & *sigma_eff(6))/M_inv(6,6) /)
589
590 c***** Derivative of d3 with respect to strain (d_d3/d_epsilon)
591
592 c**** For Tension
593 if (sigma_eff(3) > 0) then
594
595   term3 = d3_max*((ONE-k3*F_z)*exp(k3*(F_z - ONE)))/(F_z**2)
596
597   C_T_3_b = (/ (term3*dsdeEl(3,1))/sig_33_f_t ,
598   & (term3*dsdeEl(3,2))/sig_33_f_t ,(term3*dsdeEl(3,3))/sig_33_f_t ,
599   & ZERO,ZERO,ZERO/)
600
601 c**** For Compression
602 else
603
604   term3 = d3_max*((ONE-k3*F_z)*exp(k3*(F_z - ONE)))/(F_z**2)
605
606   C_T_3_b = (/ (term3*dsdeEl(3,1))/sig_33_f_c ,
607   & (term3*dsdeEl(3,2))/sig_33_f_c ,(term3*dsdeEl(3,3))/sig_33_f_c ,
608   & ZERO,ZERO,ZERO/)
609
610 endif
611
612 do i = 1,mcomp
613   do j = 1,meomp
614     C_T_3(i,j) = C_T_3_a(i)*C_T_3_b(j)
615   end do
616 end do
617
618 endif
619
620
621 do i = 1,ncomp
622   do j= 1,ncomp
623     C_T(i,j) = ZERO
624   end do
625 end do
626 c***** Tangent stiffness
627 do i=1,ncomp
628   do j=1,ncomp
629     C_T(i,j) = dsdeEl_d(i,j) + C_T_1(i,j) + C_T_2(i,j) +
630     & C_T_3(i,j)
631   end do
632 end do
633

```

```
634
635      endif
636
637      ustatev(2) = d1
638      ustatev(3) = d2
639      ustatev(4) = d3
640      ustatev(5) = F_f
641      ustatev(6) = F_m
642      ustatev(7) = F_z
643
644
645      call vzero(stress,6)
646 c *** Update stress i
647      do i=1,ncomp
648          stress(i) = sigma(i)
649      end do
650
651
652
653
654
655
656
657      if ((F_f <= 1) .AND. (F_m <= 1) .AND. (F_z <= 1)) then
658
659          do i=1,ncomp
660              do j=1,ncomp
661                  dsdePl(i,j) = dsdeEl(i,j)
662              end do
663          end do
664
665      else
666
667          do i=1,ncomp
668              do j=1,ncomp
669                  dsdePl(i,j) = C_T(i,j)
670              end do
671          end do
672
673      endif
674
675
676
677      return
678      end
679
680
```